PhD program in Translational and Molecular Medicine (DIMET)

XXIII Cicle, academic year 2009-20010

University of Milano-Bicocca
School of medicine and faculty of science

Engineered adeno-associated viruses expressing anti-PrP molecules and polyelectrolyte gold nanoparticles as new therapeutic strategies for prion diseases in mouse models

Coordinator: prof. Andrea Biondi
Tutor: dr Fabrizio Tagliavini

Dr. Fabio Moda
Matr. No. 716449

TABLE OF CONTENTS

INTRODUCTION
and
AIM OF THE THESIS

ENGINEERED ADENO-ASSOCIATED VIRUSES EXPRESSING ANTI-PrP MOLECULES AND POLYELECTROLYTE GOLD NANOPARTICLES AS NEW THERAPEUTIC STRATEGIES FOR PRION DISEASES IN MOUSE MODELS

1. NEURODEGENERATION AND MISFOLDING PROCESSES

The degenerative diseases of the nervous system are characterized by several common pathologic factors. In particular they are commonest in old age and each disease affects specific neuronal groups. The clinical features of the disease relate to the anatomy and function of the affected areas. As the disease progresses, there is often atrophy of these areas that could be so distinctive for some diseases as to be considered pathognomonic. Histopathology is generally characterized by neuronal loss associated with variable gliosis, and in many cases neurons die, by non-necrotic, often apoptotic, cell death. Microscopic examination may reveal the presence of distinctive cellular inclusions containing specific proteins in either neurons or glial cells. Unfortunately degenerative diseases of the nervous system are enigmatic conditions whose pathogenesis is poorly understood [1]. Virtually all neurodegenerative disorders involve irregular processing of neuronal proteins: the aberrant mechanism can entail a misfolding of proteins, altered post-translational modification of newly synthesized proteins, abnormal proteolytic cleavage, anomalous gene splicing, improper expression, or diminished clearance of degraded proteins [2]. One hypothesis for such diseases suggests that proteins in abnormal conformations are toxic to cells and are not eliminated by the normal lysosomal and non-lysosomal ubiquitin-proteasomal system [1].

1.1 Protein Misfolding Diseases (PMDs)

The particular protein that is improperly processed in neurodegenerative disorders can determine the malfunction of distinct sets of neurons [2] and give rise to specific diseases classified as Protein Misfolding Disorders (PMDs) [3]. Among the PMDs are Alzheimer's disease (AD), Parkinson's disease (PD), Huntington's disease (HD), Spino Cerebellar Ataxia type 1 (SCA1), Fronto-temporal Lobar Degeneration (FTLD), Amyotrophic Lateral Sclerosis (ALS) and Transmissible Spongiform Encephalopathies (TSEs). Although the proteins involved in these diseases do not share sequence or structural identity, all of them can adopt stable alternative conformations without requiring changes in their amino acid sequence. The misfolded forms of the protein have a high tendency to aggregate, forming oligomers and larger polymers [4]. Sometimes these aggregates form amyloid deposits because of their characteristic tracts [5]: i.e. a cross-β structure, with specific tinctorial properties (binding to Congo red and thioflavin S), higher resistance to proteolytic degradation and a fibrillar appearance under electron microscopy (straight, unbranched, 10 nm wide fibrils), most often present as extracellular deposits [6]. Aggregation of disease-specific proteins links these diseases (also known as aggregopathies) to intracellular pathways involved in protein refolding and degradation. Whilst protein refolding is mediated by the chaperone machinery including heat shock proteins (e.g. Hsp70 family), protein degradation involves the so-called ubiquitin-proteasome system (UPS). Targeting of cellular proteins for degradation via the UPS is a basic and well-

conserved ATP-dependent process involving two discrete and successive steps: (1) conjugation of multiple ubiquitin moieties to the substrate generating the polyubiquitin degradation signal, and (2) destruction of the tagged protein by the downstream 26S proteasome complex with release of free and reusable ubiquitin, a reaction catalyzed by de-ubiquitinating enzymes [7]. Age-related decrease of UPS function predominantly affects brain regions under chronic oxidative stress such as the basal ganglia, linking aging with neurodegeneration [8]. Ubiquitin-mediated proteolysis is not only important for cellular processes such as cell cycle, development and differentiation as well as modulation of cell surface and cellular stress response but is also involved in recognition and removal of mutant or misfolded proteins. Under physiological conditions cells maintain an equilibrium between misfolded proteins, protein refolding and clearance. Disruption of this equilibrium by excess production or decreased degradation of abnormal proteins is called proteolytic stress and results in the accumulation and aggregation of abnormal proteins with each other as well as other proteins. Aggregation of mutant, disease-specific proteins associated with ubiquitin, chaperones and proteasomes is a histological hallmark of these neurodegenerative diseases. They can appear in the cytosol (Lewy bodies in PD, Bunina bodies in ALS) or can also localize to the nucleus (HD and SCA1). In AD, prominent aggregate formation is found in the extracellular space (neuritic plaques) representing specific disease mechanisms. Sporadic aggregation of proteins is a concentration-dependent process, which has been shown to cause proteasomal inhibition probably commencing in a vicious circle until the defense mechanisms of affected cells

eventually fail. Although aggregate formation is a common feature of many neurodegenerative diseases, the relevance of visible aggregates and mechanisms of aggregate-related toxicity in the different neurodegenerative diseases is still a matter of intense research and debate. In general, aggregation is considered a multistep process starting with a protein acquiring an abnormal conformation resulting in formation of dimers and oligomeric intermediates, which can then grow to metastable β-sheet containing oligomers with fibril-like morphology termed protofibrils, which in turn can mature into protofilaments and fibers resulting in inclusions [5].

As evidence of this, Alzheimer's disease has a multifactorial pathogenesis in which one of the major features is the deposition of amyloid beta (Aβ) peptides as plaques in brain parenchyma and in vessels as cerebral amyloid angiopathy (CAA) [9,10]. Aβ is derived from a pathological enzymatic processing of the amyloid precursor protein (APP) [11]. A critical event in AD pathogenesis is the conversion of soluble Aβ into insoluble fibrils, but relative deficit in synaptic function, neurotoxicity, and the progression of the disease have all been linked to the oligomeric Aβ assemblies [12]. Pathological, genetic, biochemical and pharmacological lines of evidence all support the hypothesis that the Aβ peptide and in particular, the longer 42 amino-acid (aa) residue form (Aβ42), plays a causative role in AD [13] which is also influenced by a combination of genetic and environmental factors [14]. Another pathological hallmark of AD is the presence of intracellular neurofibrillary tangles (NFTs), composed of various hyperphosphorylated aggregates of the microtubule associated protein tau (MAPT). Thus, a diagnosis of AD

is made when a patient exhibits clinical evidence of progressive dementia and when a *post mortem* examination of the brain reveals the presence of extracellular Aβ-amyloid plaques and intracellular NFTs [15]. Another rare form of degenerative dementia often associated with amyloid deposits is Creutzfeldt-Jakob Disease (CJD) which belongs to a group of diseases named *Transmissible Spongiform Encephalopathies (TSEs)*. The protein deposited in tissue is a misfolded conformer of a normal cellular prion protein, PrP^{C}, referred to as PrP^{res} [16], reflecting the fact that the abnormal PrP protein is resistant to proteolytic degradation. This produces a smaller protease-resistant molecule of approximately 130-150 amino acids, designated PrP 27-30, which tends to polymerize into amyloid [17]. In 1982, Prusiner suggested that this new abnormal protein (named "prion") is able to convert PrP^{C} into PrP^{Sc} and is therefore responsible for propagation of the disease process and disease transmissibility [18]. The most convincing evidence for this had come from different works showing that PrP knockout mice are resistant to prion infection, because they lacked expression of the protein that was therefore linked to these diseases [19]. Mutations in the PRNP gene cause neurodegenerative process that can be transmitted experimentally to susceptible animals and, most importantly, synthetic prions can be generated *in vitro* using recombinant PrP [20]. Among PMDs, mutation in the tau gene (MAPT) cause inherited forms of diseases known as *tauopathies*. Tau is a heat-resistant phospho-protein that promotes microtubule polymerization and stabilization [21], and its biological activity is regulated by a specific degree of phosphorylation. Hyperphosphorylation of tau (HP-tau) depresses its

microtubule assembly activity and its binding to microtubules causing neuropathological alterations into the brain [22]. Recently, it has been also demonstrated that normally phosphorylated tau proteins have an important role in preventing the tubulin oligomerization prion-induced in TSEs. HP-tau loss this important function, and as consequence, single tubulin molecules can aggregate forming oligomers that are toxic for the cell [23]. Abundant tau-positive neurofibrillary lesions constitute a defining neuropathological characteristic of AD, Pick's disease, progressive supranuclear palsy, corticobasal degeneration and familial frontotemporal dementia and Parkinsonism linked to chromosome 17 (FTDP-17) [15]. As observed for PrP^{C}, also tau proteins are fundamentally important because it has been proven unequivocally that mutations in the MAPT gene cause neurodegeneration in humans [24] and in transgenic animal models over-expressing mutant forms of the protein [25]. Once considered to be relatively restricted to neurons [26], it is now known that HP-tau accumulates not only in neurons in NFTs, but also in glia in a wide range of neurodegenerative disorders and in the aging brain [6]. Sometimes, extracellular aggregates of tau protein ("ghost tangles") are also present [27].

A diverse group of PMDs is represented by *synucleinopathies* that share a common pathologic lesion composed of aggregates of misfolded and insoluble α-synuclein protein in selectively vulnerable populations of neurons (i.e. substantia nigra) and glia [28]. α-synuclein is a member of a family of proteins that also contains β-synuclein and γ-synuclein that are pleiotropic in terms of function [29]. In the central nervous system α-synuclein has been implicated in

several disorders. It was originally discovered as a non-amyloid component of senile plaques that was enriched in presynaptic termini [30], but little attention was paid to it until mutations were discovered in the gene for α-synuclein (*SNCA*) in familial PD [31] and it was found an involvement of the misfolded form of the protein in PD and dementia with Lewy bodies (DLB) [32].

Polyglutamine (polyQ) expansion diseases represent a class of inherited neurodegenerative diseases in which the underlying mutation is an expansion of a CAG trinucleotide repeat that encodes polyglutamine (polyQ) in the respective disease proteins. They are characterized by gradual and irreversible loss of specific neuronal subpopulations associated with intraneuronal accumulation of misfolded protein (i.e.: huntingtin, atrophin, ataxin, etc.). All are progressive, ultimately fatal disorders that typically begin in adulthood and progress over 10 to 30 years. The clearest example of this type of maladies is depicted by Huntington disease, a progressive neurodegenerative disorder characterized by intranuclear inclusion and cytoplasmic aggregates of huntingtin with polyQ expansion [33].

In conclusion, *transactive response DNA-binding protein 43 (TDP-43) proteinopathies* mainly include FTLD and ALS. These proteinopathies are distinct from most other neurodegenerative disorders because TDP-43 inclusions are not amyloid deposits.

TDP-43 is a nuclear ribonucleoprotein that plays a role in protein processing, particularly, modulating transcription and exon splicing. TDP-43 was recently shown to be the major component of the ubiquitinated inclusions that are their pathological hallmarks [34]. While initially considered specific to ALS and FTLD, it has become

clear that TDP-43 immunoreactive neuronal inclusions are found in other disorders, such as AD and hippocampal sclerosis [35], Guam Parkinson Dementia Complex (GPDC) [36] and DLB [37]. A proportion of familial ALS cases have been linked to structure-altering mutation in the protein superoxide dismutase 1 (SOD1), a free radical defense enzyme that in disease may undergo a toxic gain of function resulting in increased production of reactive oxygen species. Recent data demonstrated that, in some form of sporadic ALS, template-direct misfolding (TDR) of SOD1 occurs intracellularly in a way analogous to prion conversion, which may contribute to the pathogenesis of ASL [38].

Disease	Etiology	Characteristic pathology	Disease proteins deposited
Huntington's disease	Huntingtin (dominant)	Intranuclear inclusions and cytoplasmic aggregates	Huntingtin with polyglutamine expansion
Other polyglutamine diseases (DRPLA, SCA1–3, etc., SBMA)	Atrophin-1, ataxin-1–3, etc.; androgen receptor (AR) (dominant)	Intranuclear inclusions	Atrophin-1, ataxins or AR
Alzheimer's disease (AD)	Sporadic (ApoE risk factor)	Neuritic plaques and neurofibrillary tangles	Aβ peptide (from APP) and hyperphosphorylated tau
	Amyloid precursor protein (APP) (dominant)	Same as sporadic	Same as sporadic
	Presenilin 1, 2 (dominant)	Same as sporadic	Same as sporadic
Fronto-temporal dementia with Parkinsonism	Tau mutations (dominant)	Pick bodies	Hyperphosphorylated tau protein
Parkinson's disease (PD)	Sporadic	Lewy bodies and Lewy neurites	α-Synuclein
	α-Synuclein (dominant)	Similar to sporadic	α-Synuclein
	Parkin (also DJ-1, PINK1) recessive (some dominant)	Lewy bodies absent (or much less frequent)	α-Synuclein (when present)
Amyotrophic lateral sclerosis (ALS)	Sporadic	Bonina bodies and axonal spheroids	Unknown (neurofilaments)
	Superoxide dismutase-1 (dominant)	Same	Unknown
Prion diseases (kuru, CJD, GSS disease, fatal familial insomnia, new variant CJD)	Sporadic, genetic and infecti	Spongiform degeneration, amyloid, other aggregates	Prion protein

Table 1. Classification of major neurodegenerative disorders [5].

Each disease has distinctive selectivity for specific neuronal population (Table 1). For example, many of the polyQ diseases, among which SCA1, share a predilection for the cerebellum and lead to ataxia while HD mainly affects striatum and cortex. The α-synucleinopathies have a predilection for the substantia nigra, and many of the tauopathies involve cortical pyramidal neurons and hippocampus and thus manifest as dementia [39]. AD pathology is principally confined to the cortex and hippocampus while prion diseases generally affect several brain regions (cortex, brainstem, thalamus, cerebellum, etc.).

To summarize, the protein conformational changes associated with the pathogenesis of most PMDs result in the formation of abnormal proteins that are rich in β-sheet structures, partially resistant to proteolysis, which have a high tendency to form larger-order aggregates. In fact, a common feature of several PMDs, is the aggregation and deposition of the misfolded protein in different organs [3]. While the relevance of these aggregates for neuronal degeneration and their impact on cellular function is still a matter of debate, several experimental therapeutic approaches are designed to interfere with this protein aggregation.

Recent convincing experimental findings and clinical observations have suggested that protein aggregates associated with PD, AD and HD, might move from affected to unaffected areas of the brain, suggesting that prion‐like transmission of these diseases contribute to the anatomical spread of disease pathology [40].

The crucial role of the protein misfolding process is most clear in the prion disorders which are the only member of the PMDs group known

to be caused by a single gene alteration and transmissible by infection. For these reasons prion disease represents the ideal model for studying the pathological mechanism of neurodegeneration and for developing novel strategies based on gene therapy.

2. TRANSMISSIBLE SPONGIFORM ENCEPHALOPATHIES (TSEs)

Prion diseases, or transmissible spongiform encephalopathies (TSEs), are neurodegenerative disorders of humans and animals that are sporadic or inherited in origin and can be transmitted [41]. In human, the most common form is sporadic Creutzfeldt-Jakob disease (sCJD); genetic forms comprise familial CJD (fCJD), fatal familial insomnia (FFI), Gerstmann-Sträussler-Scheinker disease (GSS) and prion protein cerebral amyloid angiopathy (PrP-CAA); forms acquired by infection include Kuru, iatrogenic CJD (iCJD) and variant CJD (vCJD) [42].

Animal prion diseases occur mainly as scrapie in sheep, chronic wasting disease (CWD) in mule, deer and elk [43], bovine spongiform encephalopathy (BSE) and atypical forms termed BSE-H and BSE-L (or BASE) in cattle [44,45]. BSE, or "mad cow disease", is an example of prion disease transmission from animals to people, where the consumption of tainted beef products resulted in the outbreak of the human vCJD. Until October 2010, approximately 222 cases of vCJD occurred worldwide, most of them in UK (171) and France (25), followed by Spain (5), USA (3) and Italy (2) [46].

In Europe, the incidence of sporadic and familial CJD are approximately 1.5-2 per million per year and one per 10 million per year, respectively [47]. All forms of TSE are characterized by spongiform degeneration of the brain (Fig. 2) associated with PrP^{Sc} deposition, reactive gliosis and neuronal loss [48]. Particularly, 2 types of vacuolar changes limited to the gray matter are found. One is vacuolation of neuronal processes, observed as spongiosis or vacuolation in the neuropil, and the other type is the vacuolation of neuronal bodies, observed as single or multiple vacuoles in the perikarya of neurons.

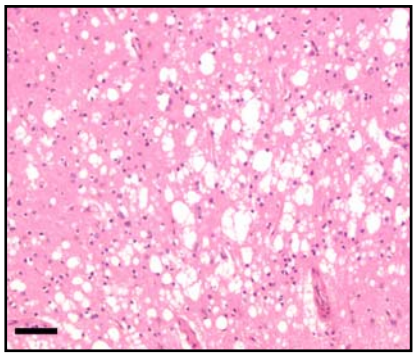

Figure 2. Spongiform changes detected in the occipital lobe of a CJD patient. Haematoxylin and eosin (H&E) stain, magnification 4X ; scale bar: 20 μm.

Despite remarkable differences in phenotypic characteristics, these disorders share a similar pathogenic mechanism, i.e. a post-translational modification of the prion protein (PrP) from a normal cellular isoform (PrP^{C}) to insoluble and protease-resistant disease-specific species (termed PrP^{Sc}) [41].

PrP^{C} is enriched in both, the lymphoreticular and central nervous system (CNS) and is tethered to the extracellular surface of cells via a

glycosylphosphatidylinositol (GPI) anchor. To date it has been shown that PrP^{C}, predominantly expressed on neurons and glia, binds copper and exerts antioxidative and neuroprotective functions [49] as well as its involvement in transmembrane signaling [50]. Unfortunately, the exact function of the protein remains still enigmatic [51].

PrP^{C} and PrP^{Sc} appear to differ mainly in their three dimensional structures [52]. Spectroscopic studies demonstrated that PrP^{C} has a high α-helical content (about 40%) whereas PrP^{Sc} contains 45% β-sheets and 30% α-helix and therefore shows remarkable amyloidogenic properties. Many features of PrP^{Sc} differ from those of PrP^{C}: (i) PrP^{Sc} is insoluble in detergents, while PrP^{C} is readily solubilized under non-denaturing conditions; (ii) PrP^{Sc} is partially hydrolyzed by proteinase K (PK) to form a fragment designated PrP27-30 (PrP^{res}), while PrP^{C} is completely degraded under the same conditions; (iii) PrP^{Sc} accumulates, whereas PrP^{C} turns over rapidly; and (iv) the patterns of PrP^{Sc} accumulation in brain are distinct from the distribution of PrP^{C} [53].

Biochemically, the properties of PrP^{Sc} appear to be determined by the three dimensional structure of the molecule. The important biochemical parameters are related to the 3 protein bands that are the molecular signature, visible by use of Western blot analytic methods. These are the 3 bands that correspond to antibody detection of a diglycosylated region of the PrP^{Sc} molecule, a monoglycosylated region, and an unglycosylated region, at around 29, 25, and 20 kDa, respectively [54]

In particular, the unglycosylated band of PrP^{Sc}, after PK digestion, may exist as 21 kDa (type 1) and 19 kDa (type 2) isoforms (Fig. 3)

which coupled with the polymorphism of codon 129 of the *PRNP* gene (Methionine/Methionine, Methionine/Valine or Valine/Valine) underline the existence of 7 molecular-variant of sCJD: MM1, MV1, VV1, MM2-cortical, MM2-thalamic, MV2 and VV2 [55].

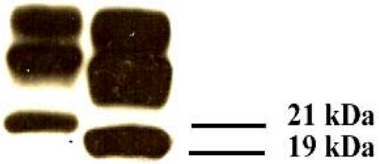

Figure 3. Immunoblot stained with anti-PrP antibody (6H4) showing type 1 (21 kDa) and type 2 (19 kDa) PrP^{res} profile.

In healthy control population, 51% are heterozygous for methionine and valine, 37% are homozygous for methionine and 12% homozygous for valine. In sCJD patients, a high prevalence of methionine homozygous patients was reported (70%). Seventeen percent are homozygous for valine and 12% are heterozygous. The polymorphism for methionine (M) or valine (V) at codon 129 of *PRNP* has been shown to influence the clinical features of sCJD [55].

2.1 CJD classification

As indicated, CJD exists in different forms that differ both clinically and neuropathologically. In contrast to genetic and iatrogenic forms, the cause of sCJD remains uncertain. However, the most favored current theory suggests that the normal prion protein in the brain undergoes a spontaneous change to the abnormal form (PrP^{Sc}), thereby

resulting in disease [46]. In this situation, the mutant PrP^{Sc} must be capable of recruiting PrP^{C} for the process of conversion [56].

2.1.1 Sporadic CJD

Sporadic CJD (sCJD) is numerically the most common form of CJD. Different sCJD phenotypes (Table 2) are determined by host genetic factors (polymorphisms at codon 129 of *PRNP* gene: MM, MV or VV) and the type of PrP^{Sc} (1 or 2). The **MM1** type corresponds to classical sporadic CJD and comprises approximately 70% of all sCJD. The mean age at onset of the symptoms is 65 years and the average clinical duration is 4 months. Neuropathological changes involve cerebral cortex, striatum, thalamus and the cerebellum; PrP^{Sc} accumulates mostly as synaptic deposits. Second, most common type, **VV2** comprise approximately 15% of all sCJD cases. The mean age at onset of the symptoms is 60 years with a mean clinical duration of 6 months. Changes are confined to the limbic system, striatum, the cerebellum, thalamus and hypothalamus and several brain stem nuclei. The involvement of the cerebral cortex depends on the duration of illness; those cases of short duration may exhibit minimal cortical changes, spongiform changes demonstrate laminar distribution while PrP^{Sc} accumulates as plaque-like, perineuronal and synaptic deposits. **MV2**-type (approximately 8%) is reminiscent of VV2-type. The mean age at onset of the symptoms is 60 years with a mean clinical duration of 17 months. Spongiform change is confined to the subcortical structures while PrP^{Sc} deposition is mostly plaque-like. In contrast to VV2-type, in MV2-type “true” plaques (Congophilic and visible in a

routine haematoxylin and eosin stain) predominates. **MM2**-type is rare (2% of all CJD) and is further sub-classified into MM2-thalamic (mean age at onset 50 years; mean disease duration 24 months), which corresponds to FFI and FSI (Fatal Sporadic Insomnia) cases and MM2-cortical (mean age at onset 65 years; mean duration 16 months), similar to MM1-type, from which it differs by limited cerebellum involvement and large (coarse) vacuoles. Finally, **VV1** is very rare (< 1% of all CJD). Mean age at onset and duration are 39 years and 15 months respectively. The distribution of lesions reveals major involvement of the hippocampal cortex while thalamus and cerebellum are less affected [55].

sCJD Variant	Previous Classification	% of Cases	Duration (mo)	Neuropathological Features
MM1 or MV1	Myoclonic, Heidenhain variants	70	3.9	"Classic CJD" distribution of pathology; often prominent involvement of occipital cortex; "synaptic type" PrP staining; in addition, one-third of cases shows confluent vacuoles and perivacuolar PrP staining
VV2	Ataxic variant	16	6.5	Prominent involvement of subcortical, including brain stem nuclei; in neocortex, spongiosis is often limited to deep layers; PrP staining shows plaque-like, focal deposits, as well as prominent perineuronal staining
MV2	Kuru-plaques variant	9	17.1	Similar to VV2 but with presence of amyloid-kuru plaques in the cerebellum, and more consistent plaque-like, focal PrP deposits
MM2-thalamic	Thalamic variant	2	15.6	Prominent atrophy of the thalamus and inferior olive (no spongiosis) with little pathology in other areas; spongiosis may be absent or focal, and PrP^{Sc} is detected in lower amount than in the other variants
MM2-cortical	Not established	2	15.7	Large confluent vacuoles with perivacuolar PrP staining in all cortical layers; cerebellum is relatively spared
VV1	Not established	1	15.3	Severe pathology in the cerebral cortex and striatum with sparing of brain stem nuclei and cerebellum; no large confluent vacuoles, and very faint synaptic PrP staining

PrP = prion protein; PrP^{Sc} = protease-resistant PrP.

Table 2. Molecular and phenotypic features of different sCJD forms [55].

2.1.2 Genetic CJD

Genetic CJD is very rare. In particular, familial forms of CJD, GSS and FFI are transmitted as autosomal dominant traits and invariably co-segregate with mutation in *PRNP* gene (chromosome 20) that encodes the prion protein [20].

There are three types of pathogenic *PRNP* mutations: point mutations leading to an amino acid substitution or premature stop codon, and insertion of additional octapeptide repeats (OPRI) (Fig. 4). This insert mutations consist of octapeptide repeats varying from 1 to 9 in total length, although an insert of 3 octapeptide repeats has not been reported in association with prion disease. To date, over 30 different mutations have been described: some are typically associated with particular clinical categories of prion disease; others are associated with a spectrum of clinical phenotypes, often with striking phenotypic variability. The PRNP E200K/129M mutation is the most frequent mutation accounting for approximately 70% of the fCJD affected families worldwide.

Clusters of affected families associated with this mutation were identified in isolated populations of Chile, Italy, Japan, Libyan Jewish community and Slovakia. All patients have dementia, 79% show cerebellar signs and 73% myoclonus. A periodic sharp wave discharge on an EEG is very characteristic of this form. A *PRNP* allele with the D178N mutation and valine at the polymorphic codon 129 (D178N/129V) is associated with the dementing form of fCJD, but when there is methionine at codon 129, the phenotype is FFI. The P102L/129M is the most frequent GSS mutation, causing the disease

in about 80% of all known GSS families [57]. Although experimental evidence from the mouse implies a role of additional factors, no genetic loci other than *PRNP* have been implicated in the pathogenesis of human prion diseases [58]. Occasionally, genetic cases are seen in which no previous family history is identified. The definitive test in relation to genetic CJD is a blood test in order that *PRNP* gene can be analyzed for searching mutations associated with the disease.

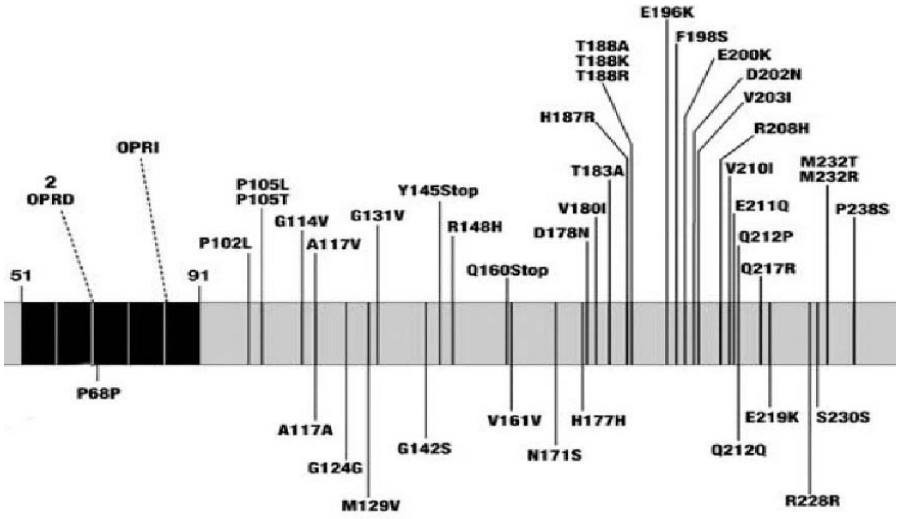

Figure 4. *PRNP* mutations associated with genetic form of CJD. P102L (129M), P105L (129V), A117V (129V), G131V (129M), F198S (129V), D202N (129V), H187R (129V), Q212P (129M), Q217R (129V), M232T (129M/V) missense mutations are associated with different clinical and neuropathological GSS syndrome; D178N (129V), V180I, T188A, E196K, E200K*, V203I, R208H, V201I, E211Q, M232R missense mutations are associated with CJD (*may be associated with insomnia as the main clinical characteristic); D178N (129M) missense mutations are associated with FFI; Y145STOP (129M) is associated with prion protein cerebral amyloid angiopathy; N171S and T183A missense mutation are associated with less specific phenotypes. Insertional mutation of 6 octarepeptide are associated with variable phenotypes including GSS, CJD and Alzheimer's atypical dementia, Huntington's.

2.1.3 Acquired CJD

2.1.3.1 Kuru

Historically, Kuru, an endemic form of CJD, was the first example of transmission of the disease. It occurred among the Aborigines in Papua New Guinea throughout the 1950s and 1960s. Kuru was horizontally transmitted by cannibalistic rituals and has not been observed in individuals born after cannibalism was abandoned [59].

2.1.3.2 Iatrogenic CJD

Iatrogenic CJD is also very rare. It occurs either by transmission during medical or surgical procedures: i.e. use of contaminated EEG depth electrodes, corneal grafting, human dura mater implants or exposure, use of human cadaveric growth hormone (hGH) and human pituitary gonadotrophin (hGNH); or by dietary exposure [46].

2.1.3.3 Variant CJD

Whereas sCJD typically presents with rapidly progressive symptoms that are usually clearly neurological in nature, variant CJD (vCJD) presents as a progressive neuropsychiatric syndrome with psychiatric and/or sensory symptoms at disease onset followed by ataxia, movement disorders (particularly myoclonus), visual abnormalities and cognitive impairment, resulting in a terminal akinetic mute state [46].

Variant CJD has a characteristic neuropathological hallmark represented by "florid plaque" (Fig. 5): fibrillary structure with a dense core rounded by a pale region of radiant fibrils, and surrounded by a ring of spongiform changes [60].

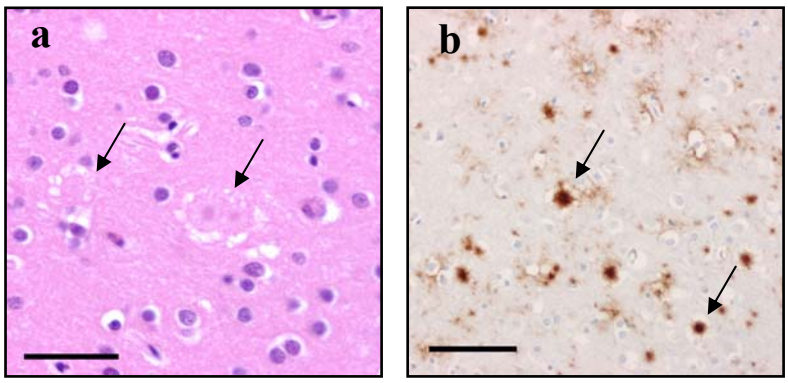

Figure 5. Florid plaques within the brain of vCJD patient. Haematoxylin and eosin stain, scale bar 20 µm (a); immunohistochemical stain to PrP^{res} 3F4 (b); scale bar: 10 µm.

These plaques occur in all layers of the cerebral cortex, but are most conspicuous at the bases of the gyri in the occipital and cerebellar cortex. They are also numerous in the molecular layer of the cerebellum. Spongiform alteration is widespread but often patchy within the cerebral cortex, mostly in a microvacuolar pattern or in relation to amyloid plaques. In contrast, confluent spongiform change is always present in the caudate nucleus and putamen, and focal vacuolation is present in most of the thalamic nuclei, the hypothalamus and globus pallidus, but the posterior thalamic nuclei (including the pulvinar) are spared [61]. All patients who have been genotyped are methionine homozygotes at codon 129 in the *PRNP* gene [60]. Unlike other forms of sCJD, vCJD shows involvement of the lymphoreticular system (lymph nodes, spleen, tonsils and

appendix). Therefore there is the possibility to find disease-related protein in a biopsy of such tissues. Tonsil biopsy has been used as a supportive diagnostic test in vCJD. A positive tonsil biopsy cannot lead to a diagnosis of definite vCJD but allows a diagnosis of "probable vCJD". Firm diagnosis has to be confirmed on autoptic brain tissue [46]. Recently, ingestion of material from BSE infected cattle has been implicated in the emergence of human vCJD, first described in the United Kingdom in 1996 [60]. There is also the possibility of ongoing person to person spread as seen with four cases of transfusion association vCJD infection to date, who received blood in 1999 or earlier from donors who were later diagnosed with clinical vCJD. Three of these individuals developed vCJD (one diagnosed in 2003 and two in 2006), whilst the fourth died from causes unrelated to vCJD, but was found on post mortem examination to have abnormal prion protein present in the spleen and a lymph node [46].

2.1.4 Variably protease-sensitive-prionopathy (VPSPr)

New subtypes of sCJD, characterized by the presence of abnormal forms of PrP with different sensitivity to PK, have been recently identified. Compared with other prion diseases, they are not exceedingly rare, as they account for about 3% of all sCJD [62, 63]. Although the affected subjects belonging to the 3 genotypes (MM, VV and MV) share several important characteristics, they also display basic variations that allow the 3 corresponding phenotypes to be distinguished (Fig. 6). In particular, VPSPr differed from known sCJD in the clinical presentation, in the histopathologic and

immunohistochemical features, and in the basic characteristics of the PrP. The most common polymorphism in VPSPr disease subtypes is VV (70%), followed by MV (22%) and MM (8%). These subtypes have been recently discovered and their characterization is still ongoing

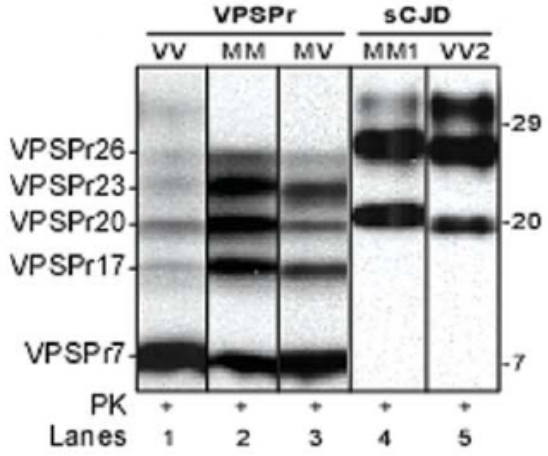

Figure 6. Electrophoretic profiles of the total brain homogenates (BHs) treated with 25l g/mL of PK and probed with the monoclonal antibody 1E4 reveal 5 PrP bands migrating approximately to 26kDa, 23kDa, 20kDa, 17kDa, and 7kDa, forming a ladder-like pattern in all 3 (129VV,129MM, and 129MV) genotypes of VPSPr (VPSPr26, VPSPr23, VPSPr20, VPSPr17, and VPSPr7) (lanes 1–3). The faint band that migrates at approximately 30kDa in VPSPr-129VV (lane 1) likely represents the incomplete PK digestion of the normal diglycosylated, N-terminus truncated PrP fragment or associated monoglycosylated full-length PrP. In contrast, BHs from sporadic Creutzfeldt-Jakob disease (sCJD) associated with the 129MM genotype and the PrPDis type 1 (sCJDMM1) or sCJDVV2 (sCJD with the 129VV genotype and PrPDis type 2) show the typical 3 PK-resistant PrP fragments of type 1 and 2 migrating between 31kDa and 19kDa (lanes 4 and 5).

2.2 Diagnosis of CJD

There is a wide scope of clinical phenomenology in human prion diseases, regarding the age of onset, presenting features, rate of progression and appearance of other clinical manifestations [64].

Because of this clinical heterogeneity, the diagnosis at early stages might be difficult. However, advances in clinical diagnostic techniques such as cerebrospinal fluid (CSF) tests and magnetic resonance imaging (MRI), allow to recognize the disease at earlier stages, but better tests are needed to identify patients as early as possible, at best at pre-clinical stage [65].

At disease onset, the symptoms and signs are not specific. Patients suffering from CJD typically present with rapidly progressive cognitive decline, which may be fulminant and progress to akinetic mutism within weeks. The diagnostic criteria for sporadic CJD produced by WHO for clinical surveillance purposes [57] are as follows:

A. Definite

Diagnosed by standard neuropathological techniques; and/or
Immunocytochemically and/or Western blot confirmed PrP^{res} and/or
Presence of scrapie-associated fibrils.

B. Probable

- Progressive dementia; and
- At least *two* out of the following four clinical features:

- Myoclonus;
- Visual or cerebellar disturbance;
- Pyramidal/extrapyramidal dysfunction;
- Akinetic mutism;

and

- A typical EEG during an illness of any duration and/or

A positive 14-3-3 CSF assay and a clinical duration to death <2 years;

A positive DWI MRI signal (i.e. hyperintense) in basal ganglia and/or cerebral cortex;

- Routine investigations should not suggest an alternative diagnosis.

C. Possible

- Progressive dementia; and
- At least *two* out of the following four clinical features:

- Myoclonus
- Visual or cerebellar disturbance
- Pyramidal/extrapyramidal dysfunction
- Akinetic mutism;

and

- No EEG or atypical EEG; and
- Duration <2 years.

Myoclonus;

- Visual or cerebellar symptoms;
- Pyramidal or extrapyramidal signs;
- Akinet mutism.

Thus, the definitive diagnosis of CJD must await the bioptically or post-mortem analysis of the CNS.

Intra-vitam diagnosis: "probable CJD" cases are diagnosed mainly on the basis of clinical symptoms, when no histopathological or biochemical confirmations are available. In particular, total Tau, phosphorylated-tau (P-tau) / total-tau (T-tau) ratio (60) and presence of 14-3-3 protein are useful, but not entirely sensitive and specific markers for the diagnosis of CJD in CSF [66]. 14-3-3 is a neuronal protein involved in cell signaling and is present in high concentrations within the CNS. It may be released into the CSF in a number of

neurological and pathological conditions affecting neuronal integrity. Therefore, its presence in the CSF is not completely specific for CJD. Total tau is remarkably increased, with values usually above 1.300 pg/mL (control value < 250 pg/mL) [67].

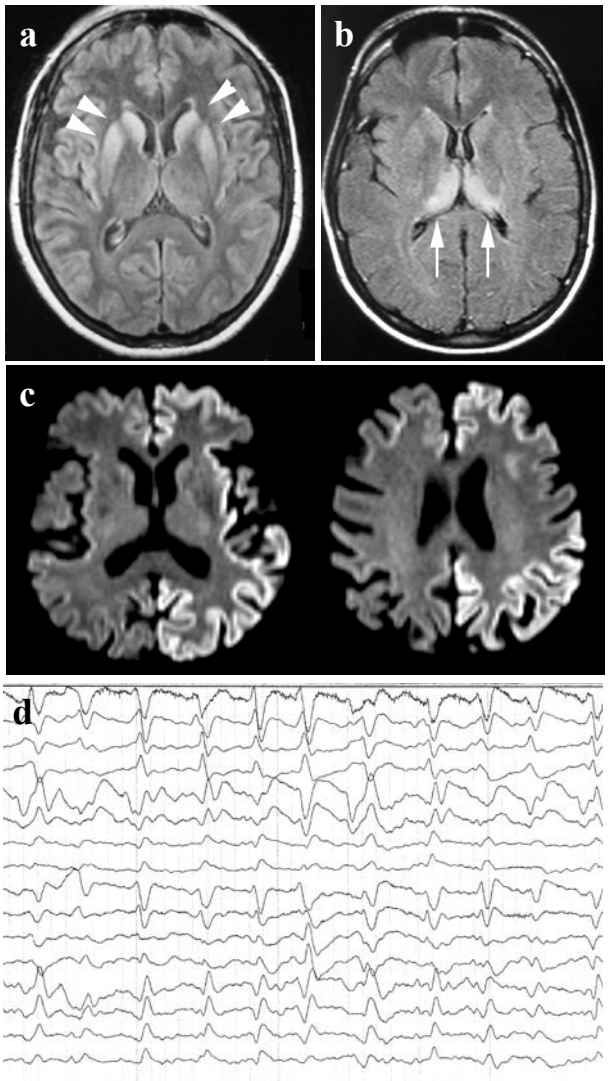

Figure 7. Sequential axial T2-weighted MRI through the basal ganglia showing high signal in caudate and putamen of a sCJD patient (a) and "pulvinar sign" in the posterior thalamic region of a vCJD patient (b); high signal present in cerebral cortex of sCJD patient (c); characteristic EEG periodic complexes (d) in sCJD patient (it has not been seen in any case of vCJD).

The potential for brain MR imaging to be a useful tool in the diagnosis of CJD is becoming increasingly recognized. In the early 90s the first few case reports have described bilateral striatal high signal on T2 or proton density weighted imaging. In the last decade it has been shown that diffusion MR is the imaging contrast of choice to identify abnormalities in patients with CJD.

Diffusion MR imaging measures the random motion of water molecules, that is a fundamental physical process for the functioning of living systems. Deposition of prion proteins and vacuole formation in the cerebral interstitium and inside neurons are considered the main cause of increased MR signal in the brain of patients with CJD.

Common MR imaging features of sporadic CJD include signal hyperintensity in the cortical ribbon of both cerebral hemispheres, in the caudate and putaminal nuclei (Fig. 7a). The cingular cortex and precuneus, the parietal, frontal, temporal and insular cortices are the cortical regions most frequently abnormal. In these areas the signal abnormalities are most frequently asymmetric; there is not a preferential affected hemisphere (Fig. 7c). Signal hyperintensities on diffusion-weighted images (DWI) are usually associated with decreased water diffusivity as confirmed by hypointensity on apparent diffusion coefficient (ADC) maps.

Less common signal abnormalities are found in the thalamus, hyppocampus, entorhinal cortex and cerebellum, despite a relatively high involvement of these structures as shown by neuropathological studies.

A recent study in 436 sporadic CJD patients and 141 controls showed that the best sensitivity and specificity in the differential diagnosis of CJD was obtained when either at least two cortical regions (temporal, parietal or occipital) or both caudate nucleus and putamen displayed a high signal in FLAIR or diffusion-weighted MR imaging [68]. Signal abnormalities on spin-density (PD) and T2-weighted MR images are currently found but they are less prominent than DWI and Fluid attenuated inversion recovery (FLAIR). DWI are especially more sensitive at detecting cortical grey matter abnormalities.

T1-weighted imaging does not usually show any signal change and there is typically no gadolinium enhancement.

Atrophy is not a common findings in patients with sporadic CJD, especially at early diagnosis. Subcortical atrophy with enlargement of the ventricles should be considered a late finding characteristic of those CJD subtypes with a relatively long course. Cerebellar signs are very frequent and electroencephalographic recordings often visualize periodic sharp wave complexes (Fig. 7d).

The usefulness of positron emission tomography (PET) and single photon emission computed tomography (SPECT) in establishing a diagnosis of CJD is debatable. Claims that there is a characteristic appearance in CJD that may be diagnostically useful should be interpreted with caution as no study has attempted to evaluate SPECT or PET as a diagnostic tool for CJD using a suitable control group. Unfortunately the time between onset of first symptoms and disease specific diagnostic tests might typically span from several weeks to months [69].

Instead of sCJD cases, diagnosis of vCJD can often be obtained by biopsy of the tonsils, which have been shown to harbor significant amounts of PrP^{Sc} in germinal centers [70], while MRI evidences the frequent presence of hyperintensity in the posterior thalamus [61]. The "pulvinar sign" (Fig. 7b) was originally thought to discriminate reliably between sCJD and vCJD, but cases of sCJD with the same neuroradiological changes have been described [71]. A serious problem is the rapid disease progression. At the time suspicion is raised and appropriate tests are done, many patients might already suffer from a severe neurological deficit. Given a short survival time in most patients, an early case identification is crucial to start the treatment.

Post-mortem diagnosis: a definite diagnosis of CJD can be made only by neuropathological, biochemical and immunohistochemical demonstration of the pathologic isoform of the prion protein within the human brain tissue (Fig. 8).

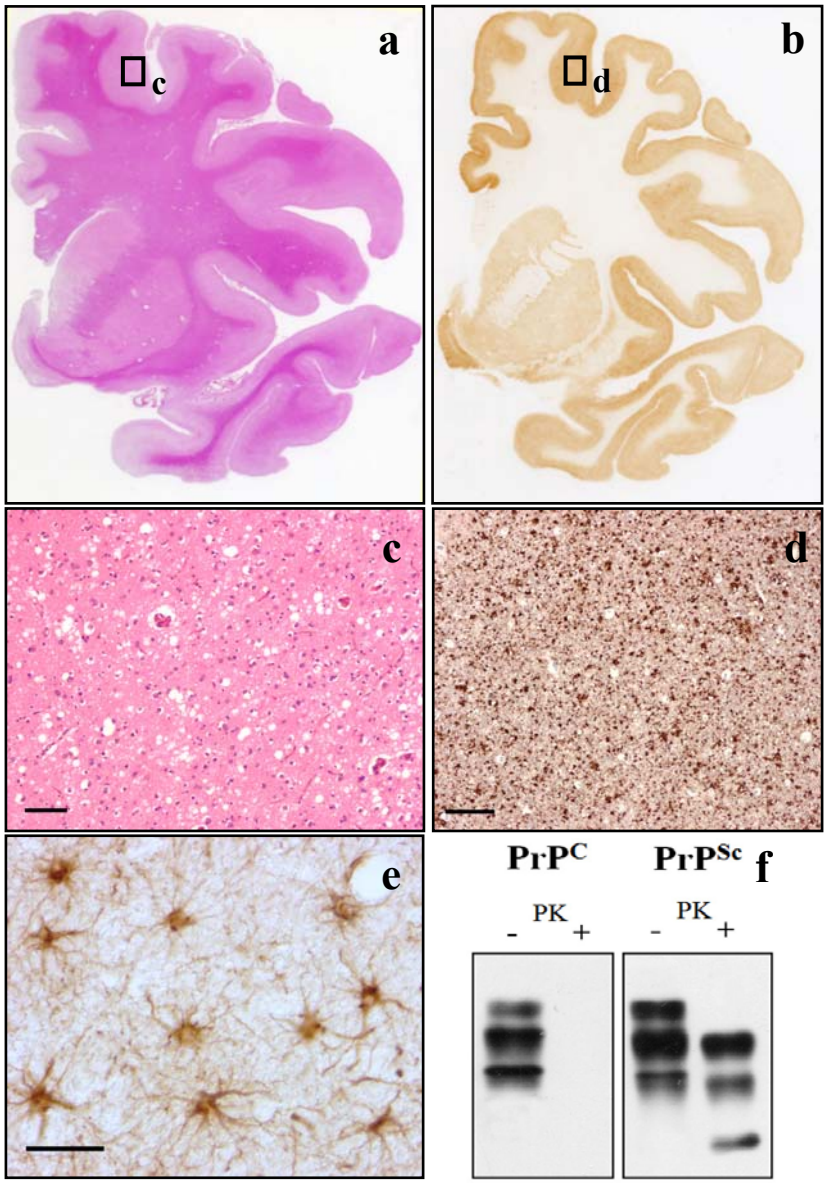

Figure 8. Macrosections of right cerebral hemisphere stained with haematoxylin and eosin (a) and immunostained (b) with a monoclonal antibody to PrP^{Sc} (clone 3F4) after PK digestion (10 µg/mL); detail of figure a (c) showing evident spongiosis into the frontal cortex (scale bar 20µm); detail of figure b (d) showing typical synaptic and focal pattern of PrP^{res} deposition (scale bar 20µm); astrogliosis (e) (scale bar 10µm); immunoblot detection of PrP^{res} with the 3F4 monoclonal antibody (f) after PK digestion (50µg/mL).

Future perspectives: PrP^C is normally expressed in white blood cells and platelets and the possibility exists that some blood cells may express the abnormal PrP isoform in affected individuals. This raises the possibility of a blood test for CJD, but would require an assay for PrP with a much higher degree of sensitivity than is currently available. However, progress is being made in this direction. Improved concentration and amplification methods coupled with the use of antibodies specific to the abnormal PrP isoform raise hope for more accurate, more sensitive and simpler diagnostic techniques in the future [57]. Moreover, using an approach called protein-misfolding cyclic amplification (PMCA), it is possible to rapidly convert PrP^C into PK-resistant PrP by using smaller amount of PrP^{Sc}. For this reason, PMCA should provide a means of detecting extremely small amounts of PrP^{Sc} in systemic tissues or body fluids and become an important tool for the pre-clinical diagnosis of prion disease. In addition, PMCA might help to facilitate our understanding of the molecular events involved in prion replication and will likely be extremely useful for identifying compounds that inhibit prion replication [72].

2.3 CJD: pathogenic mechanism

The central event in prion diseases is the conformational conversion of the PrP^C to PrP^{Sc} that has high content of β-sheet secondary structure and high tendency to form insoluble aggregates and amyloid fibrils. According to the refolding model hypothesis, PrP^C is a substrate for the PrP^{Sc} mediated conversion of PrP^C into new PrP^{Sc} molecules.

Particularly, direct interaction between PrP^{C} and PrP^{Sc} is proposed to drive the formation of nascent infectious prions (Fig. 9). The region corresponding to residues 132-140 is critical for the interaction between the two isoforms of the protein.

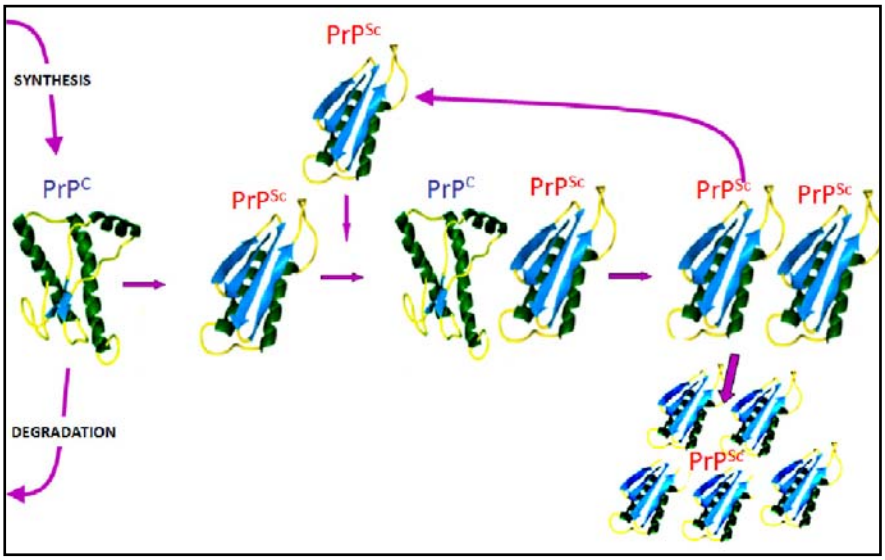

Figure 9. Model of prion conversion. Infectious PrP^{Sc} binds to PrP^{C} and catalyzes its conversion into the misfolded form.

The primary translation product of PrP^{C} consists of 253 residues; maturation of the protein involves cleavage of an N-terminal signal sequence of 22 amino acids, glycosilation at asparagine residues 181 and 197, formation of disulfide bond, removal of 22 C-terminal amino acids and addition of a glycosylphosphatidylinositol (GPI) anchor at serine residue 231. PrP^{C} is then transported to the cell surface, where it is anchored to the plasma membrane by the GPI [41]. The PrP^{C} extracellular localization makes it available to interact with PrP^{Sc} thus undergoing conformational rather than chemical modification [73]. Cellular compartments involved in PrP^{C} synthesis and trafficking are

also candidate locations for the conversion process, thus a thorough understanding of PrP^C metabolism is crucial for understanding cellular PrP^C biogenesis [74].

PrP knockout mice (*Prnp*$^{0/0}$) are resistant to prion disease without propagating infectivity [19] and PrP-null brain tissue surrounding prion-infected *Prnp*$^{+/+}$ neurografts does not develop prion neuropathological changes [75]. Moreover, the propagation of non-neuronal PrP^{Sc} in the absence of PrP^C is not by itself pathogenic and within neurons, during scrapie infection, prion accumulation can be prevented by arresting the continued conversion of PrP^c to PrP^{Sc} [76]. These studies demonstrated that the host susceptibility to prion infection and propagation requires the expression of PrP^C. To date, the exact mechanism by which PrP^{Sc} triggers further PrP^{Sc} production is unknown. In addition, the mechanism by which PrP^{Sc} or the absence of normally folded PrP^C causes tissue damage is still unclear.

Recent data show the intervention of specific cofactors in prion conversion. The fact that PrP isoforms can bind sulphated glycosaminoglycans (GAGs), glucose polymers, metal ions, lipids, nucleic acids, laminin, laminin receptor, protocadherin-2 and Bcl-2 makes them worthy of consideration as cofactors in PrP conversion [77].

Especially, increasing evidences suggest an important role of RNA as cofactor in the pathogenesis of prion diseases. Using spectroscopic approaches it has been shown that PrP interacts with RNA indicating its potential role as adjuvant in PrP^C/PrP^{Sc} conversion [78].

In addition, more than 15 miRNAs (small, non-coding RNA species that act as key regulators of gene expression) have been deregulated in

brains affected by prionopathies. This may result in an altered expression of genes involved in cell death, synapse function, and neurogenesis [79].
Detailed studies are still ongoing in order to clarify this fundamental question.

2.4 Prion transmission to mice and species barrier

The transmissibility of prions was accidentally demonstrated in 1937, when a population of Scottish sheep was inoculated against a common virus with a formalin extract of brain tissue unknowingly derived from an animal with scrapie [80]. Since then, prion transmission experiments to mice and hamsters, with infected brain material, were introduced in the 1960s [81] and 1970s [82], respectively. In 1967 Griffith J.S. introduced the possibility that the material responsible for disease transmission might be a protein that had the surprising ability to replicate in the body [83]. This launched the so called "protein-only" hypothesis and subsequently Stanley Prusiner's group coined the name "prion-only" for this new proteinaceus infective particle (PrP^{Sc}) [18]. The theory sustains that PrP^{Sc} itself is responsible for the propagation of the pathologic process and transmissibility of the disease. In particular, the incubation period for transmission of PrP^{Sc} within and between species is determined by a number of factors that include: (i) route of infection (intracerebral inoculation leading to a more rapid onset of disease than peripheral injection), (ii) strain, and (iii) dose administered. Experimental evidence indicates that ease of transmissibility decreases in the following order:

It is of note that the intragastric (i.e. oral exposure) route has the lowest efficiency, requiring in mice about 10 times more infectious material than the highly efficient intracerebral route. It is also widely recognized that lower doses increase the incubation period. When orally exposed, it appears that infection occurs via the gut. Replication of prion occurs first in the spleen and lymph nodes. The agent probably reaches the brain from the spleen via the sympathetic fibers of the splanchnic nerves, which connect to the mid-thoracic spinal cord. From here, infectivity spread caudally. Once infection has passed to the brain and spinal cord, it can reach to the peripheral tissues.

In surgically splenectomized mice the onset of clinical disease is delayed, probably as a result of a reduction in available replication sites for PrP^{Sc} [84].

Transmission of prions between mammalian species is thought to be limited by a ‘‘species barrier’’ which depends on differences in the structure of prion proteins, in the infecting inoculum and the host. The greater the homology between the PrP structure (particularly the central residues) of the donor and the host, the more likely it is that the host will acquire a specific strain. In these cases of prion transmission between different species, there is usually a longer incubation period

than seen within the same donor species. However, subsequent passage of an agent within the 'new' host is associated with a decrease in incubation period and the agent becomes "host adapted". As an example, Rocky Mountain Laboratory (RML®) and ME7 prion strains are derived from scrapie agent that has been mouse-adapted, by several passages, in mice [85]. Instead, with some host/agent combinations, it appears that the barrier is sufficiently high to prevent the transmission entirely (i.e. CJD has not been transmitted to inbred/outbred mice), while some prion strains (i.e. BSE or scrapie) are efficiently transmitted to inbred mice [86], just as BSE is transmitted to human population causing vCJD [46].

In human populations, there is an interesting observation that homozygosity at codon 129 increases susceptibility to both sporadic and iatrogenic forms of CJD, while all vCJD cases so far described are homozygotic (methionine/methionine) at codon 129. It has been speculated that heterozygosity (methionine/valine) may induce the expression of two different PrP^C proteins, resulting in a slower clinical course of the disease [57]. For this reason, it has been suggested that the 'barrier' is simply a prolongation in incubation period, and that all forms of TSE are transmissible if the animal (or human) survives long enough.

2.5 Mouse models for prion diseases

As previously described, there is a considerable evidence that the amino acid sequence homology of PrP^C from the donor versus that of the recipient species determines the so called "species barrier". This

barrier is more readily crossed in PrP knockout wild-type mice carrying the PrP transgene of the species from which the prions are derived [19]. For this reason, a number of genetically modified mouse models have been generated during the last two decades, which express PrP^{C} of heterologous species [87]. The introduction of heterologous PrP transgene by the usual procedure of pronuclear injection results in the integration of an uncontrolled number of gene copies (usually concatenates) into a random location of the genome. This in turn gives rise to transgene expression levels which vary from one transgenic line to another; moreover, the tissue specificity of expression may be influenced by the DNA sequences surrounding the integration site. These problems have been circumvented by inserting transgene directly into the target site.

In the so-called double recombination procedure, the entire PrP coding region of one allele was replaced with the heterologous PrP gene. Recombinant embryonic stem cells were isolated and used to generate mice by standard procedures [87, 88].

At present, a battery of transgenic mouse lines are available which express human (i.e. HuMTg; HuVTg) [89, 90], mink (i.e. TgMk7)[91], bovine (i.e. TgbovXV; Tg540) [92], ovine (i.e. TgovPrP4) [93], cervid (i.e. TgElkPrP12584) [94] and mouse (i.e. Tg*a*20) [95] PrP^{C}. These genetically modified mice have been utilized to investigate the physiological role of PrP^{C}, molecular aspects of species barrier effects, the cell specificity of the prion propagation, the role of PrP glycosylation, the mechanism of the prion spread, and the neuropathological role of both PrP^{C} and PrP^{res} [87]. In fact, by transmitting different form of CJD to mice containing human PrP

gene, comparative studies of human prion strains have been efficiently performed and much about human prions has been revealed: for example, the importance of PrP^{Sc} conformation for the prion properties [96] and the origin of vCJD being BSE [46].

Similarly, mice containing bovine PrP gene infected with BSE faithfully recapitulate many of the features found in BSE-sick cattle. In addition, transgenic mice carrying specific mutations or polymorphisms are useful for the study of the molecular pathomecanisms of different genetic forms of TSEs. For these reasons, mice have since then been the most frequently used experimental animals in prion research.

2.6 Prion strains characterization

The properties of PrP^{Sc} are determined by the three dimensional structure of the molecule, changes to which could result in different forms, or "strains". These strains have different properties and are characterized with different methods [97]:

1. *biochemistry*: for studying the differences in size and glycoform ratio of PK-resistant PrP^{Sc} fragments and their solubility and aggregation properties [98];
2. *immunohistochemistry:* for studying the topology and the pattern of PrP depositions in the brain of prion infected individuals;
3. *mouse bioassay:* which is used as the definitive strain-typing method. In this test animals are experimentally infected with prion. Generally, bioassay are lengthy and labor intensive and

results are not always easy to interpret. They provide important information about the susceptibility of different hosts to specific prion strain with relative time of disease incubation. Moreover, the lesion profiling is utilized for scoring the intensity of vacuolation in a selected set of neuroanatomic locations [99]. The score versus location of the brain lesions is then represented in a linear graph (Fig. 10). The severity of lesions may vary among animals, reflecting the stage in the course of the disease; advanced cases gave the most severe vacuolation. This is a well-established semiquantitative method of measuring the targeting of vacuolation to different brain regions, and reliably discriminates between TSE strains in mice. Incubation pattern and lesion profile are unique for each strain of prion that shows stable biological properties. Mouse bioassays have highest sensitivity when conducted in homologous species: for this reason, different transgenic mouse models carrying human, ovine, bovine or deer PrP^C are used. These models are genetically closeness to the specific natural prion host with whom they are infected, and the duration of the incubation period is noteworthy reduced. Fortunately, some prion strains (i.e. BSE and Scrapie) are easily transmitted to conventional inbred mice (i.e. RIII, C57Bl, VM) [100, 101] providing excellent results while keeping costs limited.

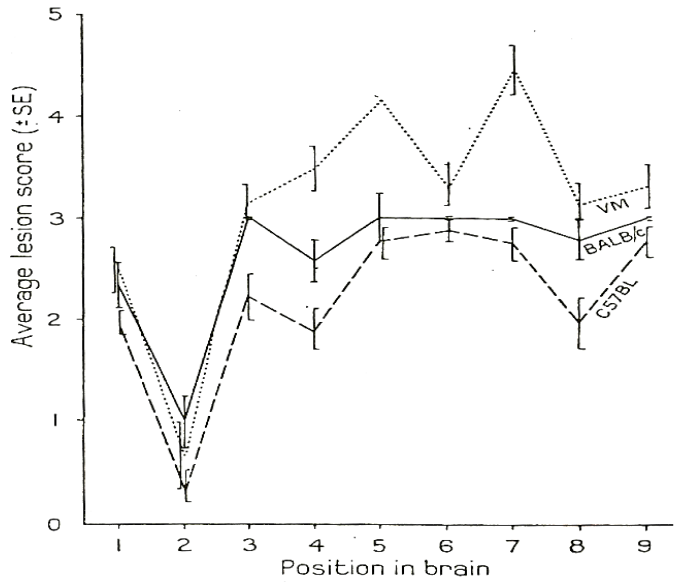

Figure 10. Distribution of brain lesions at the terminal clinical stage of three different inbred mouse strains infected with Scrapie. The 9 position used for scoring the lesion density in the mouse brain are: 1. medulla; 2. cerebellum; 3. mid-brain; 4. hypothalamus; 5. thalamus; 6. hippocampus; 7. paraterminal body; 8 and 9 cerebral cortex.

To summarize, each prion strain can be distinguished on the basis of specimen tropism, incubation period, clinical course of disease, neuropathological manifestation and PrP^{Sc} distribution in brain tissue. Collectively, the results of these various transmission studies show that distinct PrP^{Sc} conformations or subtypes with the same amino acid sequence as that of PrP can exist and that strain-specific properties are maintained in the protease-resistant core of PrP^{Sc}. Recently, the conformations of PrP^{Sc} isoforms have been studied through the use of immunoassays that recognize regions of the protein that are differentially buried or exposed depending upon the extent of

denaturation of the molecule. This approach has led to the development of the conformation-dependent immunoassay (CDI), which is capable of quantifying the concentration of PrP^{Sc} without the use of proteinase digestion to discriminate between PrP^{C} and the abnormal isomer of PrP.

The use of CDI has revealed that prion strains may differ from each other by the extent to which epitopes that are buried in PrP^{Sc} under native conditions become accessible upon partial denaturation. In addition, CDI has shown that PrP^{Sc} adopts both protease-resistant and -sensitive conformations and that prion strains can be discriminated by the composition of these two conformers of disease-associated PrP [102].

3. THERAPEUTIC APPROACHES FOR PMDs AND TRANSLATIONAL MEDICINE

The number of people suffering from neurodegenerative disorders is dramatically increasing. As of 2008, there are an estimated 30 million people with dementia worldwide. By 2050, it is projected that this data will increase to over 100 million. Alzheimer's disease, for example, affects about 600.000 people only in Italy (and more than 5 million worldwide) but this statistic, in the absence of effective treatment, is expected to dramatically increase due to the raising of the average lifespan of the people. The information in the 2009 World Alzheimer's Report makes it clear that the crisis of dementia and Alzheimer's disease cannot be ignored [103]. For this reason, research on neurodegenerative disorders are making great

efforts to try to: (i) determine the molecular basis of selective vulnerability, (ii) detect the specific pathways of protein accumulation within neurons, or glia, or both, (iii) identify the mechanisms associated with progressive neuronal loss and (iv) discover specific effective treatments. In fact, knowing that this PMDs are caused by aberrant proteins aggregation, makes it possible specific approaches to the treatment. While the relevance of these aggregates for neuronal degeneration and their impact on cellular function is still a matter of debate, several experimental therapeutic approaches have been aimed at interfering with protein aggregation. In fact the misfolding of proteins, nucleation and aggregation is a stochastic event linked to the concentration of the protein involved and influenced by cellular control and detoxification mechanisms. If aggregate formation is the causal event for neuronal cell death, reducing the concentration of the responsible protein would delay the neurodegenerative process considerably.

At present, treatments for several PMDs are exclusively symptomatic with almost no therapies available in the clinic to prevent, halt or even delay neuronal loss [104]. A common obstacle for drug therapies targeting PMDs is to cross the blood brain barrier (BBB) and many treatment strategies are based on gene transfer to localized targets in the brain. In particular, such treatments typically begin at “the bench” with basic research (in which the disease is studied at a molecular level) then progress to the preclinical level (in which the treatment is studied in specific animal model of the disease), and finally are tested to clinical level (or the patient's “bedside”). This bench-to-bedside approach to translational research is really a two-way street [105]:

basic scientists provide clinicians with new tools for use with patients and for assessment of their impact; clinical researchers make new observations about the nature and progression of disease that often stimulate basic investigations. Translational research has proven to be a powerful process that drives the clinical research engine. Especially, in the past two decades, biomedical and other research fields like gene therapy, the human genome project (HUGO), stem cell research, cloning, nanotechnology and others have revolutionized medicine and generated entirely new fields and approaches in treatment of diseases [106]. Particularly nanomedicine and gene therapy approaches have been analyzed in this thesis as new therapeutic approaches to different prion disorders.

3.1 Therapeutic approaches to prion diseases

Devising approaches to the therapy of prion diseases is beset by many difficulties. Until now, no therapeutic drug is on the market for the treatment or cure of different TSEs. In addition, no vaccination against prion disorders is available. According to the view that the accumulation of PrP^{Sc} is responsible for cell pathology, the hypothesis can be advanced that the evolution of the disease may be modified by compounds interacting with both PrP^{C} or PrP^{Sc} and the process of conversion. In particular, several *in vitro* and *in vivo* studies showed that reagents binding either PrP conformers at the contacting interface resulted efficient in blocking prion formation by inhibiting this interaction. Over the past several years, many compounds have been proposed as potential therapies for prion diseases (Table 3).

Compound	Cell-free	Cell culture	Animal/Human	Proposed mechanism	Ref.
Acridines					
Quinacrine	Binds weakly to helix 3 of PrP^{C}. No effect on PrP^{Sc} propagation	Reduces PrP^{Sc} levels in ScN2a cells (IC_{50} 300 nM), less so in ScGT1 cells	No effect on i.c. scrapie-infected mice. Ineffective in human CJD. Penetrate BBB	Accumulates in lysosomes, binds to PrP^{Sc} ?	107, 253
Bis-Acridine derivatives		Reduces PrP^{Sc} levels in ScN2a cells (IC_{50} 25-40 nM)		Binds to unknown receptor?	108
Anthracyclins (chemotherapics)					
4'-iodo-4' deoxy-doxorubicin (IDOX)			Inoculum and drug i.c. coinjected prolonged survival of scrapie-infected Syrian hamsters	May prevent amyloid by binding abnormal form of PrP	109
Anti-PrP antibodies					
FabD18	Binds PrP^{C} 132-156	Reduces PrP^{Sc} levels in ScN2a cells (IC_{50} 9 nM)		Impedes PrP^{C}-PrP^{Sc} interaction	110
Monoclonal anti-PrP 6H4	Binds PrP^{C} 144-152	Reduces PrP^{Sc} levels in ScN2a cells ($IC_{50\ ca.}$ 10 nM)	Protects mice against i.p. infection when light chain is expressed from transgene	Impedes PrP^{C}-PrP^{Sc} interaction occupying their binding domains	111
Monoclonal anti-PrP 8B4 and 8H4	8B4 and 8H4 bind PrP^{C}. Epitope 34-52, and 175-185 respectively		Modest increase in survival time of i.p. inoculated mice		112

SAF34/ SAF61	Binds PrP^C in the octarepeat region	Reduces PrP^{Sc} levels in ScN2a cells and PrP^C levels in uninfected cells		Increases the rate of PrP^C clearance which removes the substrate for PrP^{Sc} formation	113

Compound	Cell-free	Cell culture	Animal/Human	Proposed mechanism	Ref.
scFv antibody 6H4	Binds PrP^C 144-152	Paracrine antiprion activity when cocultured with ScN2a cells. Reduces PrP^{Sc} levels in ScN2a cells		Impedes PrP^C-PrP^{Sc} interaction occupying their binding domains	114
scFv antibody D18	Binds PrP^C 132-156	Paracrine antiprion activity when cocultured with ScN2a cells. Reduces PrP^{Sc} levels in ScN2a cells		Impedes PrP^C-PrP^{Sc} interaction occupying their binding domains	114
scFv antibody S18	Binds LRP/LR		Reduces peripheral PrP^{Sc} in scrapie infected mice	Inhibits LRP/LR - PrP interaction	115
ICSM18	Binds PrP^C 146-156	Reduces PrP^{Sc} levels in ScN2a cells	i.p. administration of the antibody protects mice against i.p. RML-infection	Impedes PrP^C-PrP^{Sc} interaction	116
Aptamers					
DP7	Binds PrP^C	Reduces PrP^{Sc} levels in 3F4-ScN2a cells. Blocks the conversion of PrP^C to PrP^{Sc}		Impedes PrP^C-PrP^{Sc} interaction	117

Scrapie-Associated Fibrils: SAF93	Binds PrP^{C}, prevent conversion			Impedes PrP^{C}-PrP^{Sc} interaction	118
Peptides					
PrP 106-136, PrP 109-141	Inhibit conversion	Reduces PrP^{Sc} levels in ScN2a cells		Impede conversion by binding to PrP^{C} or PrP^{Sc}	114
Compound	**Cell-free**	**Cell culture**	**Animal/Human**	**Proposed mechanism**	**Ref.**
β-sheet breaker					
iPrP13	Partially disassembly of PrP^{Sc} to a similar structure of PrP^{C}	No PrP^{Sc} reduction was seen in ScN2a treated cells	Pretreatment of inoculum decrease infectivity 1-1.5 logs in mice and delays the incubation time of treated animals	Disassembles PrP^{Sc}	119
Polycations (polyamines)					
Poly-propylene-imine (PPI)	Renders PrP^{Sc} of some prion strains susceptible to proteinase K digestion	Clears PrP^{Sc} and infectivity in ScN2a cells (IC_{50} in the nanomolar range)		Destabilizes PrP^{Sc} (disaggregates and decreases β-sheet content of Pr^{PSc})	120
DOSPA		Decreases PrP^{Sc} levels in ScN2a cells by both clearance of pre-existing PrP^{Sc} and blocking de novo formation of PrP^{Sc}		Interferes with PrP^{Sc} accumulation in ScN2a cells	121
Polyanions					

Pentosan polysulfate (PPS)	Stimulates in vitro conversion	Reduces PrP^{Sc} levels and infectivity in ScN2a cells	Increase survival time of hamster and mice i.p. infected when given hours after infection or when administered intraventricularly, also late after infection. No human (sCJD and vCJD) clinical benefits observed. Does not penetrate BBB	Interfere with PrP-glucosamino glycans interaction; stimulates PrP^{C} endocytosis	122, 123

Compound	Cell-free	Cell culture	Animal/Human	Proposed mechanism	Ref.
Heparan sulfate and heparine	Stimulates in vitro conversion of PrP^{C} to protease-resistant forms	Reduces PrP^{Sc} levels in ScGT1 cell cultures	Increase survival time in i.p. infected mice	Competitive inhibition of the interaction between endogenous GAG molecules and PrP^{C} and or PrP^{Sc}	124
Heparan sulfate mimetics (HM2602)		Reduces PrP^{Sc} levels in both ScN2a and ScGT1 cell cultures	Increases incubation time in i.p. scrapie-infected hamsters and significantly reduces splenic PrP^{Sc} levels in scrapie-infected mice treated from the time of infection	Competitive inhibition of the interaction between endogenous GAG molecules and PrP^{C} and or PrP^{Sc}	125

Heteropolyanion- 23 (HPA23)			Increases survival time of mice peripherally scrapie-infected when given days (9-12) after infection. Effective in hamsters after both i.c. and i.p. scrapie infection but only if administered within 2 h of infection		126
Dextran sulfate (DS500)		Reduces PrP^{Sc} levels in both ScN2a and ScGT1 cells (IC_{50} between nM and μM)	Increases survival time of hamster and mice peripherally scrapie-infected when given i.p. hours after infection	Interfere with PrP-glucosaminoglycans interaction; stimulates PrP^{C} endocytosis	127

Compound	Cell-free	Cell culture	Animal/Human	Proposed mechanism	Ref.
Polyene antibiotics					
Amphotericin B	Modifies rafts	Reduces PrP^{Sc} levels in ScN2a and ScGT1 cells. Inhibits endocytosis of PrP^{Sc}	Prolong survival in 263K-infected hamsters and scrapie (C506M3) infected C57Bl/6J mice. Increases the incubation time of CJD-infected African green monkeys Ineffective in human CJD	Alters membrane lipid composition by peroxidation and endocytic processes. Interacts with cholesterol disturbing the PrP^{Sc} endocytosis or directly affects conversion of PrP^{C} to PrP^{Sc}	123, 128, 129, 130

MS8209		Inhibits endocytosis of PrP^{Sc}	Strain-dependent efficacy. Modest increase in incubation time of i.p. scrapie infected mice and hamsters (C506M3 and 263K strains, respectively)	Prevent uptake of prions in periphery?	131
Filipin	Disrupt lipid rafts	Reduces PrP^{Sc} levels in ScN2a cells (IC_{50} of 2μM)		Disrupts lipid rafts, reduces endocytosis, causes release of PrP^{C} from cell surface	132

Compound	Cell-free	Cell culture	Animal/Human	Proposed mechanism	Ref.
Tetrapyrrolic compounds					
Porphyrins and phthalocyanin	Prevents propagation of PrP^{res} with submicromolar IC_{50}	Reduces PrP^{res} levels in ScN2a cells	Delay onset of disease in mice and hamsters i.p. infected when given after infection. No effects were seen after i.c. infection nor after treatment at a later stage in disease progression		133
PcTS, TMPP-Fe^{3+}	Prevents conversion	Reduces PrP^{Sc} in ScNB cells	Increases survival time in mice i.p. scrapie infected	Unknown	134
Tetracyclines					

Doxycycline		Inhibits PrP^{res} formation	Delay onset of disease and prolong survival in scrapie-infected hamster. Human clinical trial still ongoing	Direct interaction with PrP^{Sc} leads to reduction of infectivity	135
Polysulfonated-low-molecular-weight compounds					
Suramin	Decreases PrP^{C} levels in uninfected cells	Reduces PrP^{Sc} levels in both ScN2a and ScGT1 cells	Modest increase in incubation time in mice and hamsters treated around the time of i.p. scrapie-infection.	Misfolds PrP^{C} at plasma membrane, endocytosis, intracellular retention and degradation	136
Amyloidotrophic intercalators					
Congo red	Decreases PrP^{res} formation with IC_{50} of ~ 8 μM	Reduces PrP^{Sc} levels in ScN2a and ScGT1 cells (IC_{50} between 1nM and 1μM)	Modest increase in survival time of or i.p. scrapie-infected hamsters. Does not penetrate BBB	Inhibits conversion, stabilizes PrP^{Sc}	124

Compound	Cell-free	Cell culture	Animal/Human	Proposed mechanism	Ref.
Quinolines					
2,2'-biquinoline	Binds to PrP^{C}	Reduces PrP^{Sc} levels in ScN2a cells (IC_{50} 1-100nM)	Somewhat extends survival in i.c. scrapie-infected mice after intraventricular infusion		137
Recombinant proteins					

PrP-Fc(2)	Binds to PrP^{Sc}		Retard disease in mice expressing the transgene and i.c. or i.p. infected with scrapie	Blocks the recruitment of PrP^{C}	138
Phenothiazines					
Chlor-promazine		Inhibits PrP^{Sc} formation in ScN2a cells (IC_{50} 3 μM)	Increases incubation time in mice after i.c. but not i.p. infection. Penetrate BBB		139
Phosphorothioate oligonucleotides (Nucleic acids which interact with PK-sensitive PrP)					
PS-Ons	PrP^{Sc} aggregation is promoted or inhibited depending on their concentration	No PrP^{Sc} reduction was seen in ScN2a treated cells	Increases survival time in i.p. scrapie infected mice	DNA binds to recombinant PrP-molecules	140
Tyrosine kinase inhibitors					
STI574 (Gleevec)		Decreases the half life of PrP^{Sc} in ScN2a, ScGT1 and SMB cells by inducing its lysosomal degradation		Induces of the lysosomal degradation of PrP^{Sc}. Enhances the clearance of PrP^{res}	141

Compound	Cell-free	Cell culture	Animal/Human	Proposed mechanism	Ref.
Pifitrin-α (PFT)		Dose-dependent decrease of PrP^{Sc} in ScN2a cells	No effect in i.p. scrapie (263K)-infected hamster	Reduces β-amyloid induced neurotoxicity in cell culture	142
Immunostimulants					

Interferon			No effect on scrapie infected mouse and CJD infected monkeys. Ineffective in human CJD		143
Cytydil-guanyl oligodeoxynucleotide 1826 (CpG1826)			Modest increase in survival time of i.p. RML-infected mice		144
RNA interference against:					
37-67 kDa LRP/LR gene		Decreases the amount of PrP^{Sc} in ScN2a and ScGT1 cell cultures			145
prnp mouse gene		Decreases the amount of both PrP^{C} and PrP^{Sc} in ScN2a and ScGT1 cell cultures			146
Lymphotoxin-β-receptor mediated approaches					
LRS			Modest increase in incubation time in mice treated around the time of i.p. scrapie-infection.	Blocks the maturation of FDCs and prevents scrapie neuroinvasion if administered soon very after i.p. scrapie infection	147
Compound	**Cell-free**	**Cell culture**	**Animal/Human**	**Proposed mechanism**	**Ref.**
Other drugs					

Flupirtine			No difference in survival time in CJD patients		148
Curcumin	Decreases detectable PK-resistant PrP	Blocks PrP^{Sc} propagation in RML-infected ScNB cells (IC_{50} 10 nM). No effetcs were seen in ScN2a cells 22L-infected	No effective on disease progression after i.c. scrapie (263K) infection in hamsters		149
Dimethyl sulphoxide (DMSO)		Decreases the amount of PrP^{Sc} in ScN2a cells (IC_{50} 100 mM)	Increases incubation time in hamsters infected both i.p. and i.c. with scrapie		150
Cysteine-protease inhibitor E64d	No effects	Decreases PrP^{Sc} levels in scrapie-infected cells (IC_{50} 0,5 μM). No effects on PrP^{C} synthesis.			136
Statins (lovastatin and squalestatin)		Decreases the amount of PrP^{Sc} in both ScN2a and ScGT1 cells		Inhibits the export of PrP^{C} from the Golgi compartment to the plasma membrane. Affects the lipid raft localization of PrP^{C}. Reduces the amount of PrP^{C} available for conversion to PrP^{Sc}	151

Table 3. List of different compounds experimentally tested against prion propagation.

Already known chemical compounds, immunomodulants, immunotherapics, polysulphated polyanionic compounds, polyamine,

tetrapyrroles, polyene antibiotics, peptides, tetracyclic and tryciclic compounds, who showed great *in vivo* efficacy [152], were challenged in pre-clinical tests in animals. Most of them resulted effective only in increasing survival time when given prior to prion infection, but failed when administered after infection had already started [153]. Many of the compounds produced small increases in incubation time (point at which neuropathological signs are seen), but not affecting the clinical phase of disease or overall survival (point at which animals die). To date, the only approach which is effective for the prevention of symptomatic neurological disease in animals with established prion neuropathology is the knockout of neuronal PrP^C. In fact, the knockout of PrP^C approximately half way through the control incubation period completely prevents the development of disease in the mice. Recently, PrP-knockout cattle were generated that appeared to be physiologically, histopathologically, immunologically and reproductively normal [154]. These findings lead to the conclusion that PrP^C may not have essential functions for the organism and that PrP-knockout could be tolerable also for humans. The targeting of PrP^C for treatment of prion disease has thus been validated by these and other transgenic experiments which indicate that the disease can be prevented by addition or knockdown of the substrate for prion conversion [152].

An important obstacle for prion therapy is represented by the BBB. Many drugs tested in animals were given by intracerebral or intraventricular route in order to reach high brain concentrations, thus overcoming BBB. For this reason, although many of the compounds were effective in a cell culture system, they lacked any effect when

systemically administered *in vivo* because of their low penetration into the CNS [155]. Moreover, unlike in inflammatory diseases, BBB is not disrupted in patients with CJD. This limits the access of the compound to the brain and innovative brain delivery systems of these molecules have been taken into account.

3.2 Human Clinical Trial for CJD

Among anti-TSE compounds described before (Table 3), none of them revealed significant effects regarding a prolongation of survival time in CJD patients or an improvement of the state of health. At present, only a few case reports on administration of some specific drugs in CJD patients are available [152, 156]. They belonged to distinct classes such as analgesic, anti-depressant, anti-psychotic, anti-microbial and anti-coagulant drugs. Most of them were tested in observational trials only on a small number of individuals and mainly case reports for these patients are published [155-157].

Particularly, quinacrine, pentosan polysulphate, flupirtine [158] and doxycycline have been evaluated in patients fulfilling the diagnostic criteria of *probable* CJD but none of the treatments have been shown conclusively to halt disease progression. Acyclovir [159], amantidine [160], amphotericin B [128] and interferon [161] have already been shown to be ineffective in the treatment of CJD. Antiviral (HPA-23) and immunosuppressive substances (corticoids), amphotericin B, or dextranes sulfate tested in animal experiments prolonged the incubation time, but they had no influence on the prognosis [162].

Congo red and anthracycline have a similar effect, but they resulted very toxic [163].

3.2.1 Pentosan Polysulphate, Quinacrine, Flupirtine and Doxycycline

Pentosan Polysulphate (PPS)

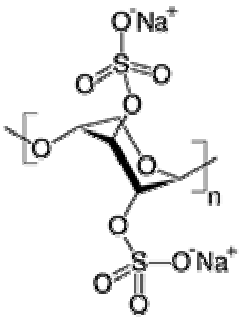

PPS does not to cross the BBB; therefore, the compound has to be administered intraventriculary. The modality of administration of this drug is invasive and not free of complications (i.e. intraventricular or intracerebral haemorrhage, seizure and also death). This has been done in a number of individuals with vCJD and sCJD [122]. There are controversial results on PPS in clinical studies. Although a prolongation of the survival time was not always reported, this finding is hard to judge because this compound has not been tested in a case-control study. PPS might still be a candidate for a clinical trial since a significant effect was observed in a mouse model of scrapie, BSE and vCJD after oral, i.v., i.p. and i.c. administration of PPS. In an observational study, continuous intraventricular PPS infusion in seven patients with various prion disorders was reported to stabilize and delay disease progression [164].

Quinacrine

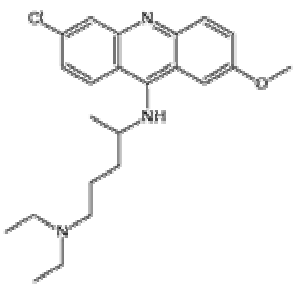

These substances belong to the group of compounds having tricyclic ring structures and an aliphatic chain. In the past, one of them was used as an antipsychotic (chlorpromazine) drug and the other as an antimalarial (quinacrine) drug [165]. Quinacrine is transported through blood brain barrier, which is important to reach high concentrations in the brain [166]. However, the results from an animals experimental study was inconclusive (Table 3). In addition, no substantial benefit in CJD patients was found in one study by comparison of quinacrine-treated patients with a cohort of historical controls with natural disease history data available. Disease progression was evaluated in 30 sCJD patients and two vCJD patients. The data were compared to untreated 125 sCJD patients.

There was no significant difference on the mean survival time in the treated and not treated group [107].

Flupirtine

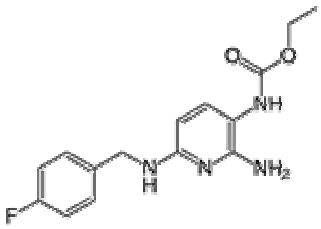

A controlled clinical trial using a prospective double blinded approach was performed for flupiritine only. Flupiritine trial was conducted in sCJD patients and 2 patients with iatrogenic prion diseases. There was no difference on the survival time, being 107 days for the treatment group and 106 for the controls. Patients treated with

flupiritine showed significantly less deterioration in the dementia tests than patients treated with placebo [148].

Doxycycline

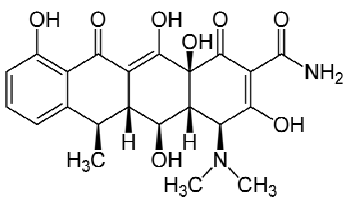

In vitro and animal studies showed that tetracyclines, are able to (i) interact with and revert the protease-resistance of PrP^{Sc} extracted from brain tissue of patients with all forms of CJD, (ii) reduce the infectivity titer in prion-contaminated material, and (iii) prolong survival of prion-infected animals. Accordingly, it has been advanced that tetracycline antibiotics with well characterized pharmacokinetic properties and safe toxicological profile could be used for prion inactivation in potentially contaminated products of medical relevance and for prevention strategies. On this ground, a small series of CJD patients observed at "Carlo Besta" Institute in the last five years received compassionate treatment with doxycycline at a daily oral dose of 100 mg from the time of diagnosis to death. The choice of this drug among others tetracyclic compounds effective in experimental models was based on the observation that doxyclycline has favorable kinetics, relatively good capacity to cross the blood brain barrier, low toxicity and good tolerability even for prolonged administration. As a matter of fact, no CJD patient chronically treated with this drug showed adverse secondary effects. The retrospective analysis revealed that the subjects treated with doxycycline (n=21) survived remarkably longer than untreated patients (n=78); in particular, the survival time (median ± SE) was 13.0 ± 4 months in the former and 6.0 ± 0.7 months in the

latter ($p < 0.001$, Logrank test). A significant difference was still present when the doxycycline-treated group was compared to an untreated group equivalent for sex, age at onset and codon 129 *PRNP* polymorphism (treated: 13.9 ± 3.8 months, untreated: 6.1 ± 0.5 months, $p < 0.01$). This result is based on an open observation, and the efficacy of doxycycline in CJD must be verified in a randomized, double-blind study versus placebo [135].

As previously underlined, a bottleneck in TSE therapy is the delivery system. Furthermore, classical therapeutic approaches were not completely efficient and resulted inconclusive in modifying disease progression in both animals and humans studies. For this reason, by taking advantage from the fields of gene therapy and nanomedicine, new experimental therapies have been planned and discussed in this thesis. In particular the attention will be focused on the use of engineered Adeno-Associated Viruses (rAAVs) and Polyelectrolyte Gold Nanoparticles (AuNPs) as delivery system for therapeutics throughout the brain of different mouse models of prion disease.

4. INNOVATIVE TREATMENTS FOR PRION DISEASES

Recent advances in molecular biology have made it possible to deeply investigate different neurological disorders at the molecular and genetic level. On this ground, while several obstacles remain which limit conventional drug therapeutic approaches, new and innovative therapies have been exploited.

Promising therapeutic approaches, based on gene therapy and nanotechnology allow a targeted and safe delivery of drugs, thereby improving controlled compound release, ameliorating patient safety, and reducing side effect. In particular, many efforts have been focused on prion diseases with the aim to identify new molecules that could interfere with *in vivo* PrP^{Sc} production and propagation.

Gene therapy is adopted as an alternative approach for treating these otherwise untreatable diseases. It should be defined as a means of drug delivery, where the drug is a nucleic acid, either DNA or RNA, delivered to neuronal cell by a specific formulation that has to fulfill two goals. First, the nucleic acid, has to be protected in a way that allows safe travel into the brain. Unprotected, naked DNA or RNA is usually prone to degradation. Second, the protective delivery agent must attach to the cell membrane and enable to entry, followed by safe passage and efficient delivery to the intracellular site of action, mostly the cell nucleus.

Different vectors, based on a variety of human or animal viruses suitable for the incorporation and transport of the gene of interest into a specific brain area, have been tested. To date, five viral vector systems are available: retrovirus, adenovirus, adeno-associated virus (AAV), herpes simplex virus and lentivirus. As adenoviruses do not integrate the host genome and are not well tolerated by the immune system, they are not relevant for gene therapy in neurodegenerative disorders. Retroviruses also exhibit less stable expression of transgenes, probably due to their random integration. This random insertion of foreign genetic material into the recipient chromosomal

DNA could also result in an insertional mutagenesis [167]. Herpes Simplex Virus are human neurotropic viruses mostly examined for gene transfer in the nervous system. The wild type HSV-1 virus is able to infect neurons. Infected neurons are not rejected by the immune system. Though the latent virus is not transcriptionally apparent, it does possess neuron specific promoters that can continue to function normally. Antibodies to HSV-1 are common in humans, however complications due to herpes infection are somewhat rare. A replication-defective HSV vector for the treatment of pain has recently entered in phase 1 clinical trial. Replication-competent (oncolytic) vectors are becoming a suitable and powerful tool to eradicate brain tumors due to their ability to replicate and spread only within the tumor mass, and have reached phase II/III clinical trials in some cases [168]. In the same way, lentivirus and AAV have already been employed for gene therapy in several brain disorders [169]. Especially, vectors based on Adeno-Associated Viruses (AAVs) are efficient in neuronal gene transfer where they lead to long term expression of molecules without apparent decline after months and years of available follow-up [170]. Interestingly, the vast majority of AAV vectors are incapable of integrating their DNA into the host genome and persist over time as transcriptionally active monomeric and concatameric episomes mediating long-term gene expression *in vivo* [171]. Moreover, AAV vectors are FDA (Food and Drug Administration) approved and are currently being used in clinical trials [172]. The AAV viral platform has already been evaluated for the treatment of many diseases, among which the more prevalent CNS protein-misfolding disorders: Alzheimer's and Parkinson's disease

[173]. The utility of therapeutic molecule delivery with AAV is actually applied and deeply analyzed also in prion diseases.

Nanomedicine is adopted as a very innovative approach for treating different diseases. In particular, nanomedicine is the medical application of nanotechnology and many efforts are intensive in the search for new methods and tools for imaging [174], sensing [175], targeted drug [176], or gene delivery system [177]. The main focus is to improve selective delivery of drugs and diagnostic agents to the diseased target sites. Nanoparticles, liposomes, polymeric micelles, dendrimers, nanogels and nanotubes can be targeted not only to an organ or tissue, but to particular cells or even an intracellular compartment. They often exhibit similarity in their size and structure to natural carriers such as viruses and serum lipoproteins, and offer multi-faceted properties for delivery of imaging and therapeutic agents to different organs, among which the CNS [178].

For this reason, they can provide the basis for the development of innovative prevention strategies and therapies for different neurological diseases. Unfortunately, clinical applications of nano-materials are currently scarce partly because of stringent safety requirements. The employment of “nano” approaches for the treatment of neurological disease gave rise to the concept of nanoneurology.

Nanoneurology is a completely new science; however, many existing neurologic treatments are at the nanoscale, such as pharmaceuticals including lithium chloride, antidepressants, and anticoagulants for stroke. Although these treatments have the appearance of

nanotechnology because of the size of the materials, subtle but fundamental differences exist. Three important differences are: (i) when ingested, small molecules and their metabolites affect the brain and its functions, as with antidepressants. Nanotechnology delivers individual molecules to specific targets, without breakdown, until the therapeutic effect is achieved, and then the material breaks down and is eliminated. With this type of formulation and construction, the quantity of delivery can be decreased 10- to 50-fold; (ii) most pharmaceuticals have fillers in them that, in some cases, facilitate release and delivery. A few new pharmaceuticals have been introduced that are nanocoated with a monomolecular layer to facilitate solubilization and transport. The therapeutics are only released when the target is reached; (iii) chemotherapy uses magnetic fields to target tumors by linking the therapeutic with a magnetic nanomaterial. It then uses an applied field to guide the particles, then triggers an external stimulus to induce release and delivers of high dose of therapeutic to the targeted area [179].

Several noninvasive medical imaging approaches, such as computed tomography (CT), magnetic resonance (MR), positron emission tomography (PET), single-photon-emission CT (SPECT), ultrasound (US), and optical imaging (OI), are currently being used. The emergence of nanosized contrast agents for these imaging techniques is anticipated to lead to progress and will broaden the understanding of biological processes at the molecular level. Combining the delivery systems with contrast agents, fluorescent, or radioactive substances allow to use imaging techniques to monitor the successful of the selective transport and the treatment [180]. Moreover the

nanoparticulated drugs allow the release over time or even the simultaneous or sequential release of multiple drugs. Once reached the target area, the active substance has to be released from the carrier at the correct rate. This can occur spontaneously by gradual diffusion, in combination with the delivery system's degradation as a result of special condition in the target tissue, such as a different pH [181], salt concentration, temperature, or the presence of certain enzymes. The accumulation of the delivery system and/or the release of the active substance in the right place can be driven from outside by influencing conditions in the target organ or tissue by means of magnetic fields [182], near-infrared radiation [183], ultrasonic vibrations [184], or heat [185]. The delivery system used and the external treatment have to be precisely matched to each other for this purpose.

Thus far, about 10 years after the regulatory approval of liposomally encapsulated doxorubicin to treat various forms of cancer, "higher functionality" nanoparticles such as gene transfer vectors are in the Investigational New Drug stage of clinical research [186]. Since then, various gene delivery systems based on nanoparticles (NPs) have been developed.

In fact, engineered nanoparticles are an important tool to realize a number of different medical applications. Although the definition identifies nanoparticles as having at least in one dimension a size of 100 nm or less, especially in the area of drug delivery, relatively large (size > 100 nm) NPs may be needed for loading a sufficient amount of drug onto the particles. The reason why these NPs are attractive for medical purpose is based on their important and unique features, such as their surface to mass ratio that is much larger than that of other

particles, their quantum properties and their ability to adsorb and carry compounds.

The composition of the engineered nanoparticles may vary: natural building blocks such as phospholipids, lipids, dextran, chitosan; or synthetic ones like various polymers, carbon, silica and metals. In that way all particles can be “customized” for a specific purpose.

The main advantage of NPs carrier technology is that they can cross BBB entrapping the original characteristics of the therapeutic drug molecule. Furthermore, this system may reduce drug leaching in the brain and decrease peripheral toxicity [187].

Passage of the BBB was suggested to be possible by the toxic effect of nanoparticle (about 200 nm) on cerebral endothelial cells. This effect was not found for a different type of nanoparticles [188]. In fact, NPs targeting to the brain usually rely on the presence of their interaction with specific receptor-mediated transport systems in the BBB. Particularly, NPs with special coating, can be specifically created to this purpose [189].

As an example, the polysorbate on the surface of the NPs adsorb apolipoprotein B and E and are taken up by brain capillary endothelial cells via receptor-mediated endocytosis.

In addition, polyethylene glycol (PEG)-treated and polyalkylcyanoacrylate coated nanoparticles were shown to cross the BBB and accumulate at high densities in the brain [190]. Drugs that have been successfully transported to the brain using nanoparticle carriers include the hexapeptide dalargin, the dipeptide kytorphin, loperamide, tubocuranine, the NMDA receptor antagonist MRZ 2/576 and doxorubicin [191]. Once into the tissue, particles generally end up

intracellularly in endosomes or lysosomes followed by degradation. However, for NPs of about 20 nm also cellular uptake without contribution of endocytic mechanisms was demonstrated [192].

Different features, among which: (i) size, (ii) composition, (iii) shape and (iv) surface charge of NPs may influence both activity, toxicity and distribution of the particles. One of the problems is the recognition of nanoparticles by the mononuclear phagocytic system (MPS) and delivery in the liver and spleen. A suitable coating on the nanoparticle can also prevent identification and removal by the immune system [193]. Surface modification with PEG resulted in prolonged presence in the circulation by preventing recognition and phagocytosis by the MPS. Another problem of nanoparticles is that they tend to aggregate especially in presence of ions as in blood. Different coatings of NPs may also be needed to prevent their agglomeration [188].

Besides acting as a delivery system, in some cases nanoparticle can act as an active therapeutic drug.

Particularly, different polyelectrolyte coated gold nanoparticles (AuNPs) showed some efficacy in curing prion infected cells and further analyses are still ongoing in order to study their effectiveness *in vivo* (preliminary results are illustrated in this work).

4.1 Gene therapy approaches to prion diseases

Gene therapy approaches for prion diseases are based on (i) mouse *Prnp* post-translational gene silencing mediated by RNA interference (RNAi), (ii) passive or active immunization, (iii) dominant negative

inhibition of PrP^{Sc} formation, and (iv) inhibition of interactions between PrP^{Sc} and PrP^{C} (or some other unknown cofactors) by using different anti-PrP molecules. Whilst it is possible to administer these molecules directly *in vivo*, their production and purification in high quantity, for multiple injections, is often challenging and expensive. For this reason AAV vectors have been engineered with the gene of interest and used with the aim of delivering and expressing anti-PrP molecules in neuronal cells via an efficient and safe way, overcoming the problem of BBB. AAV are non pathogenic, single stranded DNA Dependoviruses, which belong to the Parvoviridae family [194]. Their genome (4,6 kb) contains the two genes, rep and cap, that are replaced by the transgene of interest when used as gene transfer vectors (Fig. 11).

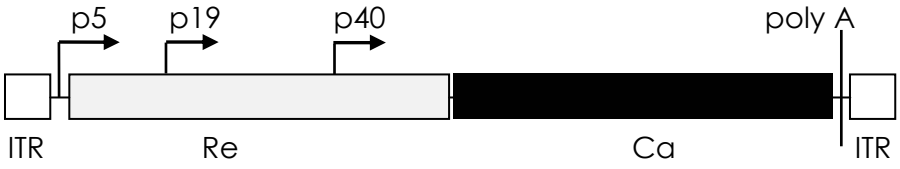

Figure 11. AAV contains a 4.6 kb linear, single-stranded DNA genome with two open reading frames Rep and Cap, which are flanked by 145 bp inverted terminal repeats (ITRs).

They are able to transduce dividing cells as well as those non-dividing, thereby constituting a tool of choice for *in vivo* brain transduction. In fact, AAV vectors do not express any viral protein and are therefore devoid of inflammatory or immunogenic properties; as a consequence, contrary to what is observed for adenoviral vectors, tissues transduced with AAV maintain the viral genomes for prolonged periods of time (several months or years) [195]. Over the

last few years more than 100 different AAV serotypes have been identified, in various species, displaying different biological properties in terms of vector yield and, most notably, extended tropism for different tissues both *in vitro* and *in vivo* [196]. For example, AAV serotype 2 is known to transducer a wide range of tissue types, including liver, muscle, lung, and central nervous system, with moderate efficiency. In skeletal muscle, AAV1 and AAV7 are known to perform well with rapid onset and high levels of transduction [197]. AAV6, which differs from AAV1 capsid by only six aminoacid residues has also shown a propensity for transduction of skeletal muscle. Several AAV serotypes have revealed distinct patterns of transduction within the nervous system [172]. In general, AAV1 and 5 exhibit higher transduction frequencies than AAV2 in all regions injected within the CNS. While AAV2 shows widespread transduction throughout the entire midbrain, AAV4 appears to transduce specific cell types, such as the ependyma and astrocytes in the subventricular zone [198]. In liver, AAV8 has been shown to be a robust vector for achieving high levels of transgene expression. Furthermore, it is able to transduce skeletal muscle throughout the body, including the diaphragm; the entire cardiac muscle and, at substantial levels, the pancreas, smooth muscle, and brain [199]. The availability of specific cell surface receptors and coreceptors is often thought to dictate the tropism of a specific AAV serotype. The cell surface receptors have been identified for only some of the many AAV serotypes: AAV-3 (heparan sulfate proteoglycan), AAV-4 (O-linked sialic acid), and AAV-5 (platelet-derived growth factor receptor). In addition, a 37-kDa/67-kDa laminin receptor has been identified as being a receptor

for AAV serotypes 2, 3, 8, and 9 [200]. The attachment receptors for the other serotypes have not yet been identified. Following receptor binding some AAV serotypes (i.e. 2 and 5) are endocytosed into the cell via clathrin-coated pits, while an alternative trafficking pathway exploited by other AAV serotype is transcytosis across epithelial and endothelial cells. Subsequent to endocytosis, processing of AAV virions within the endosomal compartment appears to be closely linked to transduction.

For example, the acidic pH of the endosomal lumen is likely to induce conformational changes of key capsid subunits necessary for priming the virus for successful endosomal release. Following the endosomal escape, perinucleae accumulation of AAV (i.e. serotype 2) virions has often been observed. The intracellular events underlying disassembly (uncoating) and nuclear translocation of AAV virions remain still unknown. AAV appears to enter the nucleus through a mechanism independent of the nuclear pore complex [201].

There are two stages to the AAV life cycle (Fig. 12) after successful infection, a lytic stage and a lysogenic stage. In the presence of helper virus (adenovirus or herpesvirus), the lytic stage ensues. During this period, AAV undergoes productive infection characterized by genome replication, viral gene expression, and virion production.

The adenoviral genes that provide helper functions regarding AAV gene expression have been identified and include E1a, E1b, E2a, E4, and VA RNA.

Herpesvirus aids in AAV gene expression by providing viral DNA polymerase and helicase as well as the early functions necessary for HSV transcription. Although adenovirus and herpesvirus provide

different sets of genes for helper function, they both regulate cellular gene expression, providing a permissive intracellular milieu for AAV productive infection.

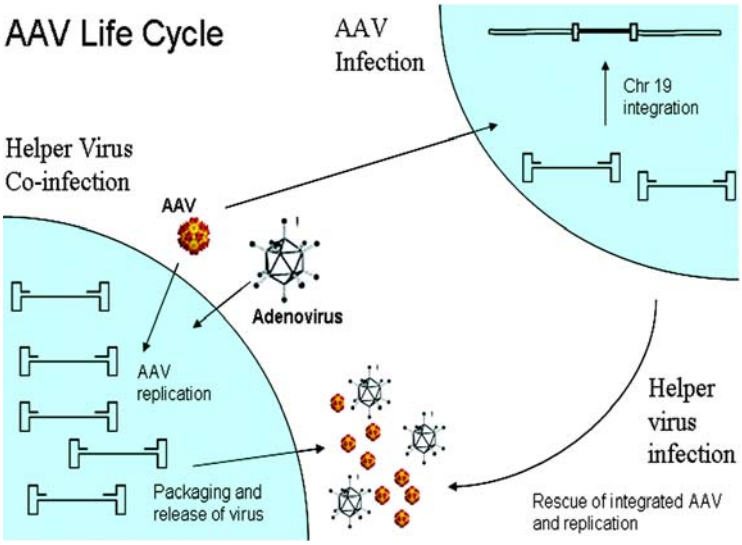

Figure 12. AAV life cycle. AAV undergoes productive infection in the presence of adenovirus coinfection. This is characterized by genome replication, viral gene expression, and virion production. In the absence of adenovirus, AAV can establish latency by integrating into human chromosome 19 (AAVS1). The latent AAV genome can be rescued and replicated upon superinfection by adenovirus.

In the absence of adenovirus or herpesvirus, there is limited AAV replication, viral gene expression is repressed, and the AAV genome can establish latency by integrating into a 4-kb region on chromosome 19 (q13.4), termed AAVS1. The AAVS1 locus is near several muscle-specific genes, TNNT1 and TNNI3. The AAVS1 region itself is an upstream part of a recently described gene, MBS85. The exact function of this gene is not clear, but its product has been shown to be involved in actin organization. Whether AAV integration into this site

is suitable for human gene therapy applications remains to be evaluated. Tissue culture experiments suggest that the AAVS1 locus is a safe integration site. Current AAV vectors do not have this ability. Most of them remain into the cell in episomal form and the development of such a vector would ensure long-term transgene expression in tissues without problems associated with insertional mutagenesis.

Among the panel of AVVs identified until now, AAV serotype 2 (AAV2) is the most serologically prevalent in human population and it is not associated with any known pathology [202]. Ongoing clinical trials are already evaluating the therapeutic efficiency of engineered AAV2 (intracerebrally injected) for the treatment of Alzheimer's disease, Canavan's disease and Parkinson's disease, while additional trials have been planned for late infantile neuronal ceroid lipofuscinosis (Batten disease) [203]. In Parkinson's disease, a loss of dopaminergic neurons leads to the loss of inhibitory gamma aminobutyric acid-sensitive input to the subthalamic nucleus. A recent study in which 12 patients with advanced Parkinson's disease had an AAV vector carrying a transgene encoding glutamic acid decarboxylase injected into the subthalamic nucleus on one side was described. The therapy was well tolerated, with no adverse effects attributable to gene therapy noted for any of the patients, who had been divided into three groups that received low, moderate, or high doses of the vector.

The clinical impression was that motor activity on the treated side was improved significantly relative to the untreated side regardless of dose. No change in cognition was noted. This clinical impression was

supported by position emission tomography scan data, which measured the reduced metabolic activity on the treated side, consistent with enhanced inhibition. Of particular interest was that motor improvement was not noted until 3 months postinjection so that it did not seem directly related to trauma associated with the injection. Also very encouraging was that the observed improvement in motor activity persisted for at least 1 year. Although the trial involved an open surgical procedure, the dramatic improvements noted, if consistent and reproducible, suggest that AAV gene therapy for chronic, degenerative neurological diseases has great promise [204].

Unfortunately, over 80% of humans may be exposed to AAV2 often resulting in a pre-existing humoral immunity that can limit the efficacy of AAV2-based gene therapies in clinical applications [205]. In fact, one of the biggest challenges facing AAV gene delivery is the host immune response. The host defense mechanism at the adaptive level is made up of cell-mediated and humoral immunity. The cell-mediated response functions at the cellular level, eliminating the transduced cells using cytotoxic T cells, whereas the humoral response produces neutralizing antibodies (Nab), preventing the readministration of vector [206].

In a recent clinical trial for hemophilia B, an unexpected liver toxicity was observed and was attributed to a CTL response to AAV-2-transduced hepatocytes [207]. Subsequently, it was discovered that the AAV-2 capsid heparin binding motif was responsible for T-cell activation [208]. This correlated well with a study in mice that showed that AAV-2 infection can activate a CTL response, whereas AAV-7 and AAV-8 do not [209].

It is noteworthy that AAV2 vectors have been also tested in mouse models of prion disorders but, considering the fact that AAV2 has a limited distribution when injected into the CNS and that prion diseases generally affect the whole brain, new serotypes of AAV capable of spreading more than AAV2 needs to be studied. The non-human primate-derived AAVs containing capsids of serotype 7, 8 and 9 have shown superior intracerebral gene transfer than AAV2, in terms of both total number of transduced cells and distribution in the brain [172]. This property has been originally described after administration to newborn mouse pups [210], and has been recently confirmed in adult mice [211]. In addition, these new AAV variants present the potential advantage to overcome preexisting humoral immunity against the prevalent human serotype 2.

Previous data, also confirmed in our laboratory, demonstrated that the AAV serotype 9 has the highest *in vivo* intracerebral diffusion and transduction efficiency if compared to the other serotypes [148]. In particular, AAV9 showed high tropism for CNS using laminin as receptor for infecting neurons specifically [200]. Considering all these properties, it has been engineered with specific anti-PrP antibodies and used as vector for gene therapy of prion diseases.

Early indications of the effectiveness of antibody against prion came from *in vitro* studies, showing reduction in infectivity of prions after cells incubation with different antibodies [212]. Particularly, those directed against the middle portion of PrP (residues 91-110 and 132-156) have been able to cure scrapie-infected cells, sometimes reducing PK-resistant PrP in brains and spleens of infected mice [110, 116]. The efficacy of these antibodies correlates with their ability to

recognize the total population of PrP^C molecules on the cell surface. Unfortunately, the systemic injection of these antibodies (passive immunization) suffers from the intrinsic problem of poor antibody diffusion from vessels into tissues, especially in the nervous system, while active immunization is limited by the host tolerance to endogenous PrP^C [112]. In addition the production of large amounts of antibodies for therapy is technically challenging and expensive and intracerebral injection of some anti-PrP IgG antibodies seemed to provoke neuronal apoptosis [213].

For this reason, as described above, it has been planned to deliver these antibodies into the CNS by exploiting the potential of AAV vectors that can package foreign DNA elements of less than 5 kb in length. In order to overcome this packaging problem, ScFv (single chain variable fragments) antibodies, smaller than the full-length antibodies, have been generated. In fact, ScFv are monovalent mini-antibodies, constituted by a single fusion polypeptide comprising the variable regions of the light and heavy chain (V_L, V_H); they maintain antigen specificity and can be engineered in AAV vectors for intracellular expression or secretion (AAV-ScFv). Moreover, lacking the Fc part they do not provoke an immune response.

To date, different ScFv antibodies have been studied in prion therapy. In particular, ScFv-D18 (direct against the PrP) [214] and ScFv-S18/N3 (direct against the 36/67 kDa laminin receptor) [215] have been studied in several models of prion disease. ScFvS18/N3 administered via stereotactic intracerebral microinjection into the hippocampus of mice, were able to interfere with PrP accumulation in the spleens of RML infected animals. In fact, after 90 days post-

infection, scFv-S18 and -N3 expression resulted in the reduction of peripheral PrP^{Sc} propagation by approximately 60 and 32 %, respectively, without a significant prolongation of incubation times and survival. These results showed the ability of rAAV vectors to migrate from the brain to the spleen of treated mice. ScFvD18 was able to reduce PK-resistant PrP levels in a concentration-dependent manner in both ScGT1 and ScN2a cell culture.

Probably, ScFvD18 binds to PrP and is able to interfere with prion metabolism (either reducing conversion or promoting degradation). In PrP^{C} the ScFvD18 epitope spans residues 132-156 and incorporates helix A. This sequence lies within the region of the protein thought to bind PrP^{Sc}, therefore, it can be argued that D18 operates mechanistically by directly blocking or modifying PrP^{C}/PrP^{Sc} interaction [216]. Molecular modelling generate a model of interaction between ScFvD18 and PrP^{C} (Fig. 13).

Promising therapeutic approaches showed that clinical signs of prion disease did not appear in AAV2-ScFvD18 treated animals until one month later than the group of untreated control. Moreover, the levels of PrP^{Sc} in the brain of treated mice was lower than that in control animals [214].

However, the protection against prion was not complete because the neuroinvasion of PrP^{Sc} into the CNS may have exerted a toxic effect on ScFvD18 expressing neurons, thereby decreasing expression and leading to the eventual loss of therapeutic efficacy.

Mice injected with AAV2-ScFvD18 could also have mounted an immune response to foreign preformed viral or expressed ScFv proteins. Several studies are still ongoing in order to elucidate these

problems while, in our laboratory, new therapeutic approaches have been planned based on engineered AAV9 vector as neuronal delivery system for ScFvD18 antibody.

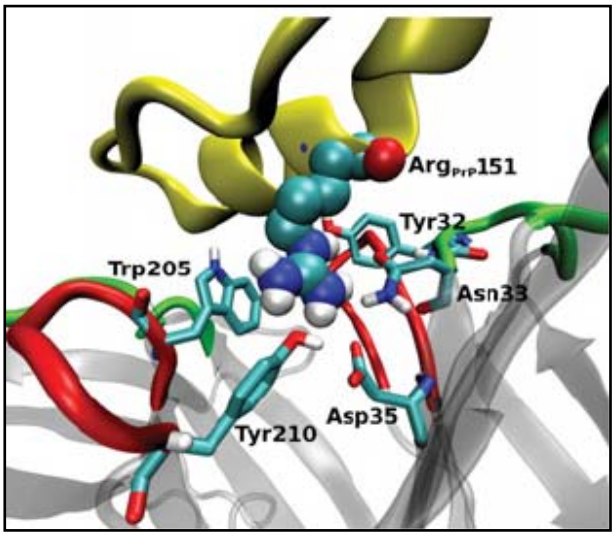

Figure 13. Model of interaction between ScFvD18 and PrP. Complex between ScFvD18 (silver) and PrP (blue). Epitope residues of PrP (yellow) interact with the six CDR loops (red, CDR3; green, CDR1,2) of the antibody. Arg151 anchors the PrP to the cavity of the antibody through the H-bond and van der Waals interactions with Tyr32, Asn33, Asp35, Trp205 and Tyr210.

Anyway, these pioneering studies form a basis of a potential and encouraging innovative therapeutic approaches that will be continuously improved.

4.2 Nanomedical approaches to prion diseases

The field of nanoparticle technology is rapidly expanding and promises revolutionary progress in diagnosis and treatment of many devastating human diseases, among which prion disorders.

Nanoparticles have been developed to allow targeted delivery and sustained release of therapeutics. Such nanoparticle-based drug formulations can interact with biological systems at both molecular and supra-molecular levels. Nanoparticles can be tailored to respond to specific cell environmental stimuli, and even to induce desired physiological responses in cells, whilst minimizing unwanted side effects. Compared to conventional drugs, they possess higher intrinsic pharmacological activity. Their main advantage is that the small dose required for therapeutic efficiency can easily fit the loading capacity of nanoparticles and would not require the administration of large amounts of potential toxic therapeutics [217].Currently, nanoparticle iron chelators have been used to treat Alzheimer's disease and other neurologic disorders associated with trace metal imbalance [218]. It has been also reported that PEGylated polymeric nanoparticles are efficient drug carrier for the delivery of active therapeutic molecules in prion diseases. Moreover, they are able to accumulate into the spleen as well as into the brain due to their appropriate long-circulating characteristic [189].

Another class of nano-compounds that possesses the ability to remove pre-existing PrP^{Sc} from infected cells is represented by cationic dendrimers. Their potency increases with the density of positive charges on their surface. Cationic dendrimers appear to accumulate together with PrP^{Sc} molecules in lysosomes, where the acidic environment facilitates dendrimer-mediated PrP^{Sc} disaggregation. Dendrimers can disaggregate a range of different amyloid proteins by interacting with specific epitopes on each protein. Potential limitations to the development of dendrimers as therapeutic compounds for

PMDs, such as prion diseases, include poor bioavailability, limited spectrum of activity, and detrimental neurological side effects [219]. Better results have been obtained with the application of polyelectrolyte coated AuNPs that showed great efficiency in prion diseases. The construction of functionalized AuNPs was started with nanogold as core and a layer-wise deposition of oppositely charged polyelectrolytes, such as the synthetic polycation polyallylamine hydrochloride (PAH) and polyanion polystyrenesulfonate (PSS). Nanogold is chosen as core due to the fact that it is non-toxic in the selected size range, monodispersed and easy to functionalize through polyelectrolyte multilayers [220]. Polyelectrolyte AuNPs showed potent anti-prion activity at half maximal effective concentrations (EC_{50}) in the range of picomolar concentration, in both ScGT1 and ScN2a cells. At the moment the exact mechanism of interaction between AuNPs and PrP is still unknown.

It is known that AuNPs coated with different numbers of polyelectrolyte layers could be cytotoxic: polycations are more cytotoxic than polyanions and a lower number of layers is more cytotoxic than a higher number of layers. This toxicity was diminished by an additional binding of different compound (i.e. albumin) to the final polyelectrolyte layer. Animal experiments confirmed that after intracranial inoculation of albumin coated polyelectrolyte NPs no toxicity leading to morphological changes in the brain has been observed [220]. So, nanoparticles surface charges and composition must be considered for toxicity and specific brain distribution profiles.

5. EVIDENCE OF PRION-LIKE TRANSMISSION FOR SOME PMDs

Hints of prion-like behavior in amyloid have emerged from studies of Alzheimer's and Parkinson's diseases. Evidence of AD transmission came from the discovery that aggregates of the amyloid-β (Aβ) peptide found in the brain of Alzheimer's disease patients could be transmitted to the brain of mice engineered to produce large amounts of the Aβ precursor protein APP.

Another study has shown that healthy tissue grafted into the brain of people with Parkinson's disease acquires intracellular Lewy bodies aggregates of the Parkinson's disease-associated protein α-synuclein.

This suggests prion-like transmission of diseased protein from the recipient's brain to the grafted cells.

Similar findings have been reported in a mouse model of tauopathy. Injection of mutant human tau in the brain of mice overexpressing normal human tau transmitted tauopathy, with intracellular aggregation of previously normal tau and spread of aggregates to neighboring regions of the brain.

Moreover, the evidence for prion-like spread of polyglutamine (polyQ) containing protein aggregates has been found [221]. Surprisingly, a prion-like mechanism of transmission has been also observed for the type 2 diabetes (T2D).

These data showed that T2D, associated with pancreatic amyloid deposits of amylin protein, was efficiently transmitted to healthy mice after intraperitoneal injection of a pancreatic homogenates obtained from T2D-sick mice [222].

PRIONS AND POTENTIAL PRIONOIDS			
Disease	**Protein**	**Molecular transmissibility**	**Infectious life cycle**
Prion diseases	PrP^{Sc}	Yes	Yes
Alzheimer's disease	Amyloid-β	Yes	Not shown
Tauopathies	Tau	Yes	Not shown
Parkinson's disease	α-Synuclein	Host-to-graft	Not shown
AA amyloidosis	Amyloid A	Yes	Possible
Huntington's disease	Polyglutamine	Yes	Not shown

Table 4. Examples of many misfolded proteins that can act like prions [221].

Therefore, not only prion diseases but also several protein misfolding diseases may be transmitted probably by sharing a common mechanism of infection (Table 4). All these findings are very recent and may provide important information about the pathogenesis of PMDs.

6. AIM OF THE THESIS

The main focus of this thesis is to gather information about the efficacy of innovative compounds, no more based on conventional drugs, to hamper or halt disease progression in different mouse models of prion disorder.

In particular, here we report the application of engineered Adeno-Associated Viruses and polyelectrolyte gold nanoparticles as new therapeutic strategies for prion diseases in mice. The study do not aim to cure patient symptoms but is focused on challenging specific molecules capable to interfere or even block the "molecular" basis of

disease. To maximize the effectiveness of each compound, different therapeutic approaches have been carried on.

Chapter one, firstly describes the intracerebral diffusion and transduction efficiency of AAV9 vector engineered with β-galactosidase reporter gene. Subsequently, the therapeutic efficiency of both AAV2-ScFvD18 and AAV9-ScFvD18 vectors, intracerebrally injected in mice, is reported.

Chapter two describes the efficiency of specific polyelectrolyte covered gold nanoparticles (2A and 5S) in curing prion infected cells. In addition, *in vivo* experiments shows the marginal efficacy of both nanoparticles to interfere with prion propagation. Because of the limited information available about the toxic effects of the particles when administered in mice, we decided to use very low dosage of compound.

Our work examines both behavioral and neuropathological modifications induced in treated mice, but also possible adverse effects related to their administration.

CHAPTER 1

ENGINEERED ADENO-ASSOCIATED VIRUSES EXPRESSING ANTI-PrP MOLECULES AS NEW THERAPEUTIC STRATEGIES FOR PRION DISEASES IN MOUSE MODELS

CHAPTER 1

MATHERIALS AND METHODS

ENGINEERED ADENO-ASSOCIATED VIRUSES EXPRESSING ANTI-PrP MOLECULES AS NEW THERAPEUTIC STRATEGIES FOR PRION DISEASES IN MOUSE MODELS

1. ANIMAL FACILITY

Animal facility is licensed and inspected by the Italian "Ministero della Salute". Current animal husbandry and housing practices comply both with the Council of Europe Convention ETS123 (European Convention for the Protection of Vertebrate Animals used for Experimental and Other Scientific Purposes; Strasbourg, 18.03.1986); Italian Legislative Decree 116/92, Gazzetta Ufficiale della Repubblica Italiana 10, 18 February 1992; and with the 86/609/EEC (Council Directive of 24 November 1986 on the approximation of laws, regulations and administrative provisions of the Member States regarding the protection of animals used for experimental and other scientific purposes). Animals are housed in group of 2-5 animals in individually ventilated cages taking into account their sociable compatibility (dominance, sex, ratio). Nevertheless, if there is any risk of unwanted inter-animal transmission (through wounds or bites) or social incompatibility, animals are housed single in a cage. Mice are daily fed with special diet food and water is provided *ad libitum*. Lighting is on an automatic 12 hours basis, including dawn and dusk steps. Changes are performed weekly. Regular veterinary visits and consulting services are provided by Dr. Cocilovo Alessandra (DVM), who is Director of "Dipartimento di Patologia Animale, Igiene e Sanità Pubblica Veterinaria" at the Università degli Studi di Milano. Veterinary care is provided by our DVM staff and includes: a program for prevention of disease, daily observation and surveillance for assessment of animal health; appropriate methods of disease control, diagnosis and treatment;

guidance of animal users in appropriate methods of handling, restraint, anesthesia and monitoring of surgical programs.

1.1 Animal strains

Six week-old C57Bl/6J and CD1® IGS mice were provided from Charles River Laboratories. Both male and female gender were included in the experiments.

2. AAV ENGINEERING WITH ScFvD18 ANTIBODY

At the beginning the antibody was engineered into the AAV2 and AAV9 vectors by the triple transfection method in HEK-293A cells by using the commercial kit AAV Helper Free System (Stratagene) which requires the use of (i) the adenovirus helper plasmid (pXX680), (ii) the AAV helper plasmid (pHelper) and (iii) the inverted terminal repeat (ITR) transgene cassette plasmid (pITR), which contains only the ITRs from the wild-type AAV (wtAAV) genome. The advantage to this system is that coinfection with adenovirus is not needed. pXX680 supplies the adenovirus proteins (E1A, E1B, E4, and E2A) along with the adenovirus VA RNAs required for helper functions. pHelper encodes the wtAAV genome lacking ITRs to circumvent packaging of the WT genome. Three days after transfection cells were lysated and, following CsCl gradient centrifugation, the AAV was isolated from the solution. Dialysis of CsCl fractions containing AAV against a physiological buffer was necessary before in vivo analysis because CsCl can exert toxic effects

on animals in the study. In order to test the infectivity of AAV2 in vitro, it was engineered with GFP reporter gene and HT-1098 cells were infected. One day after the infection FACS analysis was performed. Unfortunately *in vitro* infectivity test for AAV9 viral vectors are not currently available. Titolation of both AAV2 and AAV9 engineered vectors with ScFvD18 was detected by real-time PCR.

3. SURGICAL PROCEDURES FOR AAV INJECTIONS

The mouse (40-45 g) was anaesthetized by intraperitoneal injection of tribromoethanol (Avertin®, 100 µL/10g). It was held gently by the skin on its back, upside down so the gut falls away from surrounding organs. The needle was introduced in the lower right quadrant of the abdominal area, pulled out slightly, and some fluid was aspirated to check that the needle has not punctured the bladder or caecum. Drug was administered at a slow rate and the needle was removed. The animal remained insensate throughout the approximately 30 min surgery. All instruments (blades, scissors, forcepts, needles) were sterilized with chlorexidine. Under sterile conditions, the subject was then shaved, and cleaned at the site of the surgery, in this case the scalp. The subject was placed in position in a stereotaxic holder, (Lab Standard Stereotaxic), using the appropriate mouse/neonatal rat holding platform (Cunningham, Lab Standard from 2 Biological Instrument), and ear bars. The body temperature of the mouse was maintained by use of enough padding under the mouse to insulate temperature and use of an heat lamp positioned shining off

to the side of the cage. A small incision was made in the skin, the skin was pulled back using gentle tension and a swab soaked with a 5% hydrogen peroxide solution was used to clean the tissue from the skull. After the bregma was located the position of the syringe's needle (Hamilton Syringes, G26S) was then adjusted so that it lines up with the animal's bregma. The needle was then adjusted to the coordinates relative to the bregma, determined by using "The Mouse Brain, in Stereotaxic Coordinates", by Keith B. J. Franklin and George Paxinos, Academic Press, ISBN 0-12-266070-6. A micro-drill (Minicraft) was prepared, the skin was moved out of the way and the drill arm was very slowly lowered until there was contact with the skull and drilling begins. As soon as the burr was through the skull the drill was stopped. The resulting bone shavings were cleaned up with a sterile swab. The previously prepared 26-gauge needle on a 10 μL syringe (Hamilton), mounted on a Large Probe Holder support (Hamilton), was inserted through the incision. Once the needle was inserted, the engineered rAAV vectors (with β-galactosidase reporter gene or ScFvD18 antibody) was injected at a rate of 1 μL/2min by manual pression of the syringe plunger. Before to extract the needle from the brain, we waited several minutes (five or more). The incision was closed by autoclip wound closing system (Autoclip from 2 Biological Instrument) and antibiotic cream as well as lidocaine was then applied to the wound. Mice that survived longer than 30 min after surgery were given one dose of buprenorphine, 0.05 mg/kg s.c., at the end of surgery. The mice were then placed in a cage and put under incandescent lamp to maintain body temperature. Mice were monitored for signs of distress (frequent monitoring of wound site and

overall appearance of animal) and then infected with prion and sacrificed as described.

3.1 Stereotaxical coordinates and experimental groups

Different therapeutic approaches and inoculations were carried out in this part of the work. In particular, four experimental procedures have been performed and are clearly described below:

1. AAV9-LacZ injection (in vivo diffusion studies)

The delivery and transduction efficiency of AAV9 serotype in mouse brain have been evaluated using recombinant viruses expressing the β-galactosidase reporter gene (AAV9-βgal). Three different protocols of AAV9-βgal (5.37×10^{11} U/mL) inoculation were evaluated. In the first one C57Bl/6J mice (n=8) were stereotaxically unilaterally inoculated into the right thalamus [1.5 caudal; 1 lateral; 3.2 depth] with 5 μL of AAV9-βgal. In the second one, the amount of AAV9-βgal was improved (10 μL) and animals (n=8) were inoculated following the same stereotaxical coordinates used in the previous experiment. In the third experiment, mice (n=24) were subdivided in 4 groups named from A to D. Animals in group A were inoculated with AAV9-βgal; while mice in groups B and C were inoculated with AAV9 (empty) vectors and phosphate buffered saline (PBS), respectively. Inoculations were performed in four different regions with 2 μL of solution per site (with a total of 8μL per brain): hypothalamus [1.8 caudal; + 0.5 lateral; 5.3 depth] and thalamus [1.8 caudal; + 0.5 lateral; 3.5 depth] on the right side of the brain,

hippocampus [1.8 caudal; - 1 lateral; 1.8 depth] and cerebral cortex [1.8 caudal; - 1 lateral; 0.8 depth] on the left side.

2. AAV2-ScFvD18 injection (experimental therapeutic approach I)

CD1 mice (n=45) were subdivided in 6 groups named from A to F. Animals in groups A and B were intracerebrally injected with AAV2-ScFvD18 (5 x 10^{11} U/mL); while animals in group C were inoculated with PBS. Inoculations were carried out in six different regions with 2 µl of AAV2-ScFvD18 (or PBS) per site (with a total of 12µL per brain). Each animal was inoculated in both cerebral hemispheres following these stereotaxical coordinates: hypothalamus [1.8 caudal; ± 0.5 lateral; 5.3 depth], thalamus [1.8 caudal; ± 0.5 lateral; 3.5 depth] and hippocampus [1.8 caudal; ± 0.5 lateral; 1.8 depth]. Animals in groups D, E and F did not receive any AAV or PBS inoculation.

3. AAV9-ScFvD18 injection (experimental therapeutic approach II)

C57Bl/6J mice (n=45) were subdivided in 6 groups named from A to F. Animals in groups A and B were intracerebrally injected with AAV9-ScFvD18 (5.6 x 10^{11} U/mL); while animals in group C were inoculated with PBS. Inoculations were carried out in six different regions with 2 µL of AAV9-ScFvD18 (or PBS) per site (with a total of 12µL per brain). Each animal was inoculated in both cerebral hemispheres following these stereotaxical coordinates: hypothalamus [1.8 caudal; ± 0.5 lateral; 5.3 depth], thalamus [1.8 caudal; ± 0.5 lateral; 3.5 depth] and hippocampus [1.8 caudal; ± 0.5

lateral; 1.8 depth]. Animals in groups D, E and F did not receive any AAV inoculation.

4. AAV9-ScFvD18 (experimental therapeutic approach III)

CD1 mice (n=45) were subdivided in 6 groups named from A to F. Animals in groups A and B were intracerebrally injected with AAV9-ScFvD18 (1,4 x 10^{12} U/mL); while animals in group C were inoculated with PBS. Inoculations were carried out in six different regions with 2 µL of AAV9-ScFvD18 (or PBS) per site (with a total of 12µL per brain). Each animal was inoculated in both cerebral hemispheres following these stereotaxical coordinates: hypothalamus [1.8 caudal; ± 0.5 lateral; 5.3 depth], thalamus [1.8 caudal; ± 0.5 lateral; 3.5 depth] and hippocampus [1.8 caudal; ± 0.5 lateral; 1.8 depth]. Animals in groups D, E and F did not receive any AAV or PBS inoculation.

3.2 Post surgical care

Initial post surgical care included observing the animal to ensure uneventful recovery from the anesthesia and surgery. The incision site was closely monitored daily until the skin healed. In addition, a veterinarian or veterinary technician checked all animals post-surgery daily. If necessary, topical antibiotics were used.

4. PRION INFECTION

Rocky Mountain Laboratories (RML) and BSE prion strains were intracerebrally or intraperitoneally challenged in mice.

4.1 Inocula preparation

RML

Under sterile condition, 10% RML-infected brain homogenate (wt/vol) was prepared from pools of terminally RML-sick CD1 mouse brains using sterile saline solution (NaCl, B. Braun 0.9%), while 10% mock homogenate (wt/vol) was obtained from pools of healthy CD1 mouse brains.

Mouse-adapted BSE

Under sterile condition, 10% BSE-infected brain homogenate (wt/vol) was prepared from pools of terminally BSE-sick C57Bl/6J mouse brains using sterile saline solution, while 10% mock homogenate (wt/vol) was obtained from pools of healthy C57Bl/6J mouse brains.

4.2 Inocula sterility test

Prior to infect the animals, 100 μL of each inoculum was plated on LB medium and then incubated at 37°C for 24 hours for detecting the presence of pathogens. Only sterile homogenates were challenged in mice

4.3 Infection

Prion infections were performed 30 days after AAV2-ScFvD18 or AAV9-ScFvD18 injections.

- *AAV2-ScFvD18 experimental therapeutic approach I*

Animals in groups A (n=8) and D (n=8) were anaesthetized with tribromoethanol and intracerebrally inoculated with 30 µL of RML-infected brain homogenate, while animals in group E (n=8) were inoculated with 30 µL of mock brain homogenate. Each animal was inoculated into the right striatum following these stereotaxical coordinates: [0.38 caudal; + 0.5 lateral; 3.5 depth] using a 26 gauge needle. Animals (n=8) in groups B (n=8), C (n=8) and F (n=5) did not receive any prion infection.

- *AAV9-ScFvD18 experimental therapeutic approach II*

Animals in groups A (n=8) and D (n=8) were anaesthetized with tribromoethanol and intracerebrally inoculated with 30 µL of mouse-adapted BSE brain homogenate, while animals in group E (n=8) were inoculated with 30 µL of mock brain homogenate. Each animal was inoculated into the right striatum following these stereotaxical coordinates: [0.38 caudal; + 0.5 lateral; 3.5 depth] using a 26 gauge needle. Animals in groups B (n=8), C (n=8) and F (n=5) did not receive any prion infection.

- *AAV9-ScFvD18 experimental therapeutic approach III*

Prion infections were carried out intraperitoneally. Animals in groups A (n=8) and D (n=8) were inoculated with 100 µL of RML brain homogenate, while animals in group E (n=8) were inoculated with 100 µL of mock brain homogenate. Animals in groups B (n=8), C (n=8) and F (n=8) did not receive any prion infection.

5. SCHEMATIC ILLUSTRATIONS OF THE EXPERIMENTS

Experiment 1: AAV9 intracerebral diffusion analysis

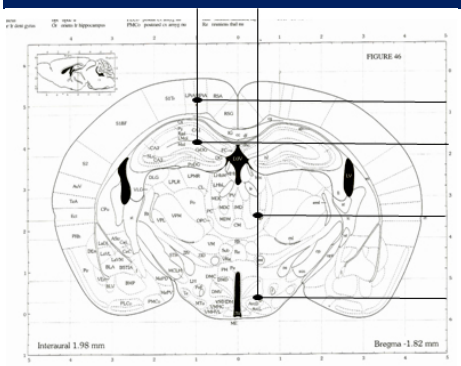

Stereotaxical injections were bilaterally performed in four different brain regions (group A, B and C). Four experimental groups have been created. Planned sacrifices were carried out every 30 days

See text for details

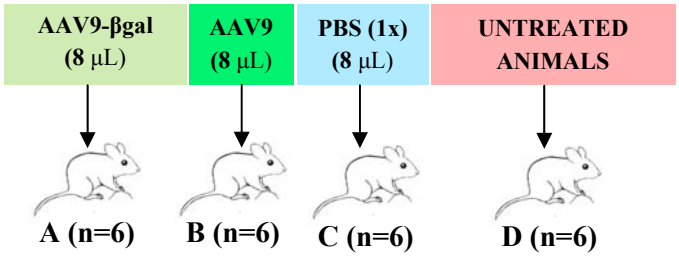

Experiment 2: AAV2-ScFvD18 therapeutic approach (I)

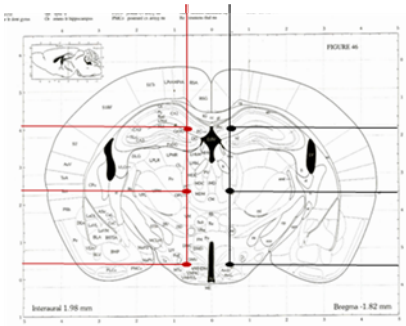

Stereotaxical injections were bilaterally performed in six different brain regions (group A, B and C). Six experimental groups have been created. One month after injection, intracerebral 10% RML infection was carried out (group A and D)

See text for details

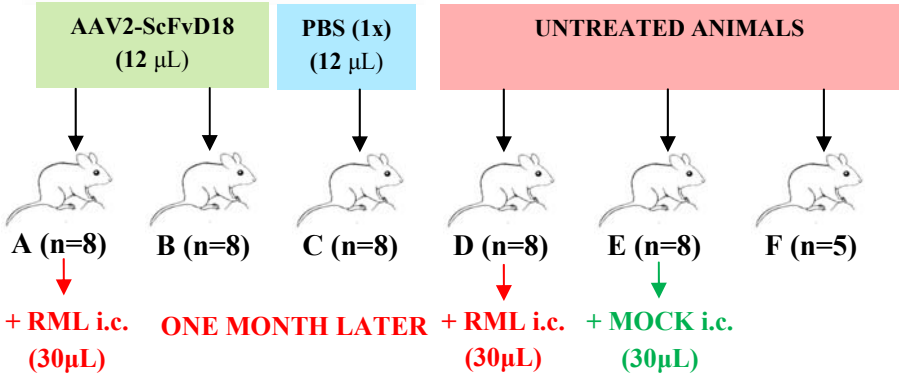

Experiment 3: AAV9-ScFvD18 therapeutic approach (II)

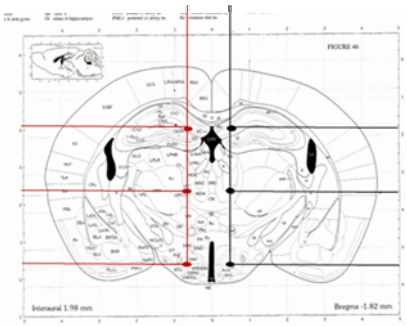

Stereotaxical injections were bilaterally performed in six different brain regions (group A, B and C). Six experimental groups have been created. One month after injection, intracerebral 10% BSE infection was carried out (group A and D)

See text for details

AAV9-ScFvD18 (12 µL) | **PBS (1x) (12 µL)** | **UNTREATED ANIMALS**

A (n=8) → **+ BSE i.c. (30µL)**

B (n=8)

C (n=8)

D (n=8) → **+ BSE i.c. (30µL)**

E (n=8) → **+ MOCK i.c. (30µL)**

F (n=5)

ONE MONTH LATER

Experiment 4: AAV9-ScFvD18 therapeutic approach (III)

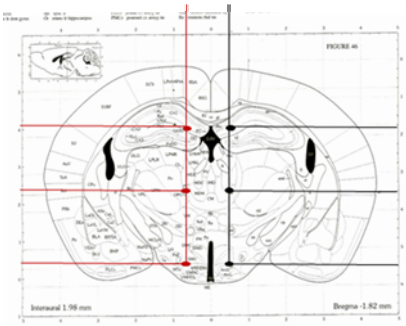

Stereotaxical injections were bilaterally performed in six different brain regions (group A, B and C). Six experimental groups have been created. One month after injection, intraperitoneal 10% RML infection was carried out (group A and D)

See text for details

AAV9-ScFvD18 (12 µL) | **PBS (1x) (12 µL)** | **UNTREATED ANIMALS**

A (n=8) → **+ RML i.p. (100µL)**

B (n=8)

C (n=8)

D (n=8) → **+ RML i.p. (100µL)**

E (n=8) → **+ MOCK i.p. (100µL)**

F (n=5)

ONE MONTH LATER

6. BEHAVIORAL MONITORING OF MICE

To examine the appearance and development of neurological symptoms of prion disease, behavioral monitoring was carried out weekly and included spontaneous locomotor activity in the open field, nest construction test, reactivity to external stimuli, horizontal and inverted screen test, awkward body posture (hunched dorsal kyphosis), suppressed righting reflex, extreme incoordination, flaccid paralysis of hindlimbs, urinary incontinence and ataxia [223]. Body weight was periodically monitored. The incubation time was calculated as the period between the day of inoculation and the appearance of clinical signs of disease, confirmed by a subsequent assessment at 3 days interval. At the terminal stage of disease, usually characterized by clasping of the hind limb, ataxia, hunched dorsal kyphosis, and suppressed righting reflex clinically affected mice were sacrificed. The survival time was calculated as the period between the day of clinical signs appearance and the day of animal's sacrifice.

7. MAGNETIC RESONANCE IMAGING (MRI)

Magnetic resonance imaging (MRI) was performed in clinically symptomatic animals and in non-infected control mice on a Brucker BioSpec 70/30 USR Tesla scanner. Mice were anesthetized with isofluorane at a dose approximately of 2.5 L/min, modulated according to the breathing frequency. The animals were positioned on an apposite bed inside the magnet and were monitored throughout the procedure for breathing frequency and body temperature with specific

probes. Twenty-six axial slices were acquired for each mouse with T2 High Resolution Turbo Spin Echo sequences. The following parameters were employed: thickness 0.60 mm without gap; TR 3000 ms; TE 27.1 ms; FOV 2.20/2.20cm; 256 matrix.

8. SACRIFICE

Specific procedures for animal sacrifice were adopted. In particular, euthanasia and intracardiac perfusion were performed.

8.1 Intracardiac perfusion

Mice were intraperitoneally anesthetized with 1 mL of Avertin 2,5% diluted (this is a lethal dose but the mouse survives for 5-20 min). This dose ensured the mouse was properly sedated. Before to proceed toes of mouse were pinched in order to judge its level of response to painful stimulus. Once mouse was sedated, abdomen was wet with ethanol. Mouse was then placed on corked surface with abdomen facing up. Using the small needles, the four paws were secured to surface spreading them as wide as possible. Skin was grabbed with forceps at the level of the diaphragm, and cut to expose the liver. Cut was performed laterally and then moving up through the ribs until the heart was easy to access. Chest flap was secured to corked surface with larger needle. Butterfly needle was placed into the left ventricle, and PBS solution with heparin (5 U/mL) was gently administered. Then the right atrium was immediately cut. PBS was administered until the liver became light gray. At this point, Glutharaldeide fixative

(0,5%) was administered for 15 min. A good indication of how well the animal was fixed, was to test tail flexibility.

8.2 Euthanasia

Mice were intraperitoneally anesthetized with Tiletamine-Zolazepam, (0,5 mg/10g). The mouse was held gently by the skin on its back, upside down so the gut falls away from surrounding organs. The needle was introduced in the lower right quadrant of the abdominal area, pulled out slightly, and some fluid was aspirated to check that the needle has not punctured the bladder or caecum. Drug was administered at a slow rate and the needle was removed. When the mouse was deeply anesthetized, intracardiac injection of Embutramide (0,2 mL) was performed and every organ was collected and processed for histological and biochemical analysis.

8.3 Sacrifice adopted for each experiment

- *AAV9-LacZ injection (in vivo diffusion studies)*

In order to study the time of highest diffusion and transduction efficiency of AAV9-LacZ, 2 animals per group were intracardially perfused at precise time point: i.e. one month, two months and three months after the inoculation. Brains were removed and prepared for histochemical analysis. The samples and sections were coded such that the study was done blind and were processed using techniques and controls that have been used in our laboratory.

- *AAV2-ScFvD18 and AAV9-ScFvD18 experimental therapeutic approaches (I and II)*

Clinically affected mice (groups A and D) were euthanized at the terminal stage of disease, while all other mice were sacrificed at the end of the experiment or monitored for the entire predicted lifespan and then culled and subjected to the necroscopy.

- *AAV9-ScFvD18 experimental therapeutic approach (III)*

In order to study possible differences in PrP^{res} deposition, 3 animals per group (A and B), randomly selected at the beginning of the experiment, were euthanized (166 days post infection). Conversely, other clinically affected mice were sacrificed at the terminal stage of disease. Mice belonging to group C, E and F were sacrificed at the end of the experiment while animals in group B were monitored for the entire predicted lifespan and then culled and subjected to the autopsy.

9. HISTOLOGICAL AND IMMUNOHISTOCHEMICAL ANALYSIS

9.1 β-galactosidase activity detection (X-gal staining)

In order to study the AAV9-βgal diffusion pathway, brain samples obtained from intracardiac perfused mice were immersed in glutharaldeide fixative 0,5% for 6 hours at 4°C and cut. β-gal activity was revealed by X-gal histochemical staining.

X-gal dilution buffer (potassium ferricyanide crystalline 5mM, potassium ferricyanide trihydrate 5mM, magnesium chloride 2mM, diluted in PBS) was freshly prepare ad warmed to 37°C prior to use. X-gal stock solution (4% in dimethylformamide) was prepared diluting 0,2 g of X-gal (5-Bromo-4-chloro-3-indolyl-β-D-galactopyranoside; Boehringer Mannheim) in 5mL of N, N dimethylformamide. X-gal stock solution was then diluted 1:40 in warmed dilution buffer.

After fixation, brains were cut in coronal slices that were rinsed 3 times in PBS and immersed in X-gal solution (37°C, overnight in the dark).

Slices were then rinsed in PBS, dehydrated and embedded in paraffin. 10µm thick serial sections were cut and counterstained with eosin.

9.2 Histological examination and spongiform profile of the CNS

All mouse tissues were collected. The brain of each mouse was cut, the left hemisphere was fixed in Carnoy solution at 4°C for 24h [224], while the right hemisphere was frozen at -80°C for biochemical analysis.

The same procedure was followed for the other organs (i.e. brain stem, muscle, spleen, liver, kidney, intestinal Peyer's patch etc.). Fixed brain samples were then cut in four standard coronal levels, dehydrated, and embedded in paraplast.

Seven-µm thick serial sections from paraffin embedded tissues were stained with hematoxylin-eosin (H&E) or probed with different antibodies (i.e.: 6H4, GFAP, CNPase and Caspase-3).

Spongiform profiles were determined on H&E-stained sections, by scoring the vacuolar changes in nine standard grey matter area as described [99].

9.3 Immunohistochemical staining

Sections were immunostained with monoclonal antibody to PrP (6H4 1:1000, Prionics), to myelin protein (CNPase 1:500, Sigma Aldrich), and with polyclonal antibody to β-galactosidase (β-gal 1:1000, USBiological), to glial fibrillary acidic protein (GFAP 1:1000, Dako) and to apoptotic cells (Caspase-3 1:100, Millipore).
Before PrP immunostaining, the sections were sequentially subjected to proteinase K digestion (10μg/mL, R_T, 5') and guanidine isothiocyanate treatment (3M, R_T, 20'), and non-specific binding was prevented using Animal Research Kit Peroxidase (Dako). Immunoreactions were visualized using 3-3'-diaminobenzidine (DAB, Dako) as chromogen.

10. GENETIC AND BIOCHEMICAL ANALYSIS

10.1 Real-time PCR

DNA obtained from brains of both AAV2-ScFvD18 and AAV9-ScFvD18 inoculated mice were subjected to real-time PCR in order to test the efficiency of AVV vector to transduce neurons.

10.2 Immunoblot analysis

Ten percent (wt/vol) brain homogenates from frozen tissues were prepared in lysis buffer (100 mM sodium chloride, 10 mM EDTA, 0.5% Nonidet P40, 0.5% sodium deoxycholate in 10 mM Tris-HCL, pH 7.4). Aliquots of cleared lysate equivalent to 100 or 200 μg were digested with 50 μg/mL of proteinase K for 1 hour at 37°C. Reactions were terminated by the addition of Phenylmethanesulfonyl fluoride (PMSF, 5mM). Treated homogenates were loaded on 12.5% polyacrylamide gels, transferred to polyvinylidene fluoride membranes and probed with anti-PrP antibody 6H4 (1:10000, Prionics) and anti CNPase antibody (1:1000; Sigma Aldrich). The immunoreactions were visualized by enhanced chemiluminescence system (Amersham).

10.3 Immunohistoblot analysis

Seven-μm thick serial sections from paraffin embedded tissues were transferred to nitrocellulose membranes and thoroughly air dried. For the detection of PrP, membranes were deparaffinized, rehydrated in TBST and treated with proteinase K (10 μg/mL, R_T, 7') and guanidine isothiocyanate (3M, R_T, 20'). Membranes were incubated with 6H4 antibody (1:1000, Prionics) and non-specific binding was prevented using Animal Research Kit Peroxidase (Dako). Samples were then probed with Alkaline phosphatase streptavidin (1:200, Vector) for 1 hour at room temperature. Alkaline phosphatase activity was detected with specific Alkaline phosphatase substrate kit III (Vector).

11. DATA ANALYSIS

11.1 Images capture

Stained sections were examined on a Nikon Eclipse E800 microscope, images captured using a Nikon Digital Camera DXM1200 and analyzed with NIS-Elements software.

11.2 Densitometric and statistical analysis

Statistical analysis were performed using the *GraphPad Prism 4.0* software. Kaplan-Meier survival curves were plotted, and differences in survival between groups of mice were compared using the Logrank test. Densitometric analysis were performed on images captured by the *Photoshop 7 program* and analyzed with *Lucia measurement software 4.6.* Using the area density tool, mean density were determined from a selected rectangular area that enclosed three glycoforms of PrP^{res} in each lane. This area remained constant for each density measurement. Mean densities were exported to Microsoft Excel 2003 and *GraphPad Prism 4.0* software for analysis. Densitometric quantization of PrP^{res} amount in each sample was analyzed by unpaired, double tailed *t*-test.

CHAPTER 1

RESULTS

ENGINEERED ADENO-ASSOCIATED VIRUSES EXPRESSING ANTI-PrP MOLECULES AS NEW THERAPEUTIC STRATEGIES FOR PRION DISEASES IN MOUSE MODELS

1. AAV9-βgal DIFFUSION AND TRANSDUCTION EFFICIENCY

The delivery and transduction efficiency of AAV9 serotype in mouse brain was evaluated using recombinant viruses expressing the β-galactosidase reporter gene (AAV9-βgal). Serial sacrifices of mice evidenced the highest enzimatic expression at four weeks post injection. In particular, AAV9-βgal resulted in enzyme-positive neuronal cells in distinct brain regions and also resulted in the greatest amount of rostral-caudal distribution of the vector genome from the sites of inoculation.

The inoculation of 5μL of AAV9 into the right thalamus of mice revealed weak β-galactosidase activity that was undetectable under stereomicroscopic. Eosin counterstained sections revealed transduced cells mainly confined to the thalamus and adjacent regions. In particular, we found that AAV9 transduced neurons specifically and not astrocytes or oligodendrocytes.

Surprisingly, the pattern of distribution observed, suggested that the AAV9-βgal was capable of undergoing axonal transport. In fact, although the injection was unilateral (right thalamus), βgal activity was also detected in the controlateral hemisphere of the brain (left thalamus).

Positive neurons were also found into the mammillary bodies and hippocampus where pyramidal cell layer of the CA1 sector and dentate gyrus were preferentially transduced (Fig. 1).

The ability of the AAV9 vector genome to undergo axonal transport has potential benefit for the treatment of many neurodegenerative diseases because the whole brain is usually affected.

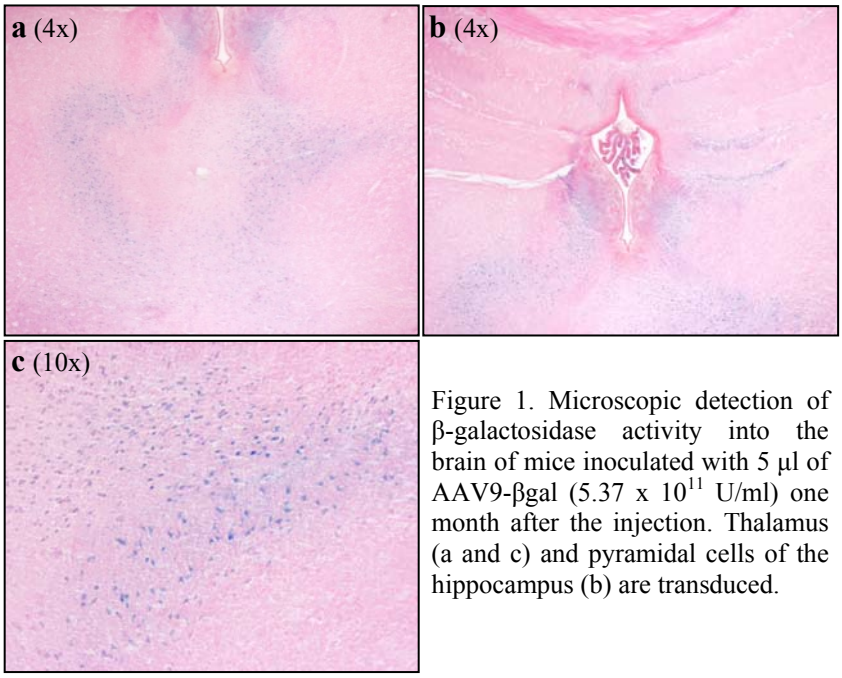

Figure 1. Microscopic detection of β-galactosidase activity into the brain of mice inoculated with 5 µl of AAV9-βgal (5.37 x 10^{11} U/ml) one month after the injection. Thalamus (a and c) and pyramidal cells of the hippocampus (b) are transduced.

The inoculation of 10 µL of AAV9-βgal into the right thalamus of mice showed increased amount of βgal positivity detectable under stereomicroscopy on macroscopic brain sections. Also in this case, although the injection was unilateral, βgal signal was present in the controlateral hemisphere of the brain (Fig. 2).

Rostral-caudal diffusion of the vector from the point of inoculation was also observed and septum and rostral mesencephalon were transduced.

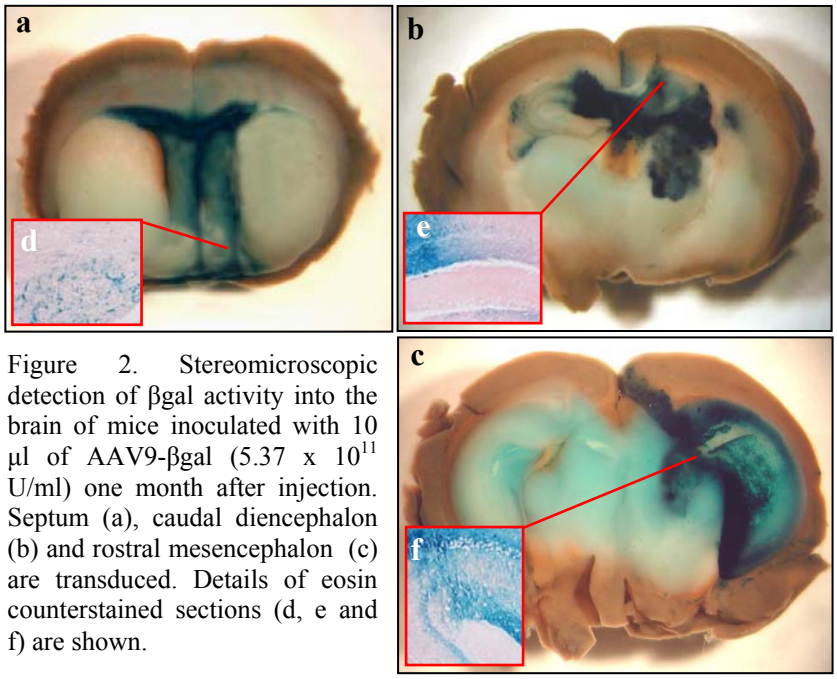

Figure 2. Stereomicroscopic detection of βgal activity into the brain of mice inoculated with 10 µl of AAV9-βgal (5.37 x 10^{11} U/ml) one month after injection. Septum (a), caudal diencephalon (b) and rostral mesencephalon (c) are transduced. Details of eosin counterstained sections (d, e and f) are shown.

High βgal activity was found into the thalamus (right hemisphere) and hippocampus (both hemispheres). Transduced neurons were also found into the septo-diencephalic region, with great involvement of the corpus callosum and septum. Weak positivity was detected in caudate and pre-optical nuclei. Thalamic nuclei and dorsal hippocampus of the rostral mesencephalon were also reached.

Injection of AAV9 into the cerebral cortex, thalamus, hippocampus and hypothalamus resulted in abundant vector genome spread to the controlateral side, especially in the hippocampus, hypothalamus and corpus callosum (Fig. 3). High signal was detected into the thalamus, hippocampus, frontal cortex, temporal cortex, septal nuclei and hypothalamus. AAV9 inoculation resulted in βgal positive

neurons in the greatest amount of rostral-caudal distribution of the vector genome (2-3 mm) from the points of inoculation.

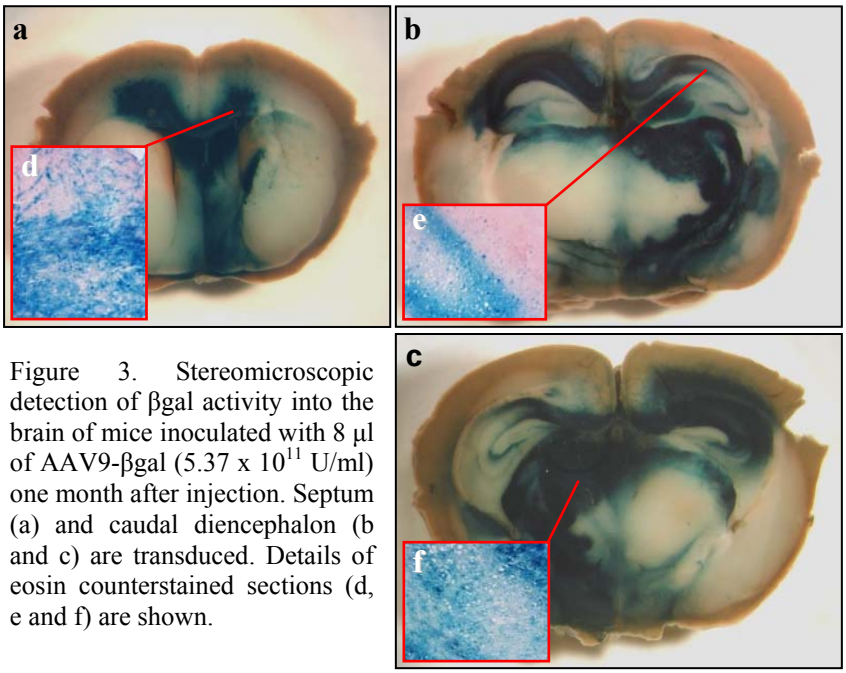

Figure 3. Stereomicroscopic detection of βgal activity into the brain of mice inoculated with 8 µl of AAV9-βgal (5.37 x 10^{11} U/ml) one month after injection. Septum (a) and caudal diencephalon (b and c) are transduced. Details of eosin counterstained sections (d, e and f) are shown.

The other mice of this group, sacrificed three months after the inoculation, showed low βgal activity, mainly confined to a small region of the caudate nucleus, thalamus and hippocampus. This could be explained by the activation of an immune response against the enzyme which led to a decreased expression of the protein.

However, genetic analysis evidenced the presence of AAV9-βgal genome into the brain of mice even after one year from the day of inoculation.

Furthermore, mice inoculated with empty AAV9 vector, monitored until two years from the day of inoculation, did not show any

neuropathological alteration. Indeed, periodical MRI analysis (Fig. 4) confirmed the lack of specific alterations AAV9-βgal related.

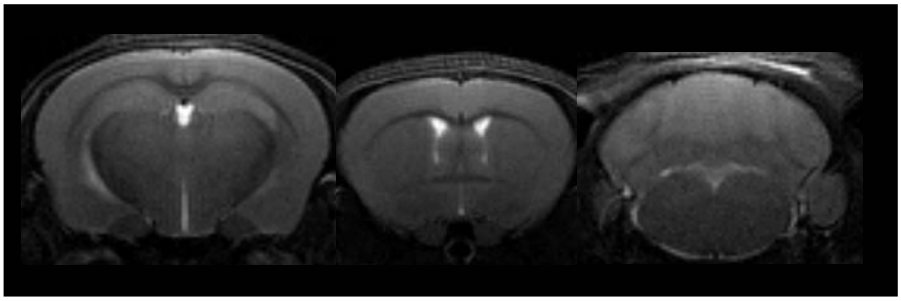

Figure 4. Periodically acquired T2 weighted MRI images confirmed the lack of neuropathological alterations into the brain of AAV9 inoculated mice.

Also histochemical (H&E stain) and immunohistochemical (Glial Fibrillary Acidic Protein stain, GFAP) analysis showed normal brain architecture without the appearance of astrocytosis (Fig. 5). Weak astrocytic activation was detected and limited to the site of AAV9 inoculation.

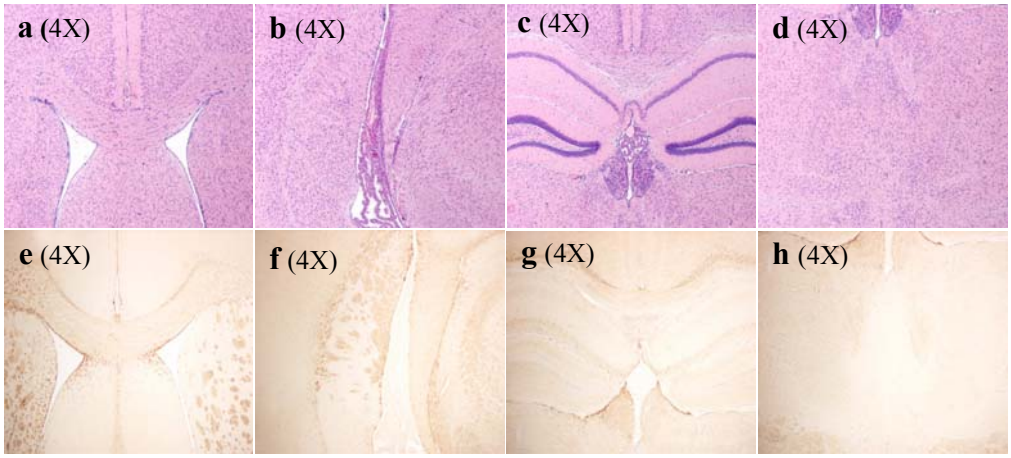

Figure 5. H&E stain of septum (a) and caudal-diencephalon (b-d) shows normal neuronal architecture, while GFAP stain did not reveal any astrocytic activation due to AAV9 injection.

2. AAV2-ScFvD18 EXPERIMENTAL THERAPEUTIC APPROACH (I)

The efficiency of ScFvD18 was initially evaluated in CD1 mice inoculated with 12 µL of AAV2-ScFvD18 vector (following the coordinates showed in materials and methods) and intracerebrally infected with RML brain homogenate. In order to accurately assess the onset of neurological symptoms, animal monitoring started 80 days after infection.

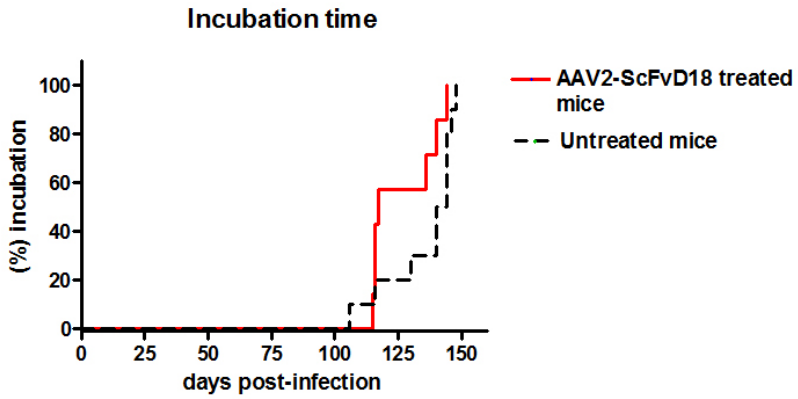

Graphic 1. Incubation time of AAV2-ScFvD18 treated and untreated mice intracerebrally infected with 10% RML.

As shown in Graph 1, there were no statistically significant differences in incubation period between AAV2-ScFvD18 treated and untreated animals (p = 0.0768, Logrank test). In particular, the mean of incubation time of treated animals was 126 ± 5 days (means ± standard error of the mean - S.E.M.) while that of control mice was 136 ± 4 days. The clinical course of disease was similar in both groups of animals and included decreased locomotor and social activities, grooming, food consumption, tail rigidity, kyphosis, uncoordinated

movements, awkwardness of gait, attenuation of righting reflex, hind limb clasping and, in the late stage of disease, tremor, hind limb paralysis and ataxia. In the first stage of the disease, most of the animals gained weight (56-60 g) and were hypoactive and apathetic in the home cage, with loss of interest in exploration of the cage. Instead, they become hyperactive in the open field, as a result of an altered response to novel environment. In the late stage of the disease, mice behavior was characterized by anxiety, fear and the animals walked in close proximity with the wall of the cage in which they were placed. In addition, circling behavior was always observed.

To note, AAV2-ScFvD18 treated animals demonstrated less pathophysiologic hind limb clasping behavior compared to untreated animals. Surprisingly, contrary to our expectations, mice treated with AAV2-ScFvD18 succumbed to experimental prion disease earlier than untreated mice (Graph. 2).

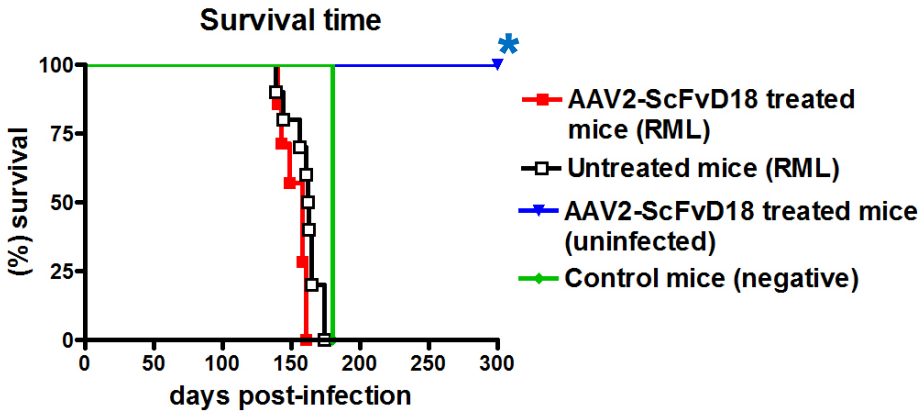

Graphic 2. Survival time of AAV2-ScFvD18 treated and untreated mice intracerebrally infected with 10% RML; *these animals were sacrificed at the end of their predicted lifespan (~700 days). Control mice have been sacrificed when all RML-infected animals were collected (~170 days).

Indeed, minimal but statistically significant differences in survival time (p = 0.028, Logrank test) of AAV2-ScFvD18 treated mice (153 ± 3 days) compared to untreated animals (160 ± 4 days) were observed. Histological examination showed striking similarities of the lesions between the groups of infected mice (i.e., the extent of vacuolar degeneration in standard brain regions) with major involvement of thalamic nuclei, hippocampus, cerebral cortex and septal nuclei (Graph. 3).

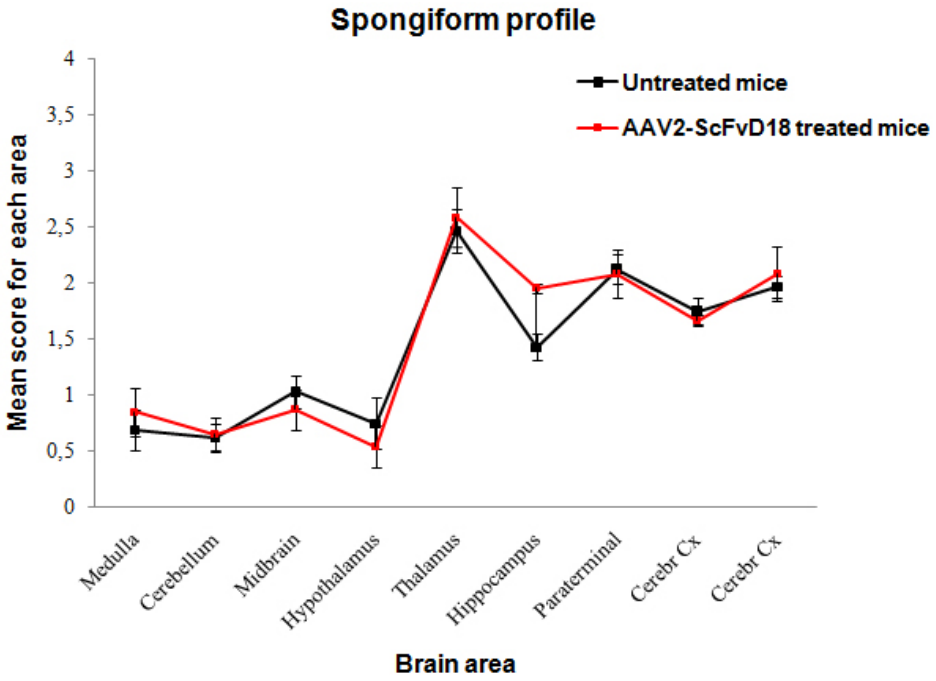

Graphic 3. Vacuolar degeneration in specific brain regions. Thalamus, hippocampus, septum and cerebral cortex were severely affected.

Small, round vacuoles were present throughout the brain in neuronal elements, but were more prevalent, bilaterally and symmetrically, into the hippocampus, thalamus and somatosensory cortex (Fig. 1).

On the contrary, hypothalamus, midbrain and cerebellum were less affected. Moderate neurodegeneration (neuronal loss) and astrocytosis were comparable between AAV2-ScFvD18 treated and untreated mice.

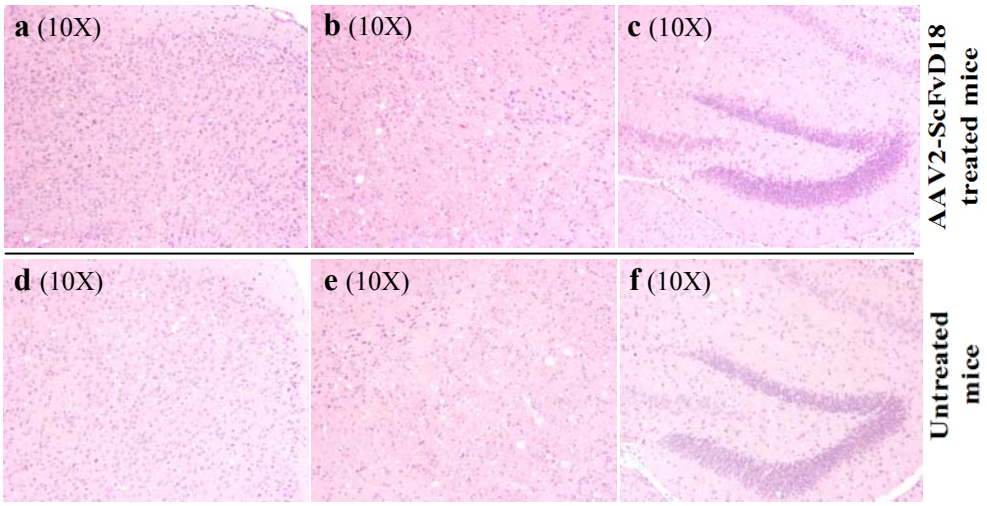

Figure 1. H&E stain illustrates the mainly affected brain area of both AAV2-ScFvD18 treated (a, b and c) and untreated mice (d, e and f). In particular, somatosensory cortex (a and d), thalamus (b and e) and hippocampus (c and f) are shown.

In particular, immunohistochemical staining for hypertrophic astrocytes (GFAP) evidenced abundant and widespread glial activation in all vacuolated area. In particular, hippocampus, thalamus and cerebral cortex were severely affected (Fig. 2).

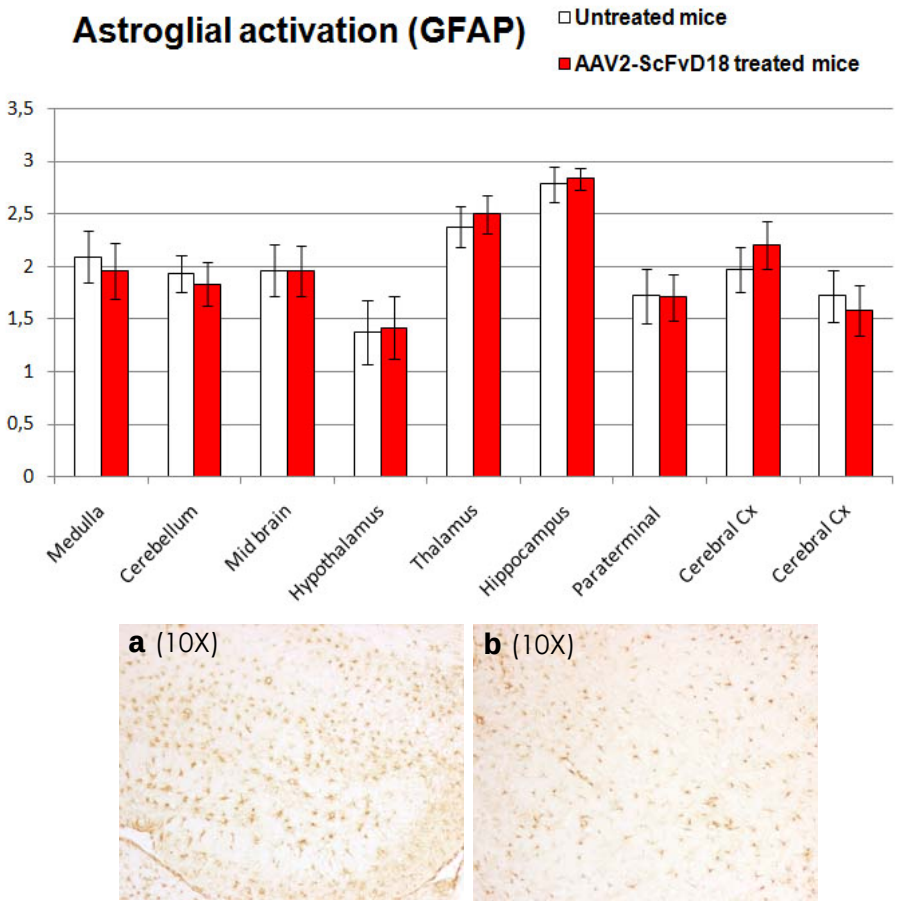

Figure 2. Astrocytic activation throughout different CNS regions of both AAV2-ScFvD18 treated and untreated mice. Comparable GFAP immunoreactivity between groups was observed and intense signal into the hippocampus (a) and thalamus (b) was detected.

PrP^{res} immunohistochemical staining with specific antibody (6H4), showed synaptic and diffuse pattern of PrP deposition

Thalamus, hippocampus, cerebral cortex and medulla were severly affected, while dentate gyrus and pyramidal cell layers of the hippocampus, hypothalamus and amygdala showed less immunoreactivity.

To note, slightly lower amount of PrP^{res} was found into the hippocampus and cerebral cortex of AAV2-ScFvD18 treated mice compared to that of untreated animals (Fig. 3).

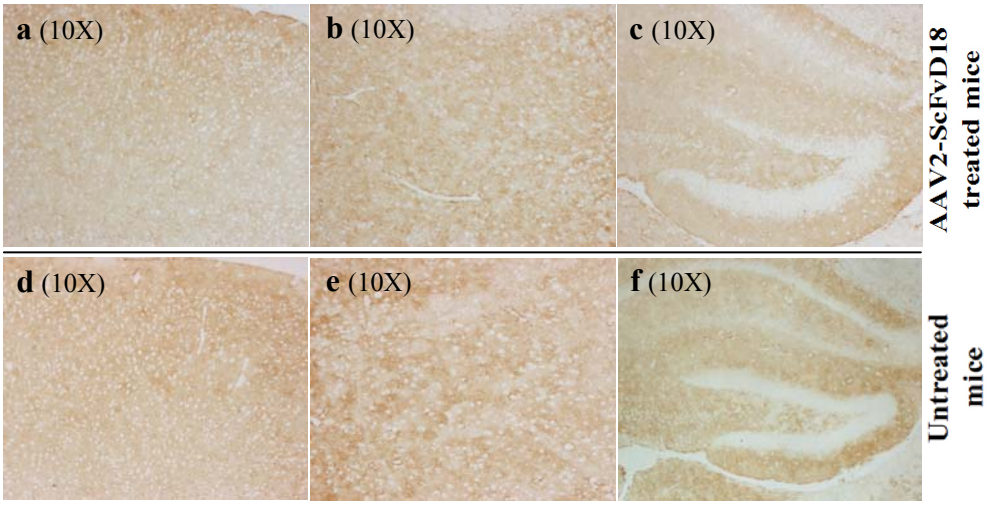

Figure 3. Anti-PrP antibody (6H4) immunohistochemical stain reveals PrP^{res} deposition in the CNS of both AAV2-ScFvD18 treated (a, b and c) and untreated mice (d, e and f). In particular, somatosensory cortex (a and d), thalamus (b and e) and hippocampus (c and f) are shown.

These data were also verified by Western blot analysis that showed similar PrP^{res} profile between groups and decreased levels of PK-resistant PrP in the brain of mice administered with AAV2-ScFvD18 (Fig. 4a).

Densitometric analysis (Fig. 4b) confirmed the presence of statistically significant lower lever of PrP^{res} in treated mice compared with untreated animals ($p = 0.025$, *t*-test).

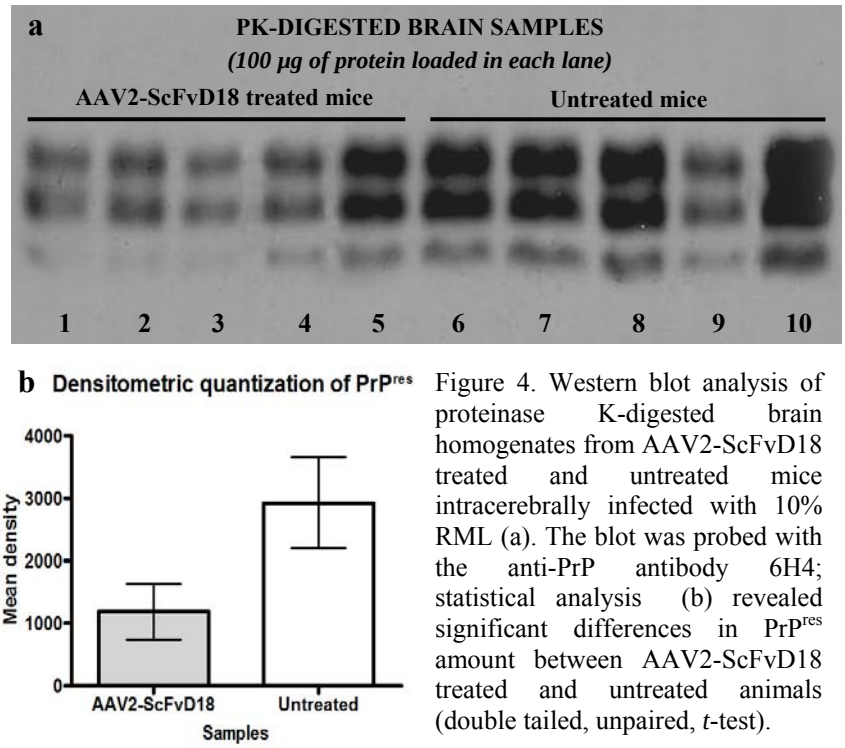

Figure 4. Western blot analysis of proteinase K-digested brain homogenates from AAV2-ScFvD18 treated and untreated mice intracerebrally infected with 10% RML (a). The blot was probed with the anti-PrP antibody 6H4; statistical analysis (b) revealed significant differences in PrP^{res} amount between AAV2-ScFvD18 treated and untreated animals (double tailed, unpaired, *t*-test).

DNA quantification of AAV2-ScFvD18 vector in terminally sick animals revealed that AAV2 genome was still present in the brain of treated mice, even after 27 weeks from the day of injection. In particular, samples loaded on lane 1, 2, 3 and 4 (Wb) were analyzed by real-time PCR and results are reported in table 1:

Lane	AAV2-ScFVD18 viral genome in terminally sick mice (genome copies/mL)	Starting concentration of AAV2-ScFvD18 vector (genome copies/mL)
1	6.5×10^6	5×10^{11}
2	2.2×10^5	5×10^{11}
3	3.6×10^6	5×10^{11}
4	4.48×10^5	5×10^{11}
5	n.d.	5×10^{11}

Table 1. Levels of AAV2-ScFVD18 viral genome (genome copies/mL) found in the brain of treated mice after sacrifice.

Mice inoculated with PBS or mock, but not infected with RML, have been monitored for the entire duration of the experiment and then culled and subjected to necroscopy. RML-uninfected mice, treated with AAV2-ScFvD18, were periodically subjected to MRI acquisitions (Fig. 5) and histochemical analysis in order to study the appearance of toxic effects following AAV injection. Neither behavioral nor neuropathological changes have never been observed.

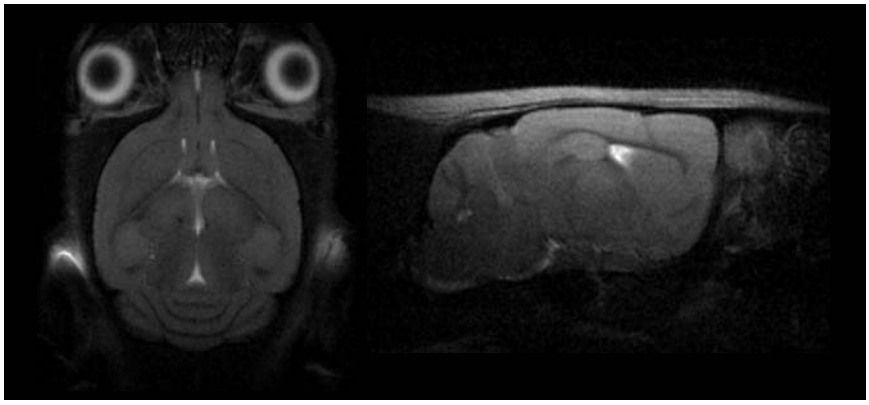

Figure 5. T2 weighted MRI images confirmed the lack of neuropathological alterations in the brain of AAV2 injected mice (RML-uninfected) even after 200 days post inoculation.

3. AAV9-ScFvD18 EXPERIMENTAL THERAPEUTIC APPROACH (II)

The efficiency of ScFvD18 was further evaluated in C57Bl/6J mice inoculated with 12 µL of AAV9-ScFvD18 vector (following the coordinates showed in materials and methods) and intracerebrally infected with BSE brain homogenate. In order to accurately assess the onset of neurological symptoms, animal monitoring started 100 days after infection.

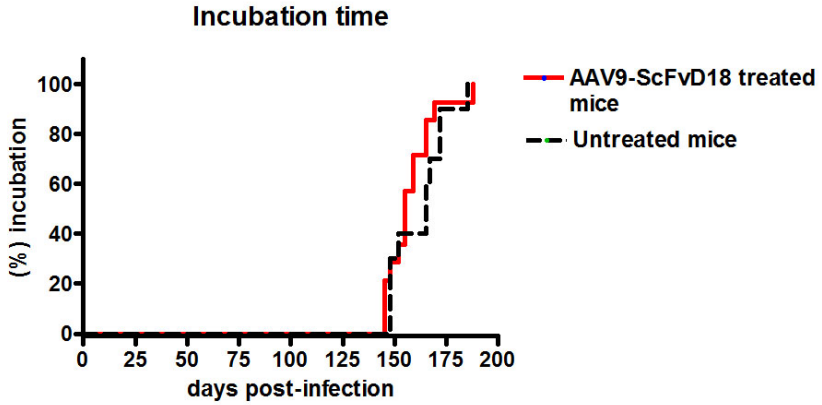

Graphic 1. Incubation time of AAV9-ScFvD18 treated and untreated mice intracerebrally infected with 10% BSE.

As shown in Graph 1, there were no statistically significant differences in incubation period between AAV9-ScFvD18 treated and untreated animals (p = 0.3918, Logrank test). In particular, the mean of incubation time of treated animals was 158 ± 3 days while that of control mice was 162 ± 4 days.

The clinical course of the disease was similar in both groups of mice and, in the first stage, was characterized by nervousness, hypersensitivity with fasciculation of the hind limbs and lack of

curiosity in the open field. Decreased locomotor and social activities, tail rigidity, weight loss, urinary incontinence, kyphosis, uncoordination, awkwardness of gait, attenuation of righting reflex, hindlimb paralysis and ataxia occurred in the late stage of disease. Survival time (Graph. 2) of AAV9-ScFvD18 treated mice (169 ± 4 days) was similar to that of untreated animals (184 ± 7 days) and no statistically significant differences were found (p = 0.078, Logrank test).

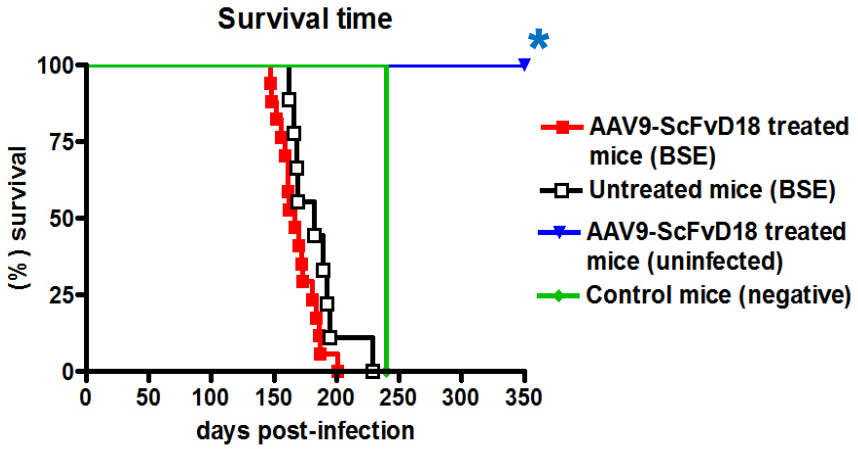

Graphic 2. Survival time of AAV9-ScFvD18 treated and untreated mice intracerebrally infected with 10% BSE; * these animals were sacrificed at the end of their predicted lifespan (~700 days). Control mice have been sacrificed when all BSE-infected animals were collected (~230 days).

Neuropathology consisted of a characteristic degeneration in areas of grey matter in brain and spinal cord. Spongiform profile showed similar pattern of vacuolation in both groups of mice with major involvement of medulla, hippocampus and thalamus (Graph. 3). Septum and cerebral cortex were also affected but with less severity. Cerebellum was completely spared.

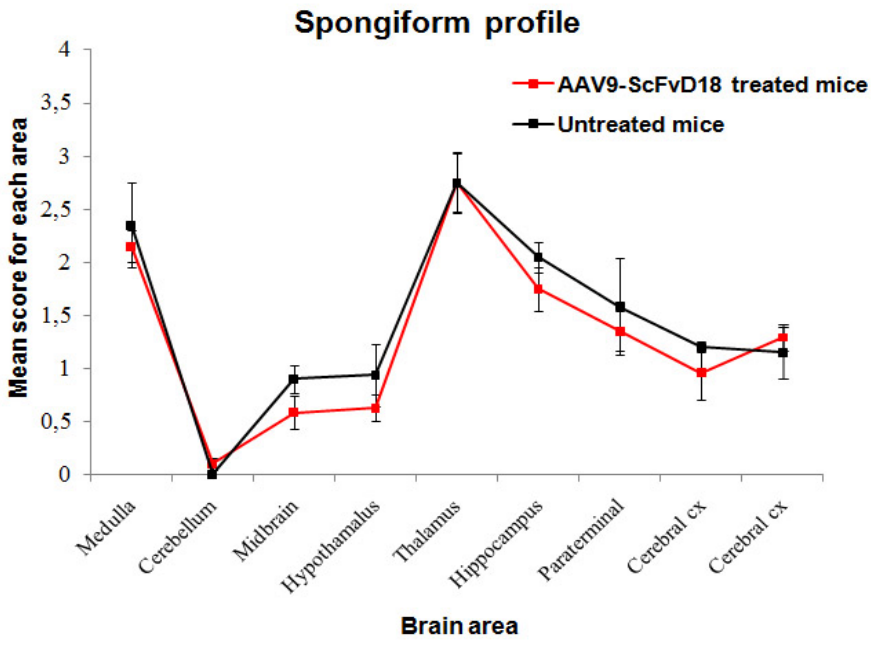

Graphic 3. Vacuolar degeneration in standard brain regions. Medulla oblongata, thalamus, hippocampus and septum were severely affected.

H&E stained sections showed severe spongiform changes into the thalamus, hippocampus and medulla, with the presence of some vacuolar confluences. Neuronal loss and glial activation were also present (Fig. 1).

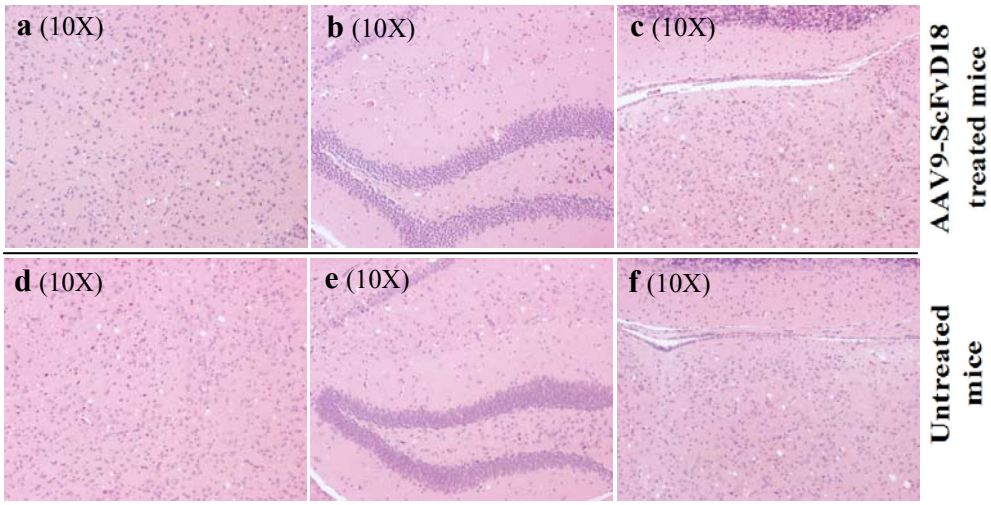

Figure 1. H&E stain illustrates the mainly affected brain area of both AAV9-ScFvD18 treated (a, b and c) and untreated mice (d, e and f). In particular, thalamus (a and d), hippocampus (b and e) and medulla (c and f) are shown.

The distribution of hypertrophic astrocytes was similar to the targeting of spongiosis and PrP^{res} deposition. As shown in Figure 2, glial activation was comparable between the groups of infected mice and severely affected the hippocampus, thalamus and medulla.

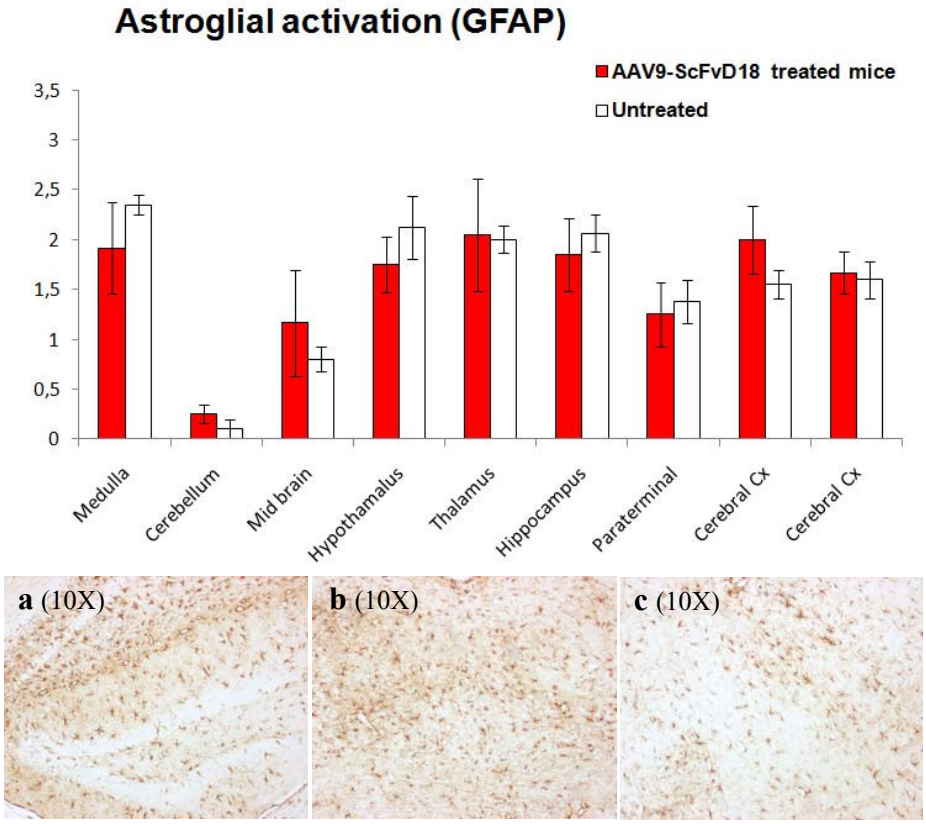

Figure 2. Astrocytic activation throughout different CNS regions of both AAV9-ScFvD18 treated and untreated mice. Comparable GFAP immunoreactivity between groups was observed and intense signal into the hippocampus (a), medulla (b) and thalamus (c) was detected.

PrP^{res} labeling showed diffuse and focal (granular and plaque-like) PrP deposits in the somatosensory cortex, striatum, thalamus, hypothalamus, septum, cerebellum, medulla oblongata, and spinal cord . The plaque-like deposits did not possess the tinctorial properties

of amyloid and were most abundant into the granular layer of the cerebellar cortex and corpus callosum (Fig. 3). Few deposits were also detected in the thalamus.

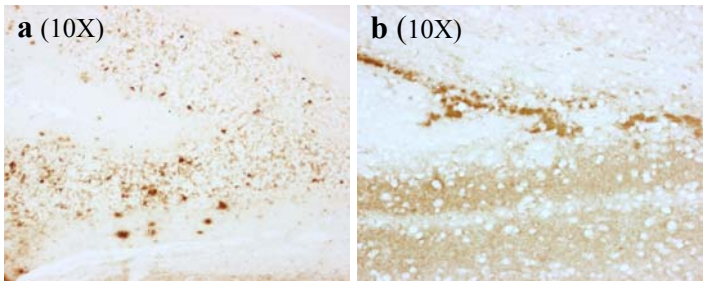

Figure 3. Plaque-like deposits of PrP^{res} in the granular layer of the cerebellar cortex (a) and corpus callosum (b) are shown.

Less PrP^{res} amount was detected in the CNS of AAV9-ScFvD18 treated mice compared to that of untreated animals (Fig. 4). Particularly, major differences were found into the hippocampus, septum and thalamic nuclei, exactly the same regions that we found to be preferentially transduced by AAV9-βgal in our diffusion studies.

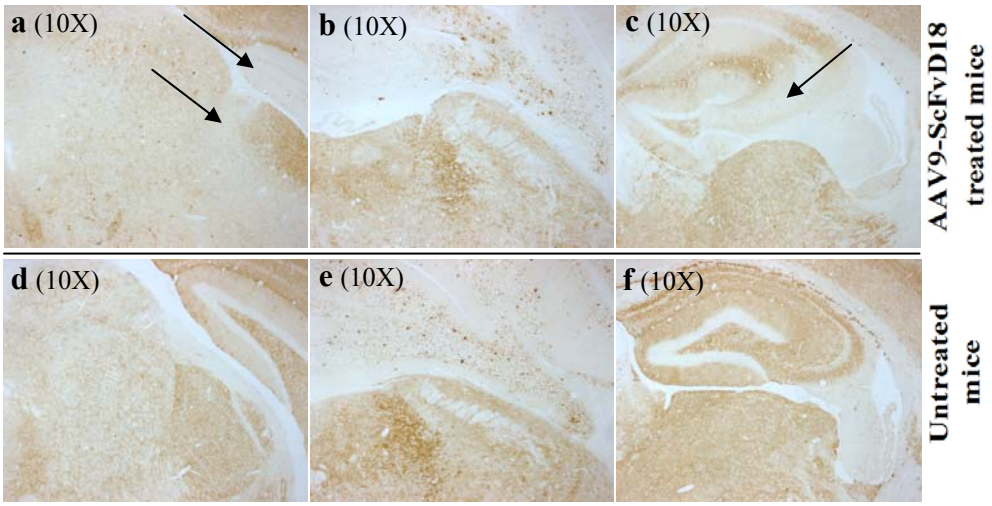

Figure 4. Anti-PrP antibody (6H4) immunohistochemical stain evidenced PrP^{res} deposition in the CNS of both AAV9-ScFvD18 treated (a, b and c) and untreated mice (d, e and f). In particular, rostral mesencephalon (a and d), medulla (b and e) and hippocampus (c and f) are shown.

These data were also verified by Western blot analysis that showed similar PrP^{res} profile in both groups of infected mice. In particular, a prevalence of a diglycosilated band, typical of cattle and humans infected with BSE, was detected (Fig. 5a).

Densitometric analysis (Fig. 5b) confirmed the presence of statistically significant lower levels of PrP^{res} in AAV9-ScFvD18 treated mice compared with untreated animals ($p = 0.047$, *t*-test).

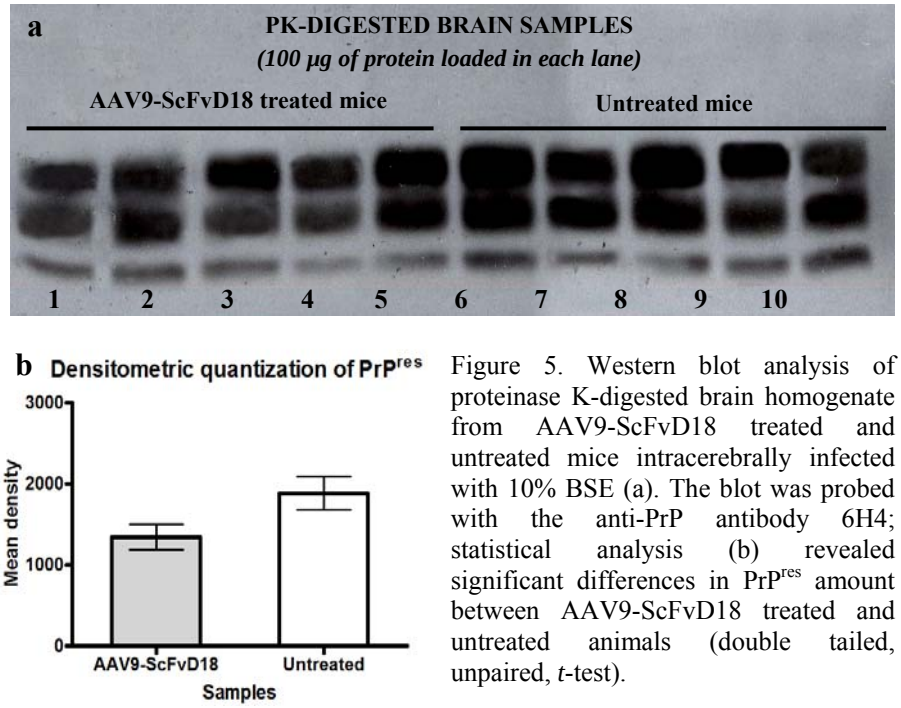

Figure 5. Western blot analysis of proteinase K-digested brain homogenate from AAV9-ScFvD18 treated and untreated mice intracerebrally infected with 10% BSE (a). The blot was probed with the anti-PrP antibody 6H4; statistical analysis (b) revealed significant differences in PrP^{res} amount between AAV9-ScFvD18 treated and untreated animals (double tailed, unpaired, *t*-test).

DNA quantification of AAV9-ScFvD18 vector in terminally sick animals revealed that AAV9 genome was still present in the brain of treated mice, even after 34 weeks from the day of inoculation.

In particular, samples loaded on lane 1, 2, 3 and 4 (Wb) were analyzed by real-time PCR and results are reported in table 1 :

Lane	AAV9-ScFVD18 viral genome in terminally sick mice (genome copies/mL)	Starting concentration of AAV9-ScFvD18 vector (genome copies/mL)
1	2.5×10^6	5×10^{11}
2	1.4×10^7	5×10^{11}
3	4.67×10^6	5×10^{11}
4	2.6×10^5	5×10^{11}
5	n.d.	5×10^{11}

Table 1. Levels of AAV9-ScFVD18 viral genome (genome copies/mL) found in the brain of treated mice after sacrifice.

Mice inoculated with PBS or mock, but not infected with BSE, have been monitored for the entire duration of the experiment and then culled and subjected to necroscopy. BSE-uninfected mice, treated with AAV9-ScFvD18, were periodically subjected to MRI acquisitions (Fig. 6) and histochemical analysis in order to study the appearance of toxic effects following AAV injection. Neither behavioral nor neuropathological changes have never been observed.

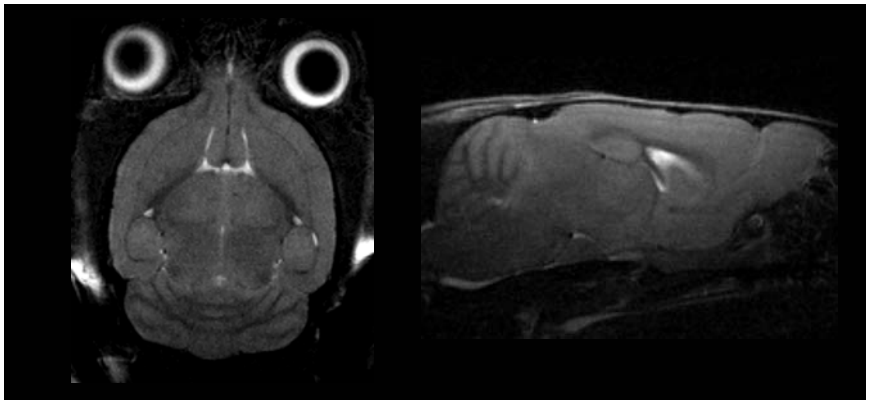

Figure 6. T2 weighted MRI images confirmed the lack of neuropathological alterations in the brain of AAV9 injected mice (BSE-uninfected) even after 240 days post inoculation.

4. AAV9-ScFvD18 EXPERIMENTAL THERAPEUTIC APPROACH (III)

In order to analyze the presence of specific neuropathological differences that could exist at an early stage of the disease between AAV9-ScFvD18 treated and untreated animals, three mice per group (A and D) were sacrificed after 166 days post infection. At the time of sacrifice, two animals per group showed initial sickness behavior (hyperactivity in the open field and slight motor deficit during the inverted screen test) while one animal per group was not symptomatic yet. Vacuolation profile revealed less spongiform changes into the septum, thalamus, hippocampus and adjacent cerebral cortex of AAV9-ScFvD18 treated mice compared to those of untreated subjects (Graph. 1, Fig. 1)

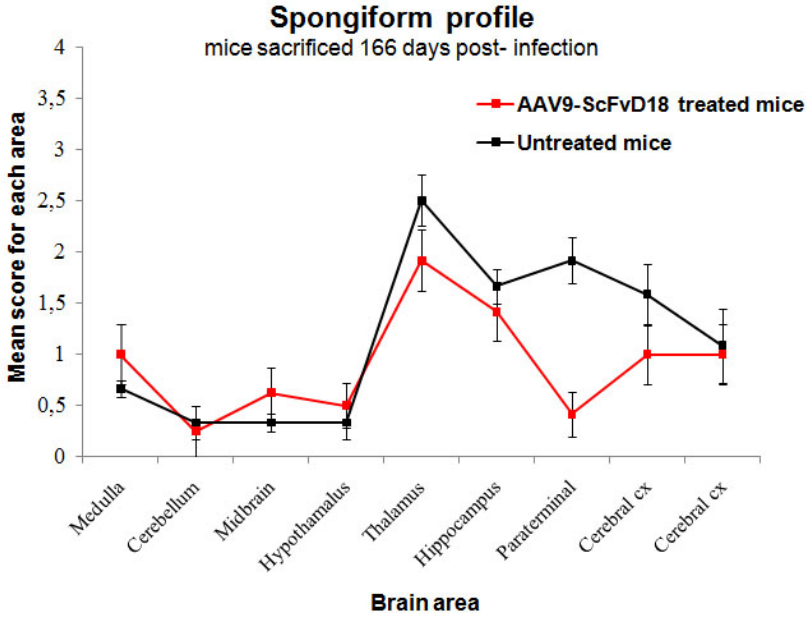

Graphic 1. Vacuolar degeneration in standard brain regions. Thalamus, hippocampus and septum of AAV9-ScFvD18 treated mice showed lower spongiform changes than that of untreated animals.

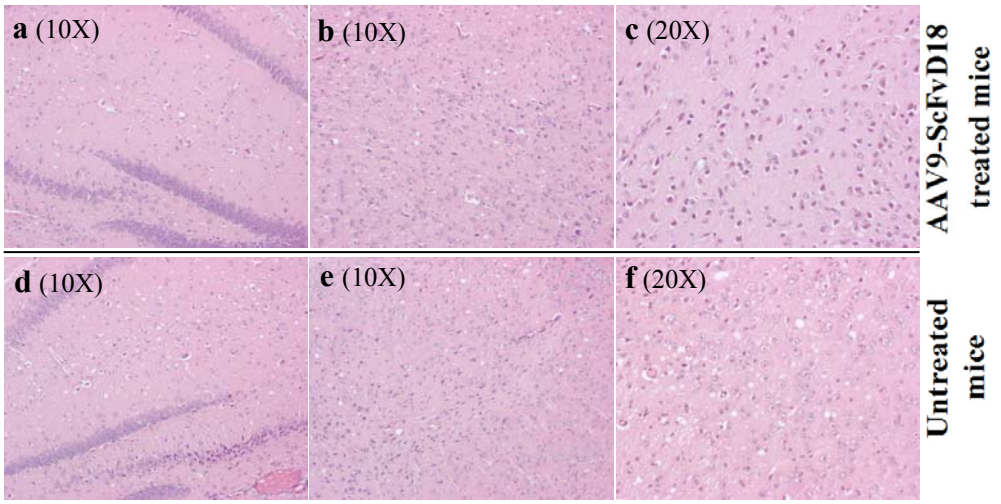

Figure 1. H&E stain shows that thalamus, hippocampus and septum of AAV9-ScFvD18 treated mice had lower spongiform changes than that of untreated animals.

Histoblots and immunohistochemical staining with specific antibody to PrP (6H4) showed synaptic and diffuse pattern of PrP^{res} deposition (Fig. 2).

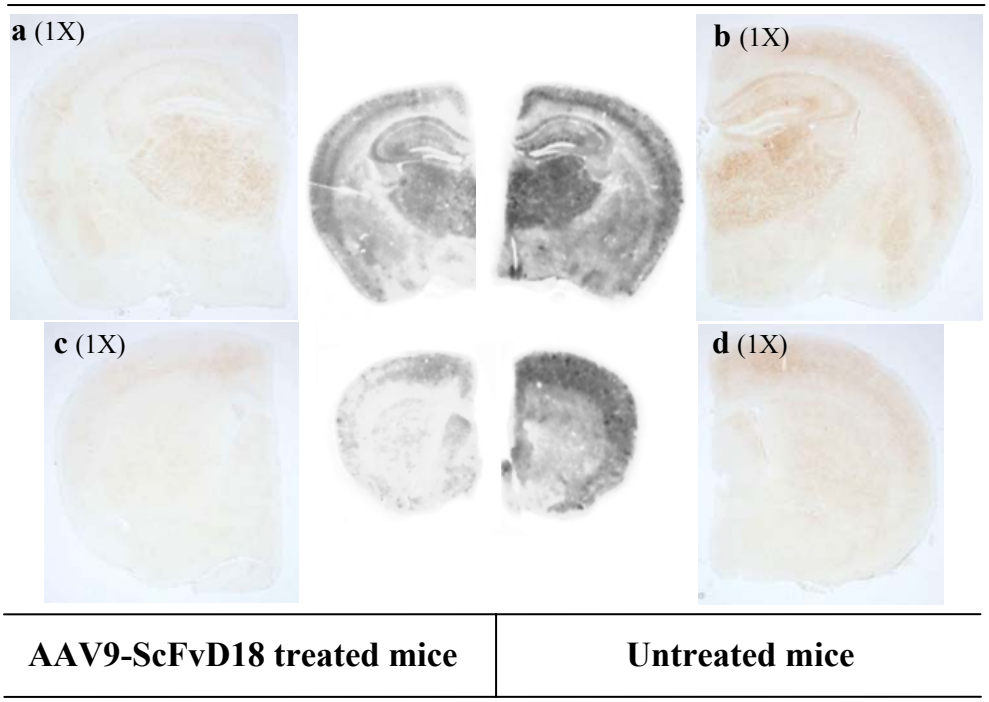

Figure 2. Anti-PrP antibody (6H4) stained histoblots and histological sections showed lower PrP^{res} deposition in the brain of AAV9-ScFvD18 treated mice (a and c) than that of untreated (b and d) animals.

Thalamus, hippocampus, cerebral cortex and medulla were prevalently affected, while dentate gyrus and pyramidal cell layers of the hippocampus, hypothalamus and amygdala showed less immunoreactivity. To note, less amount of PrP^{res} was found in the brain of AAV9-ScFvD18 treated mice compared to that of untreated animals (Fig. 3). Brain homogenates were subjected to Western blot analysis following digestion with proteinase K to determine the PrP^{res} amount (Fig. 4).

Densitometric analysis (Fig. 4) showed significantly reduced levels of PrP^{Sc} in the brain of AAV9-ScFvD18 treated mice compared to untreated group (p = 0.0005, t-test), consistent with less-advanced disease at this time point. Evident immunohistochemical differences in PrP^{res} amount between treated and untreated mice were found into the thalamus, hippocampus and septum (Fig. 3).

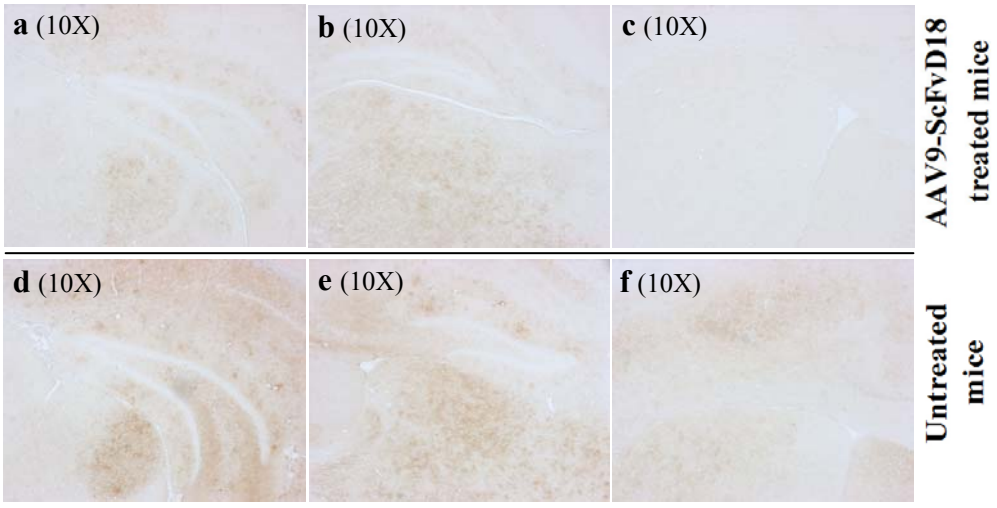

Figure 3. Anti-PrP antibody (6H4) immunohistochemical stain reveals PrP^{res} deposition in both AAV9-ScFvD18 treated (a, b and c) and untreated mice (d, e and f). In particular, region of the rostral mesencephalon (a and d), caudal diencephalon (b and e) and septum (c and f) are compared. Less PrP^{res} amount was found into the CNS of treated mice, mainly confined to the thalamus (a and d), hippocampus (d and e) and septum (c and f).

Table 1 shows the amount of PrP^{res} immunoreactivity in septum, caudal diencephalon, rostral mesencephalon and rostral cerebellum of both AAV9-ScFvD18 treated and untreated mice.

Sample	Septum		Caudal diencephalon				Rostral mesencephalon			Rostral cerebellum		
	Cerebral cortex	Septal nuclei	Thalamus	Hippocampus	Hypothalamus	Cerebral cortex	Thalamus	Hippocampus	Cerebral cortex	Cerebellar cortex	Medulla	
1	+/-	-	+	+/-	-	-	+/--	+	+/-	-	-	AAV9-ScFvD18 treated mice
2	-	-	+	+/-	-	-	+	+/-	-	-	-	
3	-	-	+/-	-	-	-	+/-	-	-	-	-	
1	-	-	+	+/-	-	+/-	-	+	+/-	-	-	Untreated mice
2	+	+/-	++	+	-	+/++	+/++	+	+	-	-	
3	+	+/-	+/++	+	-	+	+	+	+	-	-	

Table 1. Immunohistochemical analysis of PrP^{res} immunoreactivity (166 days after prion infection) in the brain of both AAV9-ScFvD18 and untreated mice.

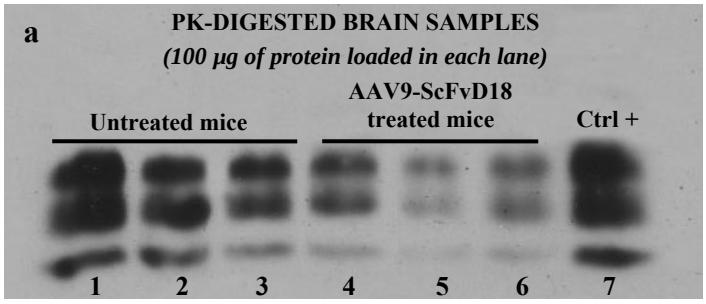

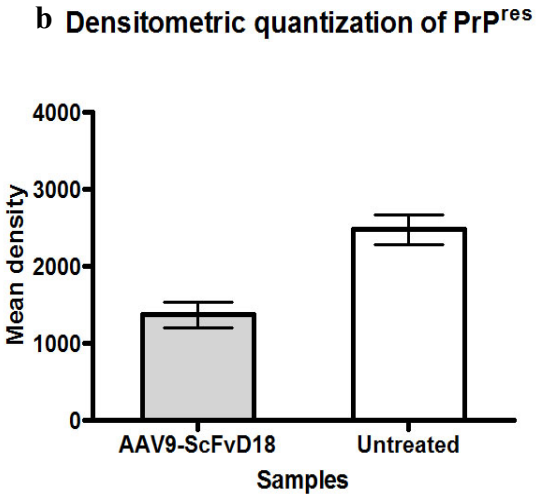

Figure 4. Western blot analysis of proteinase K-digested brain homogenates from AAV9-ScFvD18 treated and untreated mice intraperitoneally infected with 10% RML (a). The blot was probed with the anti-PrP antibody 6H4; statistical analysis (b) revealed significant differences in PrP^{res} amount between AAV9-ScFvD18 treated and untreated animals (double tailed, unpaired, t-test).

The distribution of hypertrophic astrocytes was similar to the targeting of spongiosis and PrP^{res} deposition. Different glial activation (GFAP) pattern was detected.

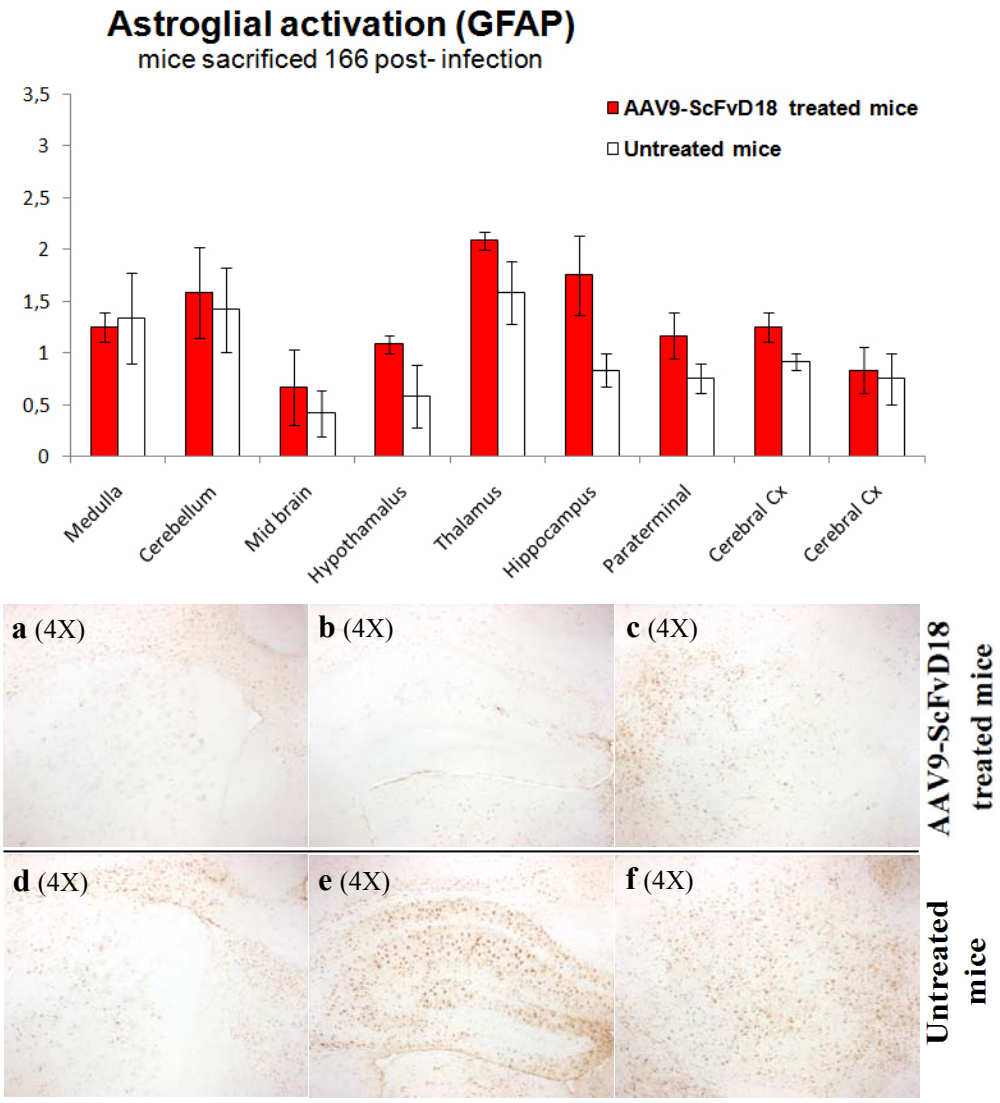

Figure 5. Astrocytic activation throughout different CNS regions of both AAV9-ScFvD18 treated and untreated mice. In particular, heavy GFAP labeling into the septum, hippocampus (a) and thalamus (b) of untreated mice was detected. On the contrary, AAV9-ScFvD18 treated mice showed less GFAP immunoreactivity in the same area.

In particular, as observed for vacuolar degeneration, septum, thalamus, hippocampus and adjacent cerebral cortex of AAV9-ScFvD18 treated mice showed less GFAP immunoreactivity compared to that of untreated animals (Fig. 5).

Unfortunately all AAV9-ScFvD18 treated mice succumbed to disease. As shown in Graph 2, there was statistically significant difference in incubation period between AAV9-ScFvD18 treated and untreated mice (p = 0.0186, Logrank test). In particular, the mean of incubation time of treated animals was 187 ± 7 days while that of control mice was 166 ± 5 days. The clinical course of disease was similar in both groups of animals. Sickness behavior included decreased locomotor and social activities, grooming, food consumption and was mainly characterized by tail rigidity, kyphosis, uncoordinated movements, awkwardness of gait, attenuation of righting reflex, hindlimb paralysis and, in the late stage of disease, tremor and ataxia.

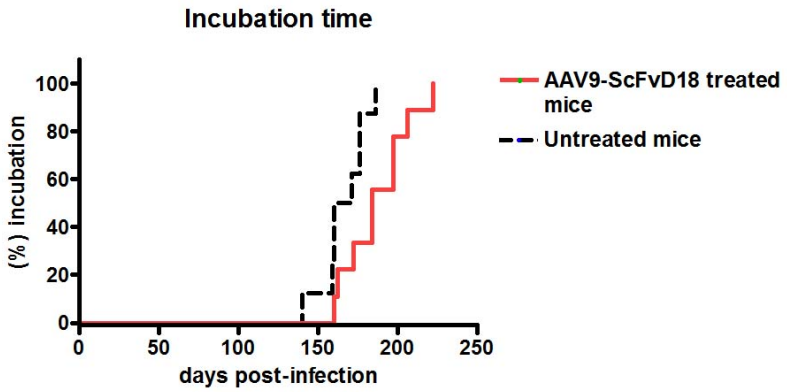

Graph 2. Incubation time of AAV9-ScFvD18 treated and untreated mice intraperitoneally infected with 10% RML.

Survival time (Graph. 3) of AAV9-ScFvD18 treated mice (202 ± 7 days) was slightly longer than that of untreated animals (188 ± 5 days) but no statistically significant differences were found between groups (p = 0.085, Logrank test).

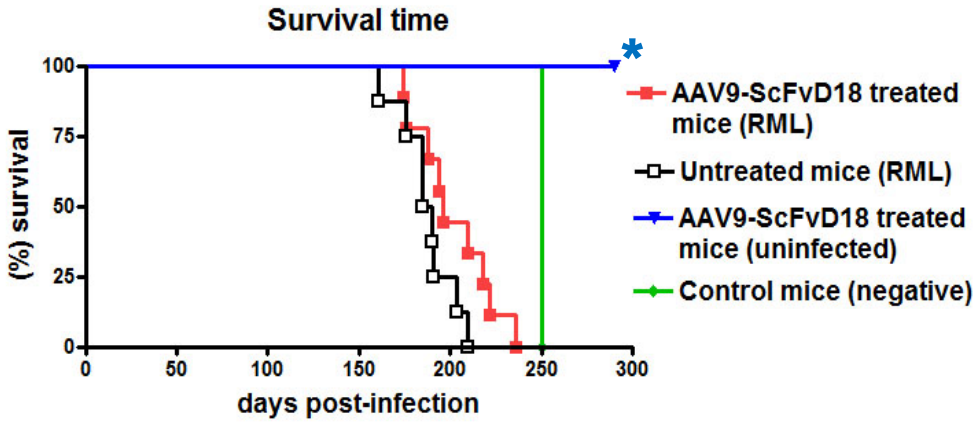

Graphic 3. Survival time of AAV9-ScFvD18 treated and untreated mice intraperitoneally infected with 10% RML; *these animals were sacrificed at the end of their predicted lifespan (~700 days). Control mice have been sacrificed when all RML-infected animals were collected (~250 days).

Histological examination showed striking similarities in lesion profile between groups of infected mice, with major involvement of thalamic nuclei, hippocampus, cerebral cortex and septal nuclei (Graph. 4). To note, hippocampus and septum of AAV9-ScFvD18 treated mice showed less spongiosis than that found into the same regions of untreated animals. Important neuronal loss was found in both groups of mice, mainly confined to the thalamus and the CA1 sector of the hippocampus (Fig. 6).

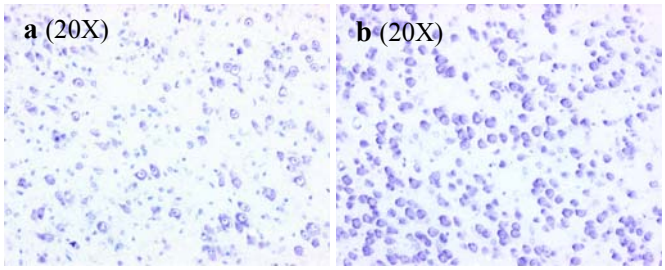

Figure 6. Nissl stain shows neuronal loss into the thalamus of both AAV9-ScFvD18 treated and untreated mice (a) compared with uninfected animals (b)

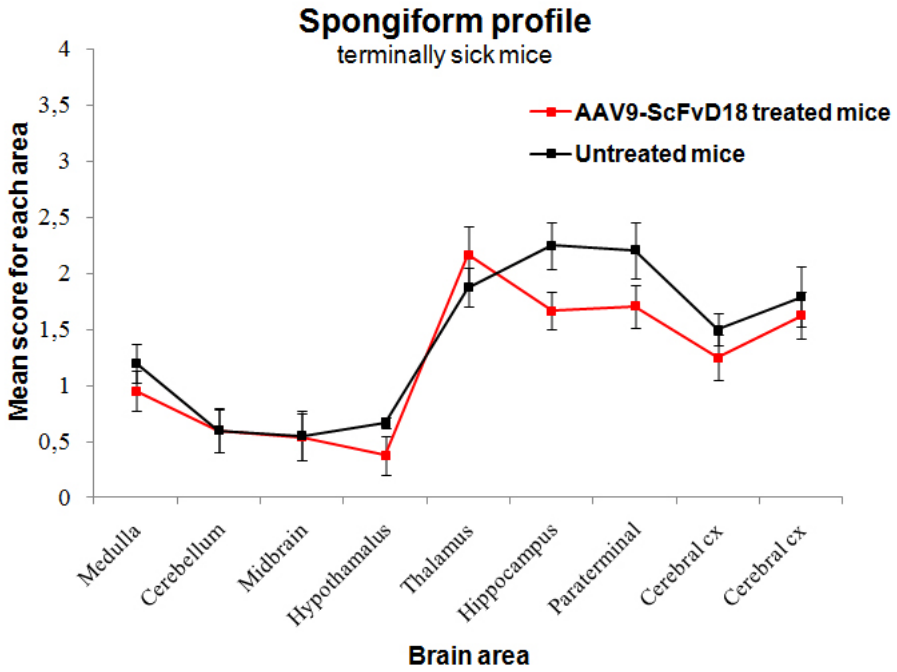

Graphic 4. Vacuolar degeneration in specific brain regions. Thalamus, hippocampus, septum and cerebral cortex were severely affected.

Hypothalamus, midbrain and cerebellum showed slight spongiform changes that were comparable between the groups of infected mice.

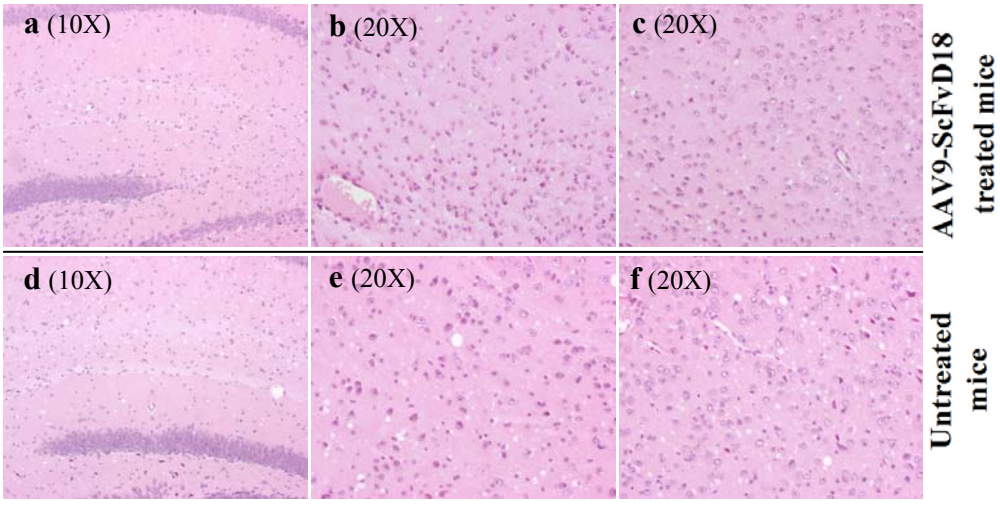

Figure 7. H&E stain illustrates the mainly affected brain area of AAV9-ScFvD18 treated (a, b and c) and untreated mice (d, e and f). In particular, hippocampus (a and d), thalamus (b and e) and septum (c and f) are shown.

Less PrP^{res} amount was detected in the brain of AAV9-ScFvD18 treated mice compared to that of untreated animals (Fig. 8). Particularly, major differences were found into the hippocampus, septum and thalamic nuclei, exactly the same regions that we found to be preferentially transduced by AAV9-βgal in our diffusion studies.

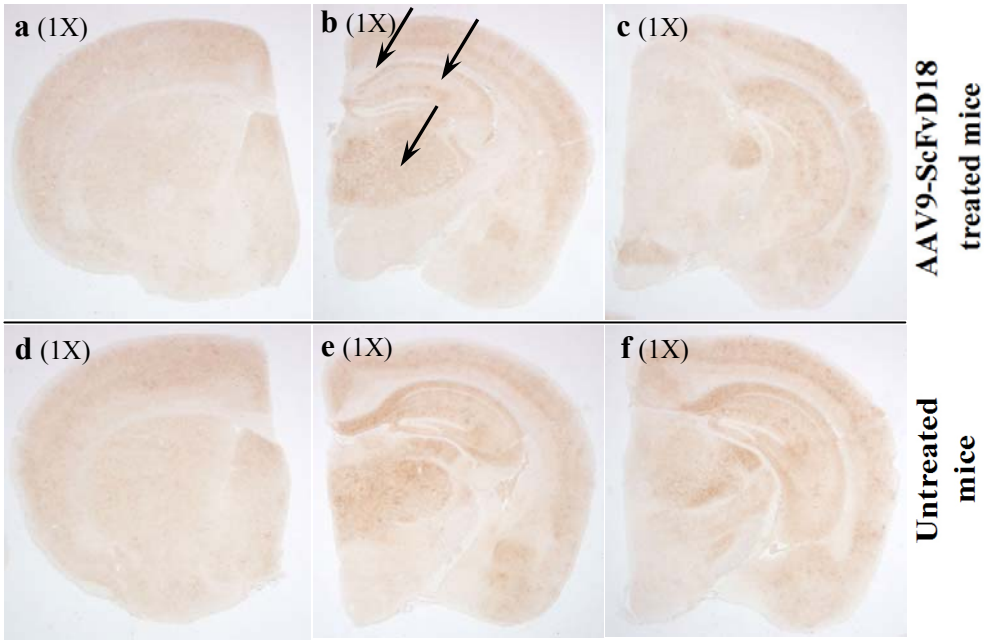

Figure 8. Anti-PrP antibody (6H4) immunohistochemical stain evidenced PrP^{res} deposition in both AAV9-ScFvD18 treated (a, b and c) and untreated mice (d, e and f). In particular, rostral mesencephalon (a and d), medulla (b and e) and hippocampus (c and f) are shown.

These data were also verified by Western blot analysis that showed similar PrP^{res} profile in both groups of mice. Densitometric analysis (Fig. 9) confirmed the presence of statistically significant lower levels

of PrP^{res} in the CNS of treated mice compared to those of untreated animals ($p = 0.0154$, *t*-test).

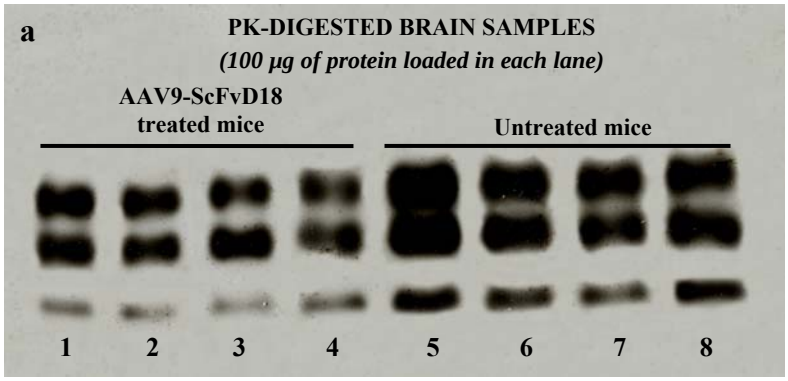

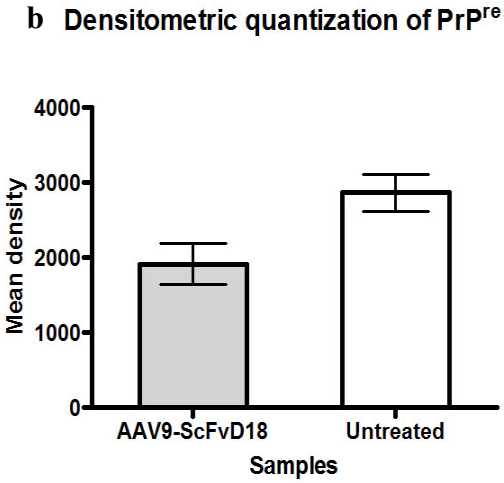

Figure 9. (a) Western blot analysis of proteinase K-digested brain homogenates from AAV9-ScFvD18 treated and untreated mice intraperitoneally infected with 10% RML. The blot was probed with the anti-PrP antibody 6H4; (b) statistical analysis revealed significant differences in PrP^{res} amount between AAV9-ScFvD18 treated and untreated animals (double tailed, unpaired, *t*-test).

Further analysis, such as GFAP immunoreactivity and AAV9-ScFvD18 genome titration are ongoing.

CHAPTER 2

A NOVEL CLASS OF POTENTIAL PRION DRUGS: PRELIMINARY IN VITRO AND IN VIVO DATA FOR MULTILAYER COATED GOLD NANOPARTICLES

Ai Tran HN*, Sousa F*, Moda F*, Mandal S, Chanana M, Vimercati C, Morbin M, Krol S, Tagliavini F, Legname G.

*(*these authors contributed equally to the work)*

Published in NANOSCALE
2010 October 14 (Epub ahead of print)
PMID: 20944860

CHAPTER 2

MATHERIALS AND METHODS

A NOVEL CLASS OF POTENTIAL PRION DRUGS: PRELIMINARY IN VITRO AND IN VIVO DATA FOR MULTILAYER COATED GOLD NANOPARTICLES

1. SYNTHESIS OF GOLD NANOPARTICLES

Monodisperse gold nanoparticles were prepared as described by Turkevich [225]. For particles with a size of 15±1 nm, 5.3 mg of $NaAuCl_4$ 2 H_2O in 25 mL of Milli-Q grade water were boiled under reflux. One milliliter of a 1% trisodium citrate solution was rapidly added to the boiling pale yellow solution, which resulted in a color change to deep red. After boiling for additional 20 min, the solution was cooled down to room temperature and stored protected from light at room temperature. All experiments described here were performed with the above colloidal nanogold stock solution.
The 46 nm gold particles were prepared using the same procedure but with 10.6 mg of $NaAuCl_4$ in 25 mL water and the fast addition of 750 µL 1% trisodium citrate solution.

1.1 Polyelectrolyte coating

The polyelectrolyte coating was applied in accordance to the method previously described [220, 226] with a few modifications. Briefly, 1 mL colloidal nanogold was added drop-wise under constant stirring to 200 µL of PSS solution (10 mg/mL) or 500 µL PAH solution (3 mg/mL). Both solutions were supersaturated to allow for an immediate coverage of the particles with polyelectrolytes. After incubation for 20 min in the dark, this solution was centrifuged for 20 min at 20,000 × g. The supernatant was removed and the particles were washed twice by centrifugation/resuspension in Milli-Q water. Prior to the next layer deposition the coated nanogold was stored in

the dark for 1 hour. The coated particles were then incubated with the oppositely charged polyelectrolyte. Each coating step was proved on a NS Zetasizer (Malvern, Milan, Italy) with dynamic light scattering (DLS) for size and monodispersity, and zeta-potential measurements for changes in the surface charge.

The concentration of the gold nanoparticles was determined at 580 nm in an UV/Vis spectrometer (ε=5.14M^{-1} cm^{-1}) [227]. For the experiments to inhibit PrP^{Sc} replication *in vitro*, particles from 1 to 5 layers were prepared, finishing with either a positive (PAH) or negative (PSS) charged layer. All particle preparations finishing with PSS were tagged as nS (n=1-5) and each one with PAH was labeled mA (m=1-5).

1.2 Observation of the coated nanoparticle's structure by TEM

High-resolution transmission electron microscopy (HRTEM) measurements were performed by diluting the coated gold nanoparticles solution with Milli-Q water to a ratio of 1:100. Then the solution was deposited on a carbon-covered 200-mesh copper grid and dried in air at room temperature. The images were acquired with acceleration voltage ranging from 18.5 to 150 kV. The non-digital images were digitized and the data analyses of the images were performed using ImageJ software.

2. PRELIMINARY IN VITRO STUDIES

2.1 Cell culture

ScGT1 cells were seeded in 10-cm plates containing 10 mL of Dulbecco's modified Eagle's medium (DMEM) culture media, supplemented with 10% fetal bovine serum (FBS) and 1% penicillin-streptomycin. ScN2a cells were cultivated in 10-cm plates, containing 10 mL of minimal essential medium with Earle's salt (EMEM) culture media, supplemented with 10% FBS, 1% non-essential amino acids, 1% L-glutamax, 1% penicillin-streptomycin. The cells were grown at 37°C in 5% CO_2 to 95% confluence for 1 week before splitting at 1:10 for further cultivation.

2.2 Drug treatment

Quinacrine was dissolved in PBS at 1 mM. Imipramine was dissolved in 100% dimethyl sulfoxide (DMSO) to a solution with a concentration of 100 mM. This solution was then further diluted into the final stock solution of 10 mM with 10% (v/v) DMSO/PBS. The final concentration of DMSO in the cell medium was never above 0.1%. The nanoparticles were diluted in PBS. The media were refreshed and drugs were added to the cultures 2 days after splitting of the cells and incubated for 5 days. Each experiment was performed using triplicate cultures.

2.3 Cell viability

ScGT1 and ScN2a cells were maintained in DMEM and EMEM, respectively, and supplemented with 10% FBS. After 1 day of incubation, media were aspirated from a confluent 10-cm plate of cells, and cells were detached by addition of 1 mL of 1X trypsin-EDTA solution. Media were added, and cell density determined by cell counting using a haemacytometer. The cell density was adjusted to 2.5×10^5 cells/mL with DMEM for ScGT1cells and 3.0×10^5 cells/mL with EMEM for ScN2a cells. A 96-well, tissue culture-treated, clear bottom, black plate (Costar) wetted with 90 μL of DMEM or EMEM, was incubated at 37°C, prior to use.

One hundred μL of the cell suspension were added to each well and the cells were allowed to settle for 2 hours, prior to the addition of the test compound. Compound library stocks were prepared as described above and diluted 1/20 with sterile PBS prior to use at the required concentrations in 96-well plates. Ten μL of the compounds were added to each well, and the plates were incubated at 37°C in 5% CO_2. Final DMSO concentration was never above 0.1% (v/v). Media were aspirated after incubation of 5 days and cells were washed twice with 200 μL of PBS. One hundred μL of 2.5 μM calcein-AM were added, and the plates were incubated at 37°C for 30 min. Fluorescence emission intensity was quantified using a SpectraMax Gemini EM or SpectraMax M5 fluorescence plate reader, excitation/emission ratio equal to 492/525 nm.

2.4 PrP^{Sc} detection by Western blot

After 5 days of drug treatment, the accumulation of PrP^{Sc} was detected by immunoblotting of lysed cells. One mL of lysis buffer (10 mM Tris-HCl pH 8.0, 150 mM NaCl, 0.5 % nonidet P-40, 0.5 % deoxycholic acid sodium salt) was added to cell plates and the cell lysates were collected after centrifugation at 2,000 rpm for 5 min in a bench microfuge (Eppendorf). The total protein amount of the samples was measured by the bicinchoninic acid assay (BCA) (Pierce).

Five hundred µL of 1 mg/mL ScGT1 or 100 µL of 1 mg/mL ScN2a cell lysates were digested by 20 µg/mL of PK for 1 hour at 37°C. The reaction was stopped with 2 mM phenylmethylsulphonylfluoride (PMSF) and the PK-digested cell lysates centrifuged at 48,000 rpm for 1 hour at 4°C in an ultracentrifuge (Beckman Coulter). The pellets were resuspended in 1X sample loading buffer. For the non-PK digested sample, 50 µg of cell lysates for ScGT1 or 25 µg of cell lysates for ScN2a were used and 2X loading buffer (125 mM Tris HCl, pH 6.8, 10% 2- mercapethanol, 4 % SDS, 0.2 % bromophenol blue, 20 % glycerol) was added in a 1:1 ratio.

The samples were boiled for 5 min at 100°C, loaded onto either a 12% or a 15% Tris-Glycine SDS- PAGE gel, and transferred overnight onto Immobilon P PVDF membranes (Millipore).

Membranes were blocked by 5% nonfat milk, incubated with 1 µg/mL anti-PrP Fab D18 followed by incubation with goat anti-human IgG F(ab)2 fragment conjugated with horseradish peroxidase. Blots were developed with the enhanced chemiluminescent system (ECL,

Amersham Biosciences) and visualized on Hyperfilm (Amersham Biosciences).

2.5 PrP^{Sc} quantification by ELISA

PK digestion of cell lysates was as described above. PK-digested PrP^{Sc} was selectively precipitated by the addition of 0.5% aqueous phosphotungstic acid (PTA, Sigma-Aldrich) solution with continuous shaking at 37°C, 350 rpm for 1 hour, and centrifuged at room temperature, 14,000 x *g* for 30 min. Pellets were dissolved and denatured in 50 µL of 8M guanidine hydrochloride (GdnHCl) in coating buffer (0.1 M sodium bicarbonate, pH 8.2) for 1 hour and diluted into 500 µL of coating buffer. Twenty µL of the suspension were transferred to 96-well MaxiSorp ELISA plates (Nunc), with each well containing 180 µL coating buffer and the plates were sealed and incubated overnight at 4°C.

To increase the immunoreactivity of PrP^{Sc}, coated proteins were denatured *in situ*. Fifty µL of 8M GdnHCl were added to each well and incubated for 10 min at room temperature. The ELISA plates were washed three times with TBST (20 mM Tris-HCl, 137 mM NaCl, 0.05% Tween-20, pH 7.5) and blocked with 200 µL of 3% BSA, made up in TBS (20 mM Tris-HCl, 137 mM NaCl, pH 7.5) sealed and incubated at 37°C. After 1 hour, the plates were washed three times with TBST, and incubated with 100 µL of anti-PrP antibody D18 (2 µg/mL) in 1% BSA/TBS, at 37°C for 2 hours. They were then washed seven times with TBST. One hundred µL of goat anti-human IgG Fab conjugated to HRP and diluted 1:1000 with 1% BSA/TBS were added

to the plates and incubated at 37°C for 1 hour. Again, plates were washed seven times with TBST, and then developed with 100 µL of 1-step TMB (3,3',5,5'- tetramethylbezidine) Turbo ELISA HRP substrate (Pierce).

The reaction was stopped by the addition of 100 µL of 2 M sulfuric acid to the plates. Absorbance at 450 nm was measured using a microplate reader (VersaMax, Molecular Devices). Dose-response curves and EC_{50} values were computed using *GraphPad Prism 4.0*.

2.6 Coated nanogold uptake studies

GT1 and N2a neuronal cell lines (1.0×10^5 cells) were seeded on 24 x 24 mm cover slips in 35 mm-plates with 2 mL of DMEM supplemented with 10% FBS, 1% penicillin-streptomycin and EMEM with 10% FBS, 1% non-essential amino acids, 1% L-glutamax, 1% penicillin-streptomycin, respectively, and were cultured for 24 h at 37°C in 5% CO_2. For the uptake 50 µL of a solution containing either nanogold particles coated with (PSS/FITC-PAH) tagged as 2A, or coated with $(PSS/FITC\text{-}PAH)_2/PSS$ called 5S were added, along with 30 µM of DiA [4-di-16-ASP;(4-(4-dihexadecylamino)styryl)-N-methylpyridinium iodide; Molecular Probes] (labeling intracellular membranes) and incubated for 2, 6, 12, 24 or 48 h at 37°C in 5% CO_2. After incubation, the culture media were aspirated and the adherent cells were washed 2 times with 2 mL of respective media, without antibiotics and sera. Then, the cells were studied by confocal fluorescence microscopy.

The experiments were repeated at least 3 times for each cell line and time. Imaging acquisition was performed with Nikon C1 laser scanning confocal unit (Nikon D-eclipse C1, Japan) attached to an inverse fluorescence microscope (Nikon D-eclipse C1*Si*, Japan) with 100 X/1.49 oil Apo TIRF objective (Nikon, Japan). Excitation was performed with an air-cooled Argon laser emitting at 488 nm for FITC (λ_{ex} = 488 nm, λ_{em} = 520 nm) and a diode laser at 561nm exciting DiA (λ_{ex} = 570 nm, λ_{em} = 630 nm), with appropriate filter sets to collect the fluorescence emission. Images were acquired and processed using the operation software EZ-C1.

2.7 Detection of *in vitro* effect of the nanoparticles on prion fibril formation and amyloid seeding assay (ASA)

Fibril formation was performed in accordance to the method previously described [228] with a few modifications. Briefly, 500 µL of 2 mg/mL ScN2a or ScGT1 cell lysates were used for PTA precipitation by adding 500 µL of PBS/4% Sarkosyl/protease inhibitor and 0.5% PTA with continuous shaking at 37°C, 350 rpm for 1 hour, and centrifuged at room temperature, 14,000 x *g* for 30 min. The pellets were washed with 500 µL of PBS/2% Sarkosyl/protease inhibitor, centrifuged and resuspended in 150 µL of water and then stored at -80^{o}C until use.

In ASA, 4 µL of resuspended PTA pellets were diluted into 400 µL of water and 20 µL of the diluted sample were added to each well containing 180 µL of reaction solution (50 µg/mL MoPrP23-230, 0.4M GdnHCl, 10 µM ThT in 1X PBS buffer) in a 96-well black plate

(BD Falcon). The nanoparticles were added in different concentrations to each well. Each sample was performed in four replicates. Each well contained one 3-mm glass bead (Sigma). The plate was covered with sealing tape (Fisher Scientific), incubated at 37°C with continuous shaking and read on SpectraMax M5 or Gemini EM fluorescence plate reader (Molecular Devices) by top fluorescence reading every 5 min at excitation of 444 nm and emission of 485 nm.

3. ANIMAL INOCULATION

Six week-old CD1 ® IGS mice were provided from Charles River Laboratories. Both male and female gendere were included in the experiments.

3.1 Preparation of brain homogenates pre-treated with functionalized nanogold

Ten percent RML infected brain homogenate (wt/vol) was prepared from pools of terminally RML-sick CD1 mice, while 10% mock homogenate (wt/vol) was obtained from pools of healthy CD1 mice brains. 2A and 5S coated nanogold colloids were separately pre-incubated with both RML and mock brain homogenates at 4°C for 24h. RML and mock brain homogenates untreated with nanoparticles were also subjected to the same pre-treatment. The final nanogold 2A concentration in both RML and mock homogenates was 25.35 nM, while that of nanogold 5S was 26.65 nM.

3.2 Inocula sterility test

Prior to infect the animals, 100 µL of each inoculum was plated on LB medium and then incubated at 37°C for 24 hours. Each sample was finally analyzed for the presence of pathogens. Sterile homogenates were challenged in mice.

3.3 Analysis of the homogenates by TEM

Mouse brain homogenates (both RML and mock) treated with 2A or 5S particles were dissolved in distilled water (1:2). 5µL of suspension were applied to Formvar-carbon-200-mesh nickel grids for 6', negatively stained with uranyl acetate and observed with an electron microscope (EM109 Zeiss, Oberkoken, Germany) operated at 80 kV at a standard magnification (X30000). Samples were evaluated for the presence and amount of 15nm nanogold particles.

3.4 Animal infection

CD1 mice (n=55) were divided in six different groups, named from A to F, housed in ventilated cages and identified by ear-tags. Each group was intracerebrally inoculated with 30 µL of a precise solution: (A) RML (n=8) or (B) mock (n=8) brain homogenate, pre-incubated with nanogold 2A; (C) RML (n=8) or (D) mock (n=8) brain homogenate, pre-incubated with nanogold 5S; (E) RML (n=8) and (F) mock (n=8) brain homogenates, untreated. Animals for each group were anesthetized with sevofluorane and inoculated into the right caudate

nucleus following these stereotaxical coordinates: [caudal 0.38; + 0.5 lateral; 3.5 depth]. Both the preparations of the inocula and their injection were carried out using sterile instrumentation and disposable equipment. Groups of mock-inoculated and uninjected mice were included as controls.

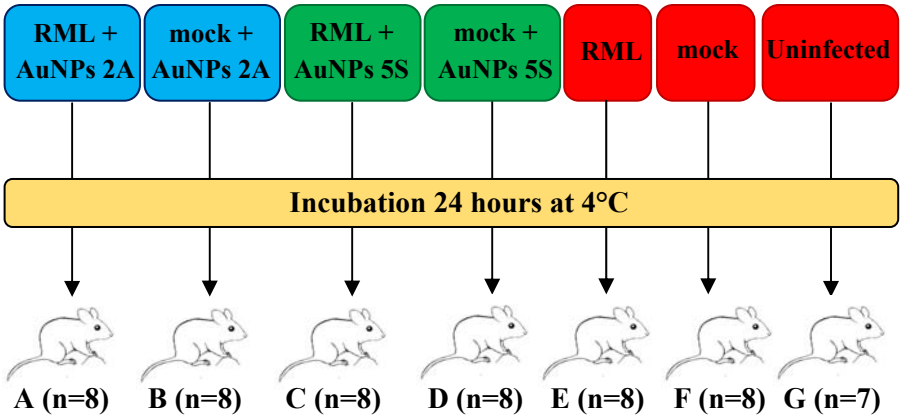

Figure 1. Schematic representation of experimental groups challenged with different combination of RML, mock and AuNPs.

4. BEHAVIORAL MONITORING

Behavioral monitoring was carried out weekly, beginning at 100 days post-inoculation, and included spontaneous locomotor activity in the open field, nest construction test, reactivity to external stimuli and inverted screen test [223]. The incubation time was calculated as the period between the day of inoculation and the appearance of clinical signs of disease, confirmed by a subsequent assessment at 3 days interval. At the terminal stage of disease (characterized by ataxia, hunched dorsal kyphosis, and suppressed righting reflex) clinically affected mice were sacrificed, while the

other mice were monitored for the entire predicted life span and then culled and subjected to necroscopy.

5. MAGNETIC RESONANCE IMAGING (MRI)

Magnetic resonance imaging was performed in clinically symptomatic animals and in non infected control mice on a Brucker BioSpec 70/30 USR Tesla scanner. Mice were anesthetized with isofluorane at a dose approximately of 2.5 L/min, modulated according to the breathing frequency. The animals were positioned on an apposite bed inside the magnet and were monitored throughout the procedure for breathing frequency and body temperature with specific probes. Twenty-six axial slices were acquired for each mouse with T2 High Resolution Turbo Spin Echo sequences. The following parameters were employed: thickness 0.60 mm without gap; TR 3000 ms; TE 27.1 ms; FOV 2.20/2.20cm; 256 matrix.

6. SACRIFICE

At the terminal stage of disease, each animal was sacrificed by euthanasia.

6.1 Euthanasia

Mice were intraperitoneally anesthetized with Tiletamine-Zolazepam, (0,5 mg/10g). The mouse was held gently by the skin on its back, upside down so the gut falls away from surrounding organs. The

needle is introduced in the lower right quadrant of the abdominal area, pulled out slightly, and some fluid is aspirated to check that the needle has not punctured the bladder or caecum. Drug is administered at a slow rate and the needle is removed. When the mouse was deeply anesthetized, intracardiac injection of Embutramide (0,2 mL) was performed and every organ was collected and processed for histological and biochemical analysis.

7. HISTOLOGICAL AND IMMUNOHISTOCHEMICAL ANALYSIS

7.1 Histological examination

All mouse tissues were collected for the study. Regarding CNS, the left hemisphere of each mouse brain was fixed in Carnoy solution at 4°C for 24h [224], while the right hemisphere was frozen at -80°C for western blot analysis.

The same procedure was followed for the other organs (i.e. brain stem, muscle, spleen, liver, kidney, intestinal Peyer's patch etc.). Fixed brain samples were cut in four standard coronal levels, dehydrated, and embedded in paraplast. 7-μm thick serial sections from paraffin embedded tissues were stained with hematoxylin-eosin (H&E) or probed with different antibodies (i.e.: 6H4, GFAP, CNPase and Caspase-3). Spongiform profiles were determined on H&E-stained sections, by scoring the vacuolar changes in nine standard grey matter area as described [99].

7.2 Immunohistochemical staining

Sections were immunostained with monoclonal antibody to PrP (6H4 1:1000, Prionics), monoclonal antibody to myelin protein (CNPase 1:500, Sigma Aldrich), polyclonal antibody to glial fibrillary acidic protein (GFAP 1:1000, Dako) and a polyclonal antibody to apoptotic cells (Caspase-3 1:100, Millipore). Before PrP immunostaining, the sections were sequentially subjected to proteinase K digestion (10μg/ml, R_T, 5') and guanidine isothiocyanate treatment (3M, R_T , 20'), and non-specific binding was prevented using Animal Research Kit Peroxidase (Dako). Immunoreactions were visualized using 3-3'-diaminobenzidine (DAB; Dako) as chromogen.

8. BIOCHEMICAL ANALYSIS

8.1 Proteinase K immunoblot analysis

Ten percent (wt/vol) brain homogenates from frozen tissues were prepared in lysis buffer (100 mM sodium chloride, 10 mM EDTA, 0.5% Nonidet P40, 0.5% sodium deoxycholate in 10 mM Tris-HCL, pH 7.4). Aliquots of cleared lysate equivalent to 100μg were digested with 50μg/ml of proteinase K for 1 hour at 37°C. Reactions were terminated by the addition of Phenylmethanesulfonyl fluoride (PMSF, 5mM). Treated homogenates were loaded on 12.5% polyacrylamide gels, transferred to polyvinylidene fluoride membranes and probed with anti-PrP antibody 6H4 (1:10,000, Prionics) and anti CNPase

antibody (1:1,000; Sigma Aldrich). The immunoreactions were visualized by enhanced chemiluminescence system (Amersham).

9. DATA ANALYSIS

9.1 Images capture

Stained sections were examined on a Nikon Eclipse E800 microscope, images captured using a Nikon Digital Camera DXM1200 and analyzed with NIS-Elements software.

9.2 Statistical analysis

Statistical analyses were performed using the *GraphPad-Prism 4.0* software. Kaplan-Meier survival curves were plotted, and differences in survival between groups of mice inoculated with RML (positive control) and RML pre-incubated with nanogold 2A or nanogold 5S were compared using the Logrank test. Densitometric analysis were performed on images captured by the *Photoshop 7 program* and analyzed with *Lucia measurement software version 4.6.* Using the area density tool, mean density were determined from a selected rectangular area that enclosed three glycoforms of PrP^{Sc} in each lane. This area remained constant for each density measurement. Mean densities were exported to Microsoft Excel 2003 and *GraphPad Prism 4.0* software for analysis. Densitometric quantization of PrP^{Sc} amount in each sample was analyzed by unpaired, double tailed *t*-test.

CHAPTER 2

RESULTS

A NOVEL CLASS OF POTENTIAL PRION DRUGS: PRELIMINARY IN VITRO AND IN VIVO DATA FOR MULTILAYER COATED GOLD NANOPARTICLES

1. NANOPARTICLES EXPERIMENTAL THERAPEUTIC APPROACH

The efficiency of different polyelectrolyte covered gold nanoparticles (AuNPs) was evaluated in CD1 mice inoculated with pre-treated AuNPs brain homogenates (RML and mock).

The physical characteristics of the coated nanoparticles are given in Table 1.

Nanoparticles	Size (DLS) (nm)	Zeta potential (mV)	Concentration (nM)	Number of particles/mL
	Mean ± SD	Mean ± SD		
NG-15nm	19.9 ± 0.2	-40.0 ± 0.4	33.0	$1.99 \times 10^{+13}$
1A*	105.1 ± 2.9	52.8 ± 0.9	18.7	$1.12 \times 10^{+13}$
2A	128.9 ± 9.9	63.0 ± 0.9	30.3	$1.83 \times 10^{+13}$
3A	112.8 ± 6.3	58.8 ± 0.9	32.7	$1.97 \times 10^{+13}$
4A	110.9 ± 3.2	65.4 ± 5.4	14.2	$8.55 \times 10^{+13}$
5A	110.1 ± 1.4	56.4 ± 3.2	14.2	$8.55 \times 10^{+13}$
1S*	59.0 ± 1.7	-50.7 ± 1.3	37.9	$2.28 \times 10^{+13}$
2S	88.7 ± 5.4	-48.1 ± 3.8	29.2	$1.76 \times 10^{+13}$
3S	103.8 ± 0.6	-56.0 ± 3.3	24.5	$1.48 \times 10^{+13}$
4S	98.6 ± 5.0	-49.8 ± 6.1	16.1	$9.72 \times 10^{+13}$
5S	94.0 ± 0.7	-53.6 ± 0.5	14.2	$8.55 \times 10^{+13}$
NG-46nm	45.7 ± 0.3	-32.4 ± 3.2	82.9	$4.99 \times 10^{+13}$
2A	86.9 ± 1.8	50.8 ± 0.8	61.3	$7.38 \times 10^{+12}$
5S	155.4 ± 8.3	-39.6 ± 0.83	34.0	$4.10 \times 10^{+12}$

Table 1. Physical characteristics of the nanoparticles. *A - outermost layer PAH and S - outermost layer PSS. The mean particle size and zeta-potential were obtained from cumulative measurements (SD, n=6).

Several layers (1-5) of oppositely charged polyelectrolytes (PAH and PSS) were deposited via LbL technique onto nanogold particles with a size diameter of 19.9 ± 0.2 nm (DLS). DSL usually gives a larger diameter than electron microscopy because it also measures the ionic shell (citrate) around the hard core (gold). As an example, Fig. 1

showed the HRTEM image of a coated (2A) nanogold particle. The particle is around 15 nm in diameter and, in the dehydrated form in ultrahigh vacuum, the 2 layers coating measures less than 1 nm. The thickness is not perfectly homogenous, but the coating is covering the particle surface completely.

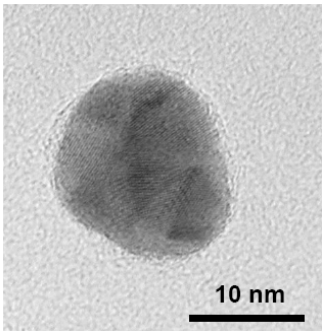

Figure 1. HRTEM image of a 2A coated nanogold particle; it was acquired with an acceleration voltage of 200 kV.

The concentration was determined via UV-VIS absorption spectrometry using the Beer-Lambert law (abs at 518 nm and ε at 5.14 × 107 M-1cm-1) [227]. Up to now, UV-VIS absorption spectrometry could only determine the nanogold concentration. From Table 1 can be noted that the diameter of particles, when coated with PAH, are bigger in comparison with PSS, this could be attributed to the nature of individual polyions. PSS is a strong, short-chain (~23-mer) polyelectrolyte while PAH is a weak, long-chain (~259-mer) polyelectrolyte. Thus, a possible explanation could be that in the PAH layer the longer molecules connect to the particles surface only in a few positions, and PSS intercalate in the open structures condensing them on the surface. Previous experiments with SERS (surface

enhanced Raman spectroscopy) and Raman spectroscopy, indicated that if PSS is the starting layer, citrate is substituted by PSS and the polyanion is oriented with the aromatic moieties parallel to the gold surface. When PAH is the starting layer, it replaces the citrate and connects with the gold surface via its amino group. In addition to the increase of diameter, the coating was confirmed by the change in charged surface (zeta-potential measurements); when the polycation PAH is the deposit, a positive charge is given; when the polyanion PSS is the deposit, a negative charge is given. It is interesting to note that although citrate-reduced nanogold already carries a negative charge, an increase of negative charge is observed when PSS is the starting layer, giving additional confirmation of the coating. Finally, experiments were performed to investigate if the curvature of the nanogold had an effect on functionality. To this purpose, gold nanoparticles possessing a bigger diameter (45.7 ± 0.3 nm) were also prepared and tested.

Potency of known drugs such as quinacrine and imipramine was used as control for anti-prion activity in our cell models. Table 2 indicates the potency of either quinacrine or imipramine to be similar to previous publications [229], namely EC_{50} of quinacrine was 0.4 ± 0.1 and 0.3 ± 0.1 μM for ScGT1 and ScN2a, respectively; whereas for imipramine EC_{50} was 6.2 ± 0.4 and 5.5 ± 0.5 μM for ScGT1 and ScN2a, respectively. As a control, citrate stabilized gold particles without polyelectrolyte layers did not show any detectable prion inhibitory activity.

The number of layers, in addition to the surface charge of the outermost layer for the coated nanoparticles influenced the neuronal

ScGT1 and ScN2a cell survival, as shown in Table 2. Cytotoxicity was determined by measuring surviving cells after incubation in the drug-doped medium for 5 days, assayed with calcein-AM in a fluorescence plate reader. For these experiments, carried out in 96 well-plates, cells were grown from a starting density of 25,000 ScGT1cells and 30,000 ScN2a cells per well. The cell viability was between 92-100% for positively charged particles (1-5 A) and 74-100% for negatively charged particles (1-5 S) (Table 2).

Compounds	**PrP^{Sc} inhibition***		**% cell viability ± SE†**	
Small molecules	**ScGT1 (EC_{50} ± SE, µM)**	**ScN2a (EC_{50} ± SE, µM)**	**ScGT1**	**ScN2a**
Quinacrine	0.4 ± 0.1	0.3 ± 0.1	100 ± 4	100 ± 2
Imipramime	6.2 ± 0.4	5.5 ± 0.5	100 ± 7	100 ± 5
Nanoparticles	**ScGT1 (EC_{50} ± SE, pM)**	**ScN2a (EC_{50} ± SE, pM)**	**ScGT1**	**ScN2a**
Positive surface charge –PAH (NG-15nm)				
1A	8.3 ± 0.5	8.4 ± 0.6	100 ± 6	100 ± 3
2A	8.8 ± 0.2	24.5 ± 1.0	100 ± 1	97 ± 1
3A	10.1 ± 0.2	20.4 ± 0.5	100 ± 7	96 ± 3
4A	25.4 ± 1.3	25.1 ± 1.2	100 ± 6	100 ± 5
5A	20.1 ± 1.1	30.0 ± 1.4	100 ± 3	92 ± 1
Negative surface charge –PSS (NG-15nm)				
1S	121.4 ± 6.5	248.7 ± 12.9	95 ± 2	92 ± 5
2S	99.8 ± 4.7	220.3 ± 11.8	97 ± 1	87 ± 3
3S	70.1 ± 3.2	149.5 ± 6.1	74 ± 7	90 ± 3
4S	50.3 ± 2.0	130.1 ± 5.4	100 ± 2	90 ± 7
5S	35.0 ± 1.4	129.9 ± 7.1	84 ± 8	93 ± 4
NG-46nm				
2A	10.3 ± 0.3	30.2 ± 1.7	100 ± 4	94 ± 2
5S	89.7 ± 3.5	329.5 ± 10.7	90 ± 1	91 ± 6

Table 2. PrP^{Sc} inhibition and cellular toxicity of quinacrine, imipramine and the nanoparticles in ScGT1 and ScN2a cells. *Compound concentration required to reduce PrP^{Sc} level 50% versus untreated cells. †Cell viability at EC_{50} values was determined by calcein-AM cytotoxicity assay and expressed as an average percent of viable cells versus control untreated cells. Standard errors from three experiments are given.

Moreover, the concentration at which a complete inhibition of PrP^{Sc} formation in ScGT1 and ScN2a cells takes place could be determined from the SDS-PAGE gels. Particle preparations were added at different concentrations to scrapie-infected cells, and the inhibitory activity was measured over 5 days. PrP^{Sc} levels were quantified, either by western blot or by ELISA.

The resulting EC_{50} of the particles with a positive outermost layer (mA) were in the range of 8.3 ± 0.5 - 25.4 ± 1.3 pM in ScGT1 and 8.4 ± 0.6 - 30.0 ± 1.4 pM in ScN2a cells (Table 2). In both cases, the influence of size and number of layers on efficacy is limited. However, prion inhibition by particles with a negative outermost layer (nS) showed an increase in efficacy with a higher number of layers. In particular, EC_{50} of 1S was 121.4 ± 6.5 pM and 5S was 35.0 ± 1.4 pM in ScGT1 while EC_{50} of 1S was 248.7 ± 12.9 pM and 5S was 129.9 ± 7.1 pM in ScN2a cells (Table 2). In order to investigate a possible influence of the particle curvature on the efficacy of prion inhibition, bigger gold nanoparticles were used. For 46 nm nanogold particles, the efficacy and cytotoxicity was only tested exemplarily for 2A and 5S coatings. Both tested cell types showed viability (Table 2) in the range of 90-100% and therefore it was not significantly different from those observed for the smaller nanogold (15 nm). Prion inhibition of 2A -46 nm was similar to 2A, and 5S -46 nm was 3 times less effective than 5S (Fig. 2 and Table 2).

The uptake mechanism of nanogold particles coated with 2A or 5S was followed in the two different types of immortalized neuronal cells used in this study, GT1 and N2a.

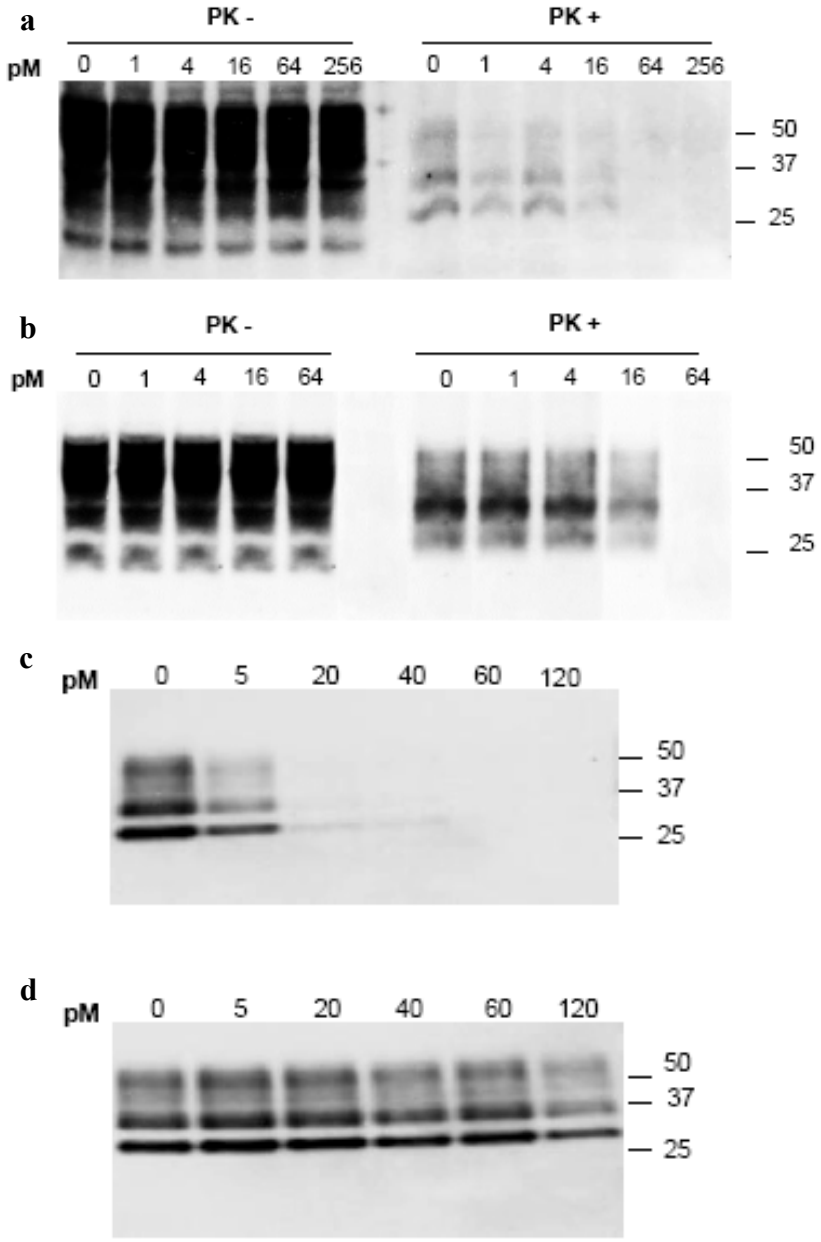

Figure 2. Treatment of ScGT1 cells with nanoparticles 2A, 5S and 2A -46 nm, 5S -46 nm. After 2 days in cell culture, the media were refreshed and the nanoparticles added at the indicated concentrations and incubated for 5 more days. Cell lysate proteins were quantified, treated with or without PK and immunoblotted using anti-PrP Fab D18. Five- hundred μg of ScGT1 protein cell lysates were digested by 10 μg PK and 50 μg protein was used for non-PK samples; ScGT1 cells treated with 2A (a); ScGT1 cells treated with 5S (b); ScGT1 cells treated with 2A -46 nm (c); ScGT1 cells treated with 5S -46 nm (d).

In Fig. 3 examples for the GT1 and N2a cells are shown at 2 and 24 hours, after 5S coated nanogold uptake. The particles were internalized mainly by endocytosis.

Co-localization was found for the red fluorescent dye DiA, incorporated in the phospholipid membrane of the endosomes, and green color, due to FITC-PAH, bound to the particles resulting in a yellow signal (Fig. 3a, b, c). This co-localization can be clearly seen in the images of the 3D optical sectioning depicted in Fig. 3a.

Images were acquired 2 hours after starting the incubation of GT1 cells with the coated nanogold particles.

Particles attached to the cell surface show a clear green fluorescence (3rd section, white circle). When the coated particles are localized in endosomes the signal is yellow due to co-localization of the red lipid-staining dye and the FITC from the particles (7th section, arrow). Even after 24h the GT1 cells are still presenting the yellow signal of nanogold in vesicles, with some clustering taking place, which could be indicative for exocytosis of the particles (Fig. 3b).

The same uptake mechanism could be observed for N2a cells. After 2h of incubation (Fig. 3c), a homogenous distribution of the nanogold particles in endosomes located in the cytosol could be seen.

Since potent anti-prion activity for 2A and 5S was found in scrapie-infected cells, these two particles were chosen to test their ability to inhibit recombinant PrP fibril formation in amyloid seeding assay (ASA) [228].

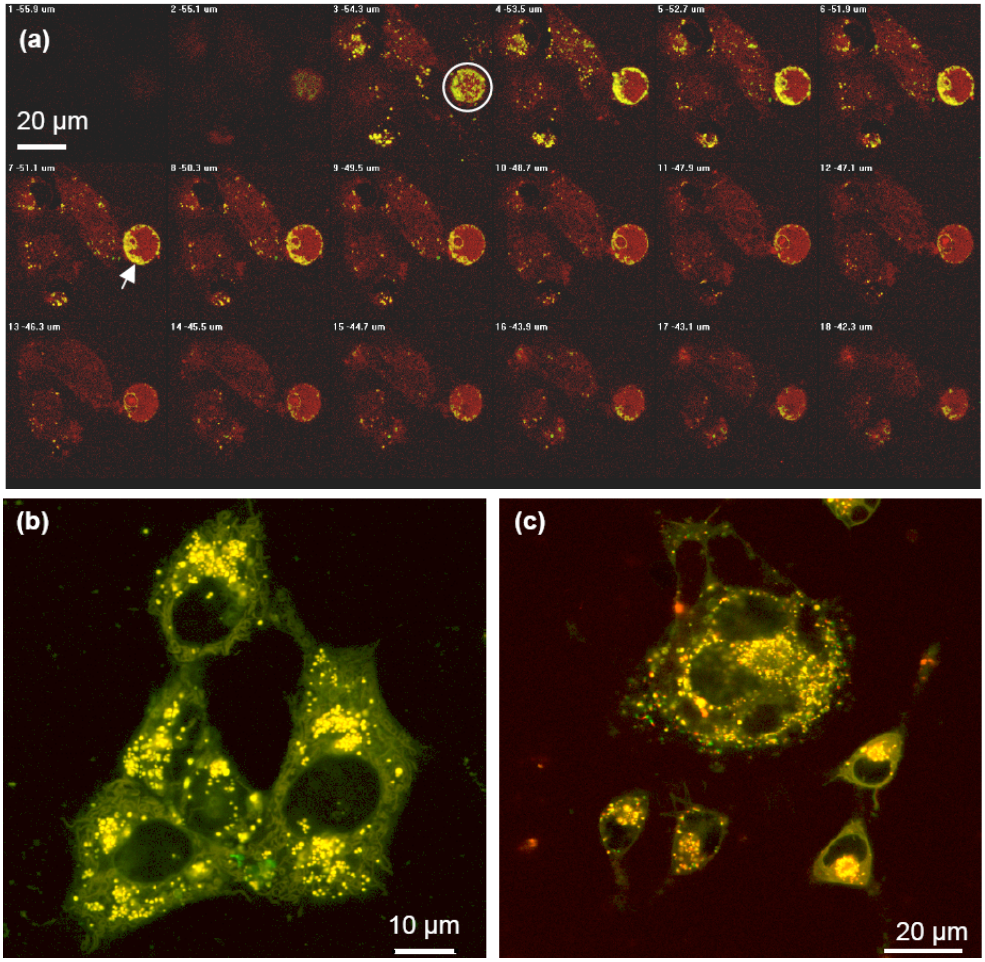

Figure 3. Uptake of coated nanoparticles into immortalized neuronal cells. The particles were labeled with FITC (green) and cell membranes were stained with DiA (red). Co-localization of particles in vesicles is indicated by a yellow signal. 3D optical sectioning of GT1 cells incubated for 2 hours with 5S coated nanogold (a). The white circles in section 3 indicate nanogold attached to the cell's surface and therefore showing only green fluorescence. The arrow in section 7 indicates endosomes filled with nanoparticles and therefore appearing yellow. 5S coated nanogold in GT1 cells after 24 hours of incubation (b). 5S coated nanogold in N2a cells after 2 hours of incubation (c).

Using full-length recombinant MoPrP(23-230) as template and ScN2a- and ScGT1-PTA precipitated prions as seeds in a standard ASA assay, 2A and 5S extended the lag phase by 5-15 hours, at concentrations of 50 pM and 200 pM respectively, therefore showing a much slower kinetics than the control (Fig. 4).

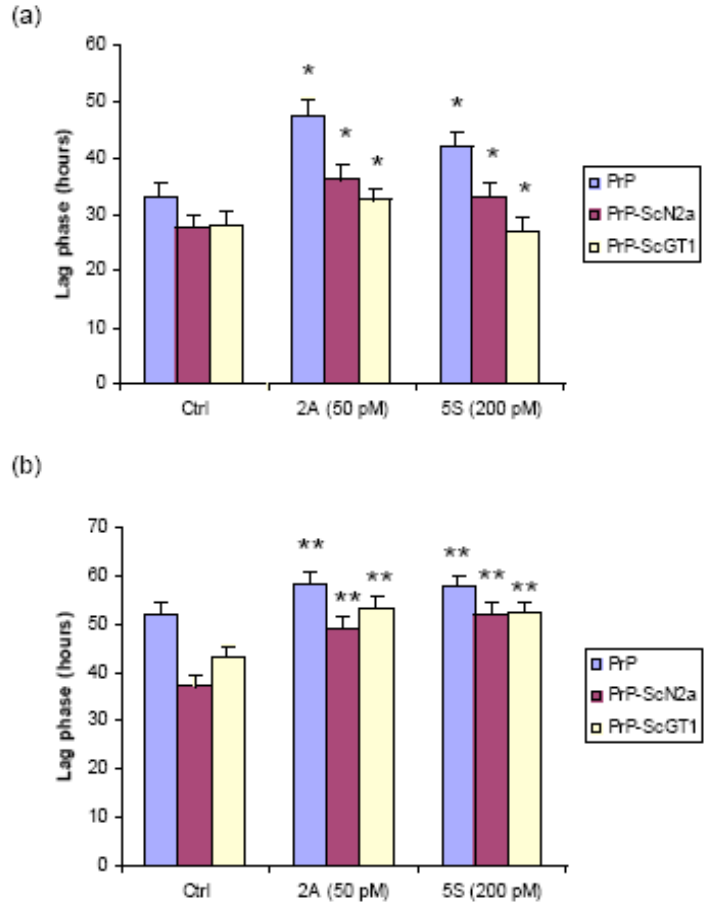

Figure 4. Effect of the nanoparticles on fibril formation and ASA. Lag phase of amyloid-formation kinetics are compared between (a) SpectraMax M5 and (b) Gemini EM instruments (Molecular Devices) in the assays, using full-length MoPrP(23-230) and amyloid seeding with ScN2a- and ScGT1-PTA precipitated protein in presence of coated gold nanoparticles. Fifty pM of 2A coated nanogold or 200 pM of 5S coated nanogold were added to each well. The Student's *t*-test (two-tailed) was used to determine significant differences among measurements (n=4). **P*<0.05, ***P*<0.01.

Given the potency of 2A and 5S in delaying of PrP fibril formation, we suggest that these nanoparticles may interact directly with PrP to prevent its conversion to the pathogenic PrP^{Sc}-like form.

In standard recombinant PrP fibril formation assays using MoPrP(23-230) alone, both 2A and 5S exhibited PrP amyloid fibril forming inhibitory activity. In addition, in ASA, PrP^{Sc} proteins from PTA-precipitated ScGT1 or ScN2a cell extracts were able to seed amyloid

PrP formation, and to promote fibril formation exhibiting much shorter lag phase kinetics. On the contrary, in the presence of nanoparticles, the lag phase of amyloid PrP formation was extended significantly in ASA. In light of these results, the ASA could also be utilized to study the mechanistic steps involved in the inhibitory effects of different drugs screened for prion diseases, and in particular of nanogold particles.

CD1 mice were intracerebrally inoculated with 30 μL of 10% RML brain homogenates pre-incubated with a nanomolar concentration of gold particles 2A or 5S. Before the inoculation, TEM (transmission electron microscopy) analysis of AuNPs-treated homogenates confirmed the presence of scattered particles in the whole samples (Fig. 5).

Figure 5. TEM analysis of different AuNPs pre-incubated brain homogenates was performed and scattered particles were always observed.

The incubation period of mice treated with both 2A (139 ± 3 days) and 5S (135 ± 2 days) were significantly longer (respectively p = 0.0021 and p = 0.023, Logrank test) than that of control animals infected with pure RML homogenate (128 ± 2 days) (Graph. 1).

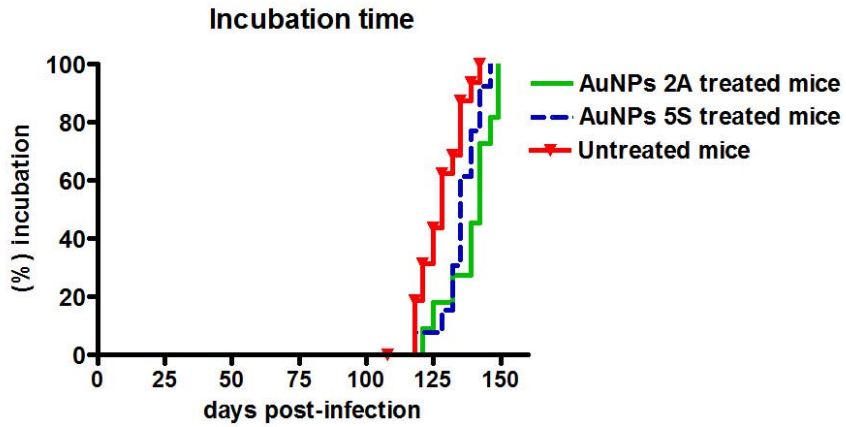

Graphic 1. Incubation time of 2A or 5S AuNPs treated and untreated mice intracerebrally infected.

From a behavioral standpoint no particular differences were observed during disease progression for nanogold 2A- or 5S-treated animals and RML control mice. The initial clinical signs consisted in hyperexcitability, followed by marked lethargy, until reaching complete ataxia in the terminal stage of disease. The clinical course of the disease was similar to that of CD1 mice treated with AAV2-ScFvD18 and infected with RML (for clinical details see therapeutic approach I). Only 2A-treated animals showed a modest but statistically significant increase of survival time compared with controls (163 ± 3 vs 152 ± 3 days; p = 0.025 Logrank test), whereas treatment with nanoparticle 5S was not as effective (151± 1 vs 152 ± 3 days; p = 0.075, Logrank test) (Graph. 2).

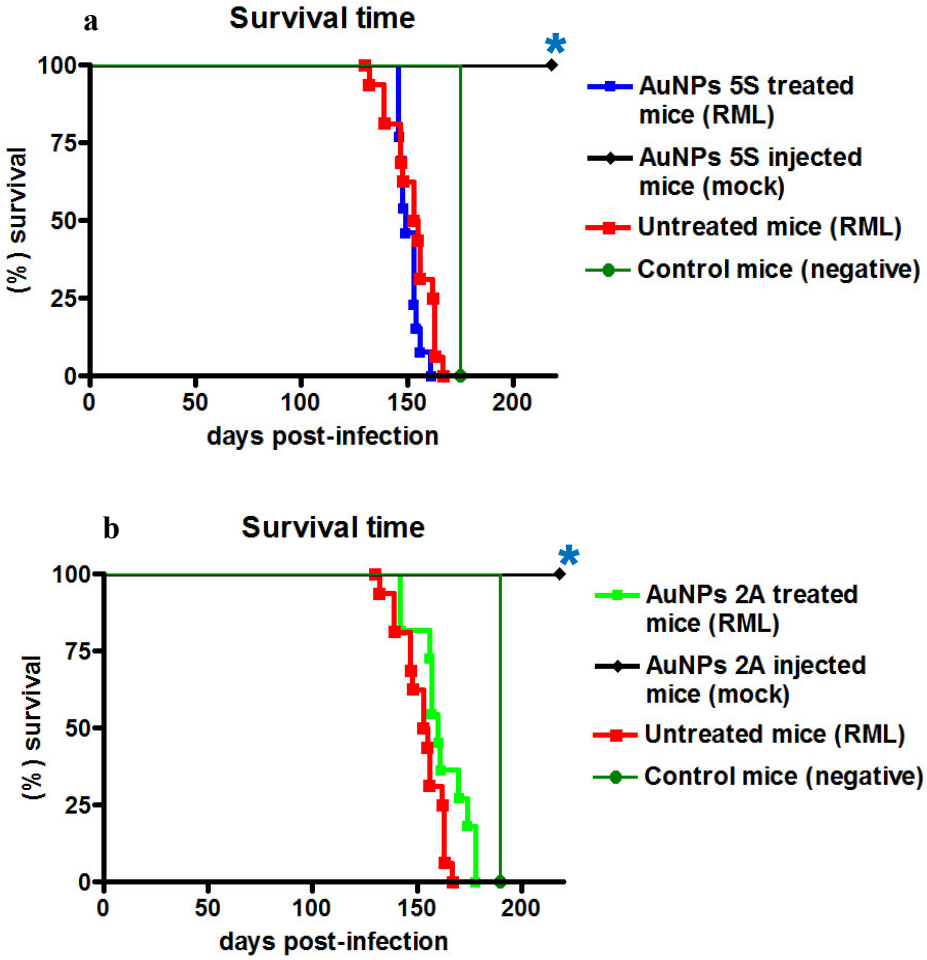

Graphic 2. Survival time of 5S (a) and 2A (b) AuNPs treated mice compared to that of untreated animals; * these animals were sacrificed at the end of their predicted lifespan (~700 days). Control mice have been sacrificed when all RML-infected animals were collected

Histopathological assessment of H&E stained sections was carried out on all mouse organs (brain, spleen, liver, kidney, lung, muscles, etc.). Neuropathological results (Graph. 3), showed similar moderate spongiform alterations in each group of mice with a major involvement of the hippocampus (Fig. 6a, b, c), thalamus (Fig. 6d, e, f), and somatosensory cortex.

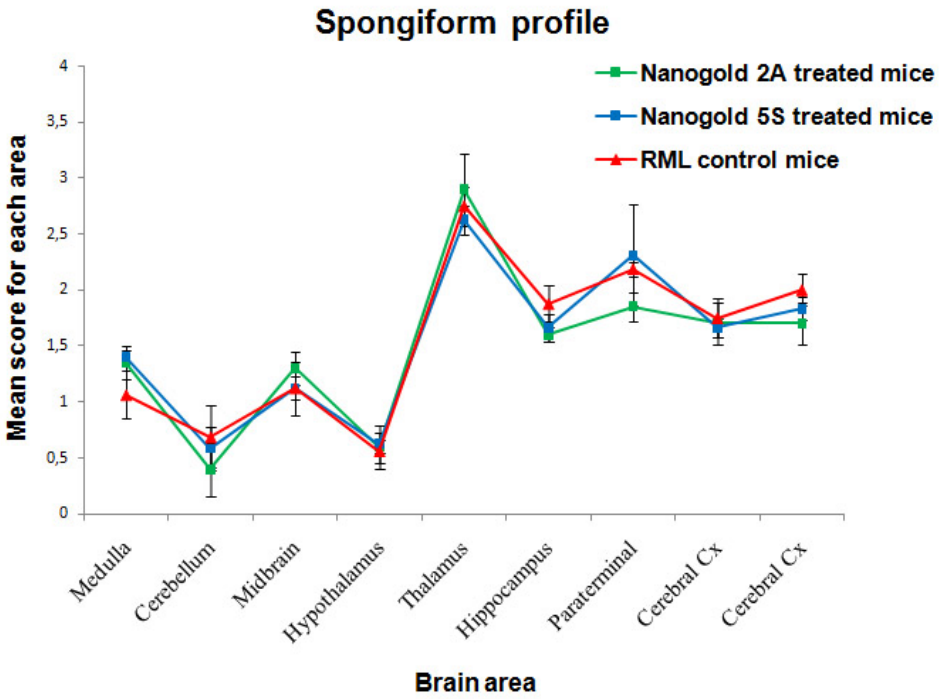

Graphic 3. Vacuolar degeneration in standard brain regions. Thalamus, hippocampus, septum and cerebral cortex were severely affected.

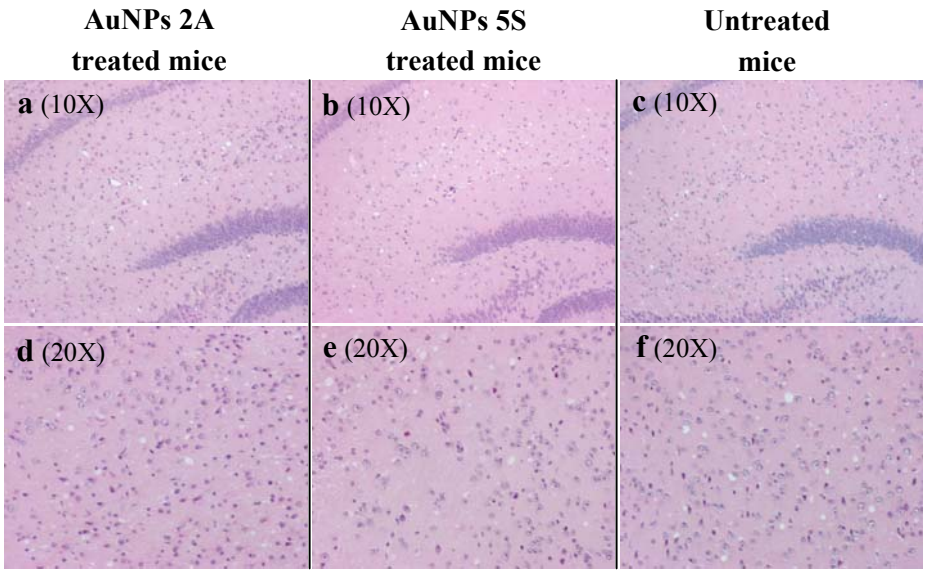

Figure 6. H&E stain shows the mainly affected brain area of AuNPs 2A treated mice (a and d), AuNPs 5S treated (b and e) and untreated animals (c and f). In particular, hippocampus (a, b and c) and thalamus (d, e and f) are shown.

Immunohistochemistry showed PrP^{res} immunoreactivity in the form of synaptic and diffuse deposits in the cerebral cortex, basal ganglia, hypothalamus, hippocampus, brainstem, cerebellum, and thalamus, which was often affected by coarse PrP^{res} deposition (Fig. 7). In particular, AuNPs 5S treated mice and control animals showed similar amount of PrP^{res} deposition, while AuNPs 2A treated subjects evidenced high amount of PrP immunoreaction.

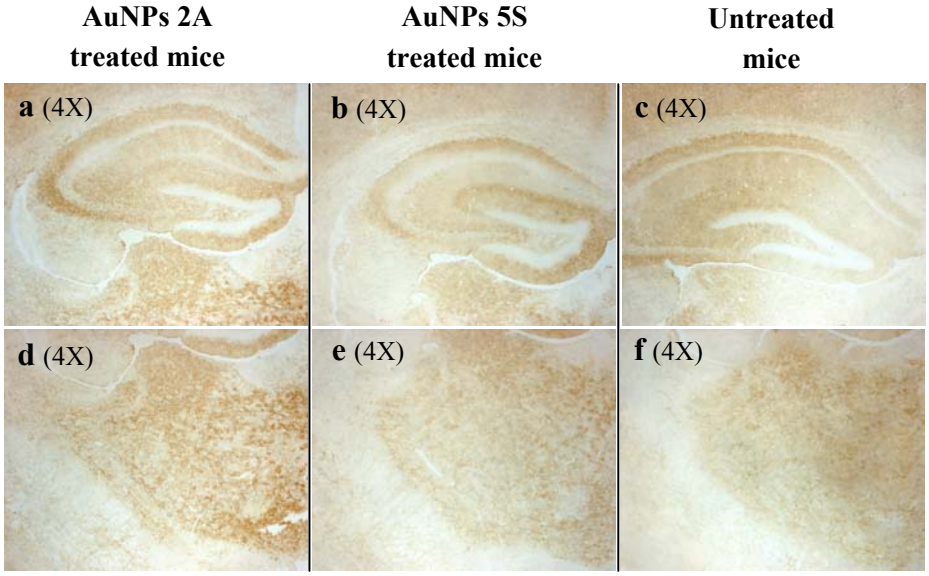

Figure 7. Anti-PrP antibody (6H4) immunohistochemical stain reveals PrP^{res} deposition in the brain of AuNPs 2A treated mice (a and d), AuNPs 5S treated mice (b and e) and untreated animals (c and f). In particular, hippocampus (a, b and c) and thalamus (d, e and f) are shown.

Immunoblot analysis of brain homogenates revealed the same PrP^{res} profile for all groups of mice (Fig. 8a); densitometric analysis, confirmed the presence of similar PrP amount in both AuNPs 5S treated and untreated mice (p = 0.8534, t-test), while AuNPs 2A treated mice showed higher amount of PrP^{res} than that of untreated animals (p = 0.0075, t-test).

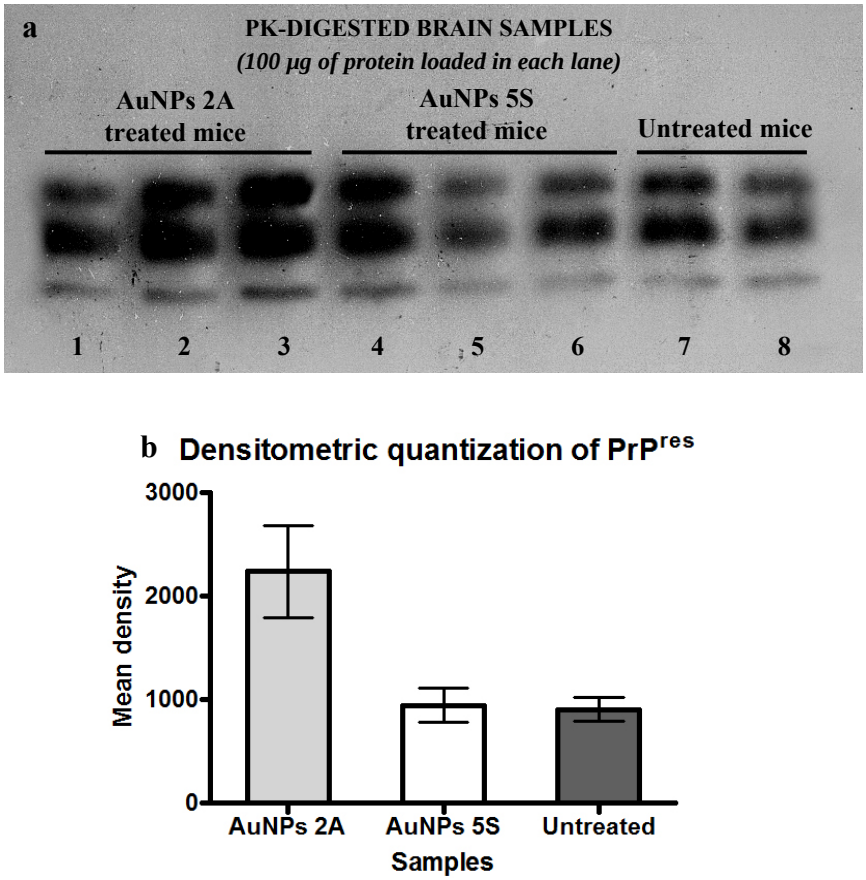

Figure 8. Western blot analysis of proteinase K-digested brain homogenates from 2A or 5S AuNPs treated animals and untreated mice intracerebrally infected with 10% RML (a). The blot was probed with the anti-PrP antibody 6H4; statistical analysis (b) revealed significant differences in PrP^{res} amount between AuNPs 2A treated animals and controls, while no differences were observed between AuNPs 5S treated and untreated mice (double tailed, unpaired, *t*-test).

Glial immunoreaction (GFAP) was comparable between the groups of infected mice and was mainly detected in the hippocampus, thalamus, brainstem and the granular layer of the cerebellar cortex (Fig. 9).

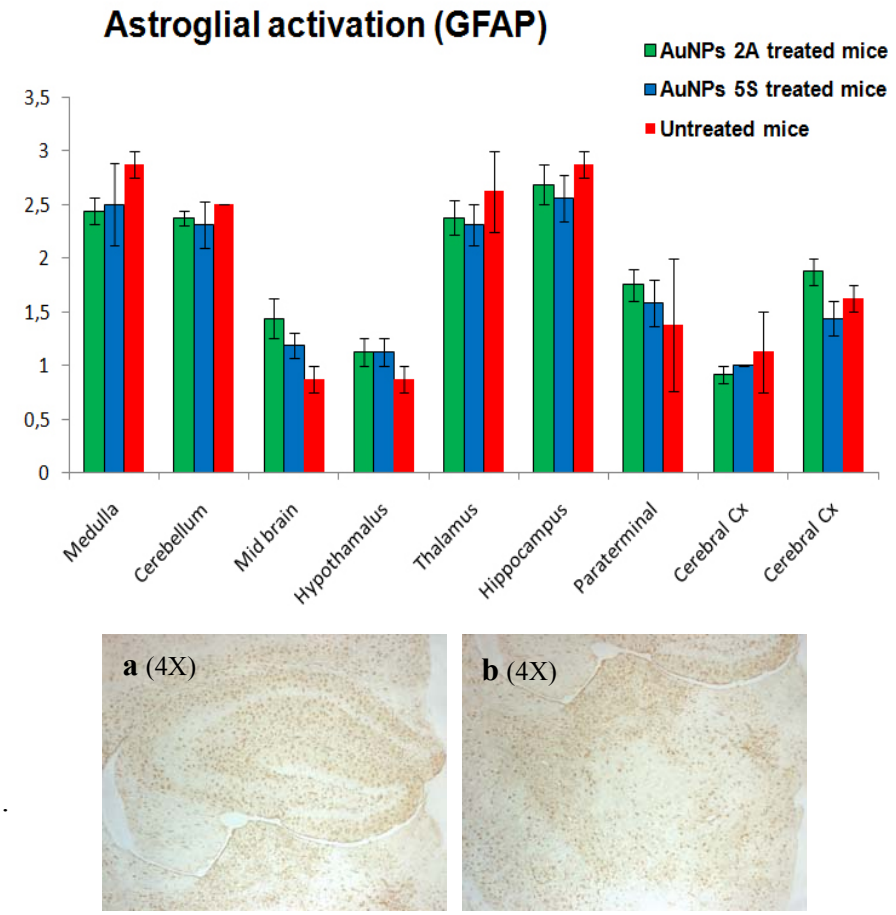

Figure 9. Astrocytic activation throughout different CNS regions of AuNPs treated and untreated mice. The same activation pattern between groups was observed; in particular heavy GFAP labeling into the hippocampus (a) and thalamus (b) was detected.

Kidneys, spleens and livers from mice inoculated with both RML and mock nanogold-treated homogenates were analyzed, and indicated the lack of acute systemic toxicity following the injection of the particles (Fig. 10).

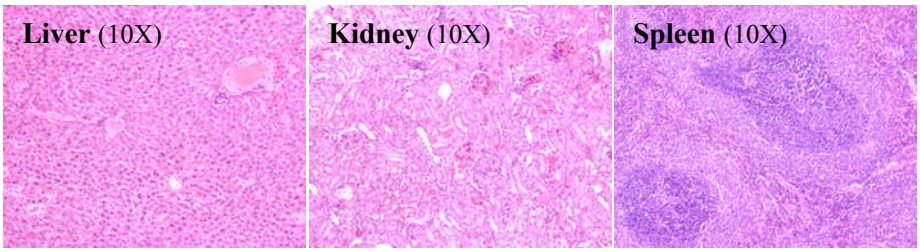

Figure 10. H&E stain of liver, kidney and spleen of either 2A or 5S AuNPs treated mice did not show any pathological alteration related to the intracerebral inoculation of the particles.

Even the brains of mice inoculated with 2A or 5S pre-treated mock homogenates did not reveal specific alterations related to a potential toxic effect of the particles on the CNS. These results were also confirmed by MRI analysis to which the animals were periodically subjected during the experiment (Fig. 11).

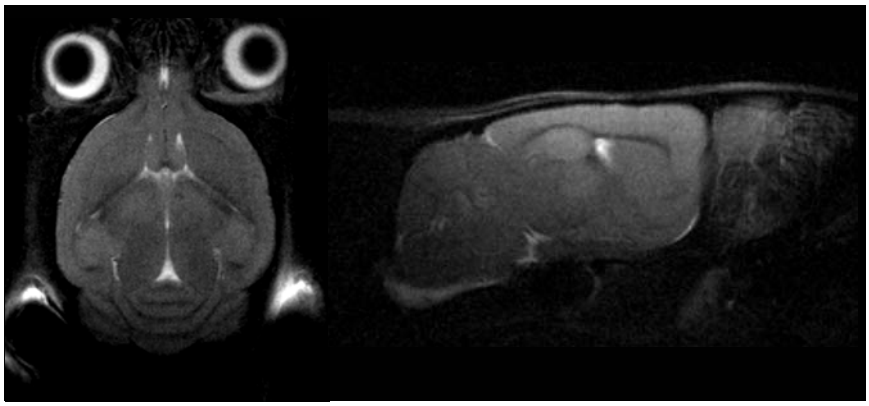

Figure 11. T2 weighted MRI images confirmed the lack of neuropathological alterations in the brain of both 2A or 5S AuNPs injected mice (~200 days after the inoculation).

DISCUSSION, SUMMARY and FUTURE PERSPECTIVES

1. DISCUSSION

Among human TSEs, sporadic Creutzfeldt-Jakob disease (sCJD) is the most commonly diagnosed prion disorder, occurring with a relatively uniform incidence of around one individual per million per annum. Although a wide range of ages at onset has been reported, most cases of sCJD occur in the seventh decade of life, with male and female being affected equally. The disease usually presents as a rapidly progressive dementia accompanied by other neurological abnormalities, among which ataxia, myoclonus, visual abnormalities, and pyramidal and extrapyramidal signs are common. Diagnostic tests include the electroencephalogram (EEG), which shows a characteristic abnormality with periodic triphasic complexes in approximately 65% of patients. Brain scans using Magnetic Resonance Imaging (MRI) of patients with sCJD often show an increased signal in the basal ganglia, with variable patterns of intensity in the cerebral cortex. In the CSF of most patients, levels of 14-3-3 and phopshorylated tau proteins are increased, making them a valuable diagnostic criteria for this disorder. The etiology of sCJD is unknown. It has been suggested that this disease might occur as a consequence of a random event that results in the generation or spontaneous conversion of PrP^{C} into the pathological form PrP^{Sc} in the brain. The mechanisms that stabilize PrP^{C} structure are largely unknown but, once it assumes its pathological conformation, that is PrP^{Sc}, this can bind to another PrP^{C} molecule and induce a conformation change. This starts a self-perpetuating vicious cycle allowing PrP^{Sc} to replicate without DNA, using the host cell's PrP^{C} as a template. Most inherited prion diseases (in autosomal

dominant fashion) such as GSS, FFI or inherited forms of CJD (fCJD) are the result of a point mutation in PrP^{C} that increases the propensity to assume an abnormal conformation.

The resistance of PrP^{Sc} to protease digestion forms the basis for biochemical detection of the pathological hallmark of prion disease. When tissue homogenates are examined by Western blot analysis using antibodies to PrP, samples containing PrP^{Sc} show immunoreactivity even after treatment with proteinase K. In 1996, a variant of CJD form (vCJD) with unusual clinical, biological, and pathological features was identified by the National CJD Surveillance Unit in the United Kingdom. A causative relationship with the epidemic of BSE in cattle seemed likely. Clinically, there were a relatively young ages at onset (mean 27 years, range 12 to 74 years). The length duration of illness (mean 13 months) and the clinical presentation were also characteristic. The latter includes psychiatric and/or sensory manifestations at onset followed by severe progressive ataxia, extrapyramidal and pyramidal signs, and a progressive dementia that in some cases is severe. In vCJD the EEG is abnormal but does not exhibit the characteristic abnormalities seen in sCJD. Cranial MRI scans show a symmetrical area of hyperintensity in the posterior thalamus (the "pulvinar sign") that is highly characteristic and has been incorporated into the clinical diagnostic criteria for vCJD. Pathologically, "florid" plaques, extensive accumulation of PrP^{Sc} and spongiform changes most marked in the caudate nucleus and putamen are typical of this form of disease. In the thalamus, there is extensive neuronal loss and gliosis in posterior nuclei, corresponding to the abnormalities on MRI. In vCJD, Western blot

analysis of the brain shows a characteristic PrP^{res} isotype with a predominant diglycosylated band and an unglycosylated band that averages around 19 kDa. This glycosylation pattern is similar to that in Western blot of PrP^{res} in cattle with BSE and in other species (i.e. mice) that have been infected with BSE. Generally, the transmission of prion between different species is quite ineffective due to differences in the PrP sequence (species barrier). This barrier does not provide absolute protection; therefore, transmission of scrapie to cattle and transmission of BSE from cattle to humans resulted in the emergence of vCJD. In transmissible prionoses, exogenous PrP^{Sc} present in the inoculum is responsible for the conformational transformation of host PrP^{C}. Upon entering an organism by oral administration, PrP^{Sc} initially replicates within the lymphoreticular organs, including the spleen, lymph nodes and tonsils, for months to years prior to neuroinvasion and the onset of neurological symptoms. Therefore, infected but asymptomatic individuals are a reservoir of infectious material. Since PrP^{C} is also expressed by follicular dendritic and other lymphoid cells, accumulation of PrP^{Sc} in the lymphatic organs of presymptomatic humans infected with BSE has been demonstrated by immunohistochemistry. PrP^{Sc} replication occurs because it does not elicit an immune response [49]. This is related to the inability of the immune system to distinguish between PrP^{C} and PrP^{Sc}. In fact, the prion protein is a self-antigen; hence, active immunization is not known to elicit a classical immune response. As observed in many *in vitro* studies, passive immunotherapy could be feasible in curing prion-infected cells. However, the major problem in using passive immunotherapy *in vivo* is that antibodies are generally

excluded from transport to the brain, because of the blood-brain barrier (BBB).

At present, there is no treatment that would arrest and/or reverse progression of prion disease in non-experimental settings, although many approaches have been investigated. The aim of most therapeutic interventions for these conformational disorders is to reduce the amount of the substrate (PrP^{C}) and its availability for the structural alteration; therefore interfere with the conversion either directly or indirectly and promote removal of the disease-associated conformers. The expression of host PrP^{C} is essential for both prion propagation and pathogenesis: PrP-null mice are resistant to prion disease and unable to replicate infectivity, disease incubation time is determined by PrP^{C} expression levels, and prion neurotoxicity is confined to PrP-expressing neural tissue. Thus the expression of host PrP^{C} is necessary for prion-induced neurotoxicity, suggesting the generation of a toxic intermediate form during prion conversion, or possibly the toxicity of early oligomeric forms of PrP^{Sc}. Removing PrP^{C}, the substrate for prion conversion, is therefore an appealing therapeutic target. Proof of principle of the validity of strategies targeting PrP^{C} came from the use of the adult onset model of PrP^{C} depletion. Transgenic animals in which PrP was depleted in neurons at nine weeks of age provided a system for testing the effects of PrP depletion in prion infection. PrP-expressing mice were infected with prions at one week of age, eight weeks prior to transgene mediated PrP depletion. Prion infection was allowed to develop over this time, with establishment of early spongiform change, astrocytosis and PrP^{Sc} deposition by the time neuronal PrP knockout occurred. This transgene mediated removal of

neuronal PrP^C during established prion infection allowed the animals to survive for long term without symptoms and led to a reversal of early spongiform change. The animals were effectively clinically cured [19]. In particular, among the numerous molecules harboring an anti-prion activity, antibodies against PrP were able to block PrP^{Sc} propagation in chronically infected prion cells [110]. Especially, we focused our attention on ScFvD18, an antibody fragment composed by the variable regions of the heavy and light chains. The extracellular location of PrP^C enables the potential use of this antibody, exploiting the potential of different selective gene therapy approaches. In fact, the activity of ScFvD18 was attributed to its ability to specifically recognize the total population of PrP^C molecules on the cell surface. The epitope of the antibody includes residues 132-156 of PrP^C. This sequence lies within the region of the protein though to bind PrP^{Sc}, an essential step for prion propagation.

We decided to selectively target ScFvD18 into the CNS of mice using an innovative adeno-associated virus-based drug delivery system. Important *in vivo* analysis with ScFvD18 have been already done and demonstrated that AAV2-ScFvD18 treated mice, intraperitoneally infected with RML, had an important delay in the appearance of clinical signs of disease if compared to untreated littermates [214]. These findings support the hypothesis that ScFvD18 binds to PrP^C and interferes with PrP^C-PrP^{Sc} interaction thus preventing PrP^{Sc} deposition into the brain. We decided to start our experiments with AAV2-ScFvD18 because this vector is nonpathogenic to humans, it is devoid of inflammatory or immunogenic properties thus allowing diffusion, long lasting and sustainable expression of therapeutics (months or

years) into the brain. [195]. The efficacy of AAV2 was recently supported by its application in different human clinical trials for Alzheimer, Parkinson, inborn errors of metabolism and other neurodegenerative disorders [204]. Unfortunately, over 80% of humans may be exposed to AAV2 often resulting in a pre-existing humoral immunity that can limit the efficacy of AAV2-based gene therapies in clinical applications [205]. However, considering the fact that AAV2 has a limited distribution into the CNS and that prion diseases affect several brain structures, it was necessary to select a new serotype of AAV capable of spreading more than AAV2. Previous data, confirmed in our laboratory, demonstrated that a new identified AAV serotype 9 had a higher in vivo diffusion and transduction efficiency than serotype 2 [230, 196].

In detail, we demonstrated that delivery of AAV2 vector (engineered with βgal reporter gene) unilaterally injected into the thalamus of C57Bl/6J mice led to an efficient but barely transduction of the cells closeness to the injection site. This serotype has been shown to be predominantly neurotropic by infecting only neuronal cells with the highest βgal expression detected one month after the injection. We subsequently showed that AAV9 vector was able to spread into the CNS and to transduce neurons better than AAV2. Particularly, AAV9 was able to undergo retrograde axonal transport and, as observed for AAV2 serotype, the highest βgal expression was reached one month after the inoculation. This serotype was predominantly neurotropic using laminin as receptor for neuronal infection [200]. Moreover, it has the potential advantage to overcome preexisting humoral immunity against the prevalent human serotypes (i.e. AAV2) thus

increasing the possibility of therapeutic success when translated from rodents to humans.

For these reasons, ScFvD18 was engineered in both AAV2 and AAV9 vectors and challenged in different mouse models of prion disease

In the first therapeutic approach, we tested the AAV2 vectors because they have already been employed in several human clinical trials without showing adverse effects after injection. Thus, AAV2-ScFvD18 was inoculated into the thalamus, hypothalamus and hippocampus of CD1 mice because of their prevalent involvement in PrP^{res} deposition following RML infection. Like humans, also the animals well tolerated the treatment and slight astrocyte reaction was mainly confined to the site of AAV inoculation. Neither the intracerebral AAV injection nor the viral particles themselves had any obvious effect on the behavior of the mice for the entire duration of the study. Also MRI and histological analysis, periodically performed, confirmed the lack of toxic or pathological effects related to the ScFvD18 expression into the CNS. Importantly, we were able to detect AAV2-ScFvD18 genome into the brain of mice even after 25 weeks from the day of inoculation. This is an important data because it confirmed that neuronal transduction was successful.

One month after AAV administration, at the time of highest ScFvD18 expression, mice have been intracerebrally (i.c.) infected with RML. This strain cause a widespread, diffuse and synaptic pattern of PrP^{Sc} deposition throughout the brain of mice, which is very similar to that of people affected by the MM1 form of sCJD (see p. 23).

After infection, animals monitoring was periodically performed. Changes in species-typical behaviors also occur long before end stage

motor symptoms and correlate with early loss of presynaptic terminals in the dorsal hippocampus.

Unfortunately, the treatment was not as effective in modifying or delaying the incubation time or survival of treated animals compared to that of untreated counterparts. Both AAV2-ScFvD18 treated and untreated mice became symptomatic and succumbed to disease at the same time.

Neuropathological analysis revealed important lesions into the hippocampus, which gave rise to an important vestibular problem: mice began to walk in circling. In addition, lesions into the ventro-medial portion of the hypothalamus, that is known to be a crucial centre in the control of ingestive behaviors, were responsible for hyperphagia and obesity of the mice. Tail rigidity was the result of spinal cord involvement in the disease while motor disfunction was the consequence of neuronal damage found into the cortex and in thalamic, caudate, putamen and septal nuclei. In particular, the thalamus, which is a major link between the external world and the cerebral cortex, was severely affected. It receives afferents from the spinal pathway to the ventroposterior nucleus (touch, pain, movement, temperature), and cerebellothalamic tracts from the deep cerebellar dentate nucleus to the ventral anterior and ventrolateral thalamus. Thus, disfunctions in thalamic areas could underline positive and negative sensory symptoms such as paraesthesia, pain or numbness. Since severe deficits, such as tremor and ataxia were caused by lesion to the dentate nucleus, the loss of its projection areas in the thalamus may also had a role in the motor coordination problems ultimately experienced by most patients with prion diseases.

Detailed histological and immunohistochemical analysis revealed similar neuropathological alterations between groups, except for lower PrP^{res} amount found into the CNS of AAV2-ScFvD18 treated mice compared to untreated animals. Moreover, densitometric analysis of PrP^{res} amount underlined that this difference was statistically significant. Surprisingly, although decreased level of PrP^{res}, the survival time of treated mice was significantly shorter compared to that of untreated group, while the incubation time was not different. In order to explain these results we need to do some considerations. In fact, it has commonly been assumed that pathological PrP itself is the primary cause of neurodegeneration in prion disease, based on the temporal and anatomical correlation between the accumulation of this protein and the development of neuropathological changes. However, there are a number of situations where this correlation is weak or absent. Several reports showed the absent link between infectivity or disease progression and PK-resistant PrP^{Sc} [231]. It has been also demonstrated that tissue containing little or no PK-resistant PrP can be infectious with high titres of TSE infectivity [232]. For example, in several kinds of transmission experiments, significant pathology and/or clinical disfunction develop with little accumulation of PrP^{Sc}. Some familial prion diseases (i.e. GSS) are not transmissible and are not accompanied by the accumulation of PK-resistant PrP. For this reason, the amount of PrP^{Sc} does not automatically predict disease progression. Conversely, there are examples of PrP^{Sc} accumulation in the absence of neuropathological alterations or clinical symptoms. These discrepancies have led to the growing recognition that alternative molecular forms of PrP, distinct from infectious PrP^{Sc}, or

other cofactors may be the proximate causes of neurodegeneration in prion diseases [233].

Actually, PrP^{Sc} is classically distinguished from its normal cellular precursor PrP^{C} by its detergent insolubility and partial resistance to proteolysis. Although molecular diagnosis of prion disease has historically relied upon detection of protease-resistant fragments of PrP^{Sc} using PK, it is now apparent that a substantial fraction of disease-related PrP (PK-sensitive) is destroyed by this protease. In particular, in inherited prion disease, PrP^{Sc} isoforms may be generated with unique physicochemical properties, reflected by sensitivity to PK digestion and PrP^{Sc}/prion infectivity ratios that can be very different from the PrP^{Sc} types propagated in sporadic and acquired forms of human prion disease. For this reason, it is becoming increasingly evident that the pathogenesis of both human and animal prion diseases may sometimes involve the propagation of PK-sensitive isoforms of PrP^{Sc}. To note, in our therapeutic approach, we infected the animals with RML prion strain. Recent studies on RML showed that only a minority of total disease-related PrP is PK-resistant [234]. In RML brain homogenate obtained from infected CD1 mice, under optimized conditions of proteolysis which destroy PrP^{C}, ~80% of total PrP^{Sc} do not resists degradation, whereas only ~20% of total PrP^{Sc} resists degradation with PK [235].

Taken into account all these observations, we may hypothesize that the expression of ScFvD18 could inhibit PrP^{res} formation while promoting the propagation of a PK-sensitive PrP^{Sc} probably more aggressive than the PK-resistant one. Considering the fact that PrP^{Sc} detection in our study was based on classical PK-treatment of the

samples, the PK-sensitive forms of the protein were lost. As support of our hypothesis, the presence of a PK-sensitive PrP more aggressive than the PK-resistant one have been also observed by Chiesa et al. [236] in Tg(PG14) mice. These mice carry a transgene encoding the murine homologue of a nine-octapeptide insertion associated with a familial prion disease in humans. Tg(PG14) mice spontaneously developed a fatal neurological illness that recapitulated several key features of human prion disorders, including ataxia, neuronal loss, synapse-like deposition of PrP, and astrogliosis. The development of clinical symptoms and neuropathological changes correlated closely with the accumulation of an aggregated and PK-resistant form of PrP. This mutant protein resembled PrP^{Sc} in its biochemical properties with one important exception: it was ~20 to 50 times less protease resistant than the PrP^{Sc} associated with most standard prion strains. This difference in protease resistance raises the possibility that Tg(PG14) mice harbour an unusual form of PrP that is highly pathogenic but that is structurally and biologically distinct from PrP^{Sc}. This work has been cited only to show that different forms of PrP^{Sc} could be involved in disease progression, and that analytic methods are very important for a correct sample analysis

We have also to consider that the infective PrP^{Sc} itself may not be the only responsible for the propagation of the disease and other unknown molecules (cofactors) could be involved in this process.

Other possible reasons for the failure of the first attempt may be the following: (i) the lack of ScFvD18 effectiveness could be partially explained by the high amount and the low dilution of infective material used for animals' infection following standardized

procedures. The injection of devastating amount of infective PrP^{Sc} into the brain of mice could have masked a potential benefit of ScFvD18 antibody; (ii) the incomplete protection could be related to a downregulation of ScFvD18 expression due to the progressive reduction of scFv expressing neurons, thereby leading to the loss of therapeutic efficacy; (iii) an immune response of mice against a foreign preformed viral vector or expressed ScFvD18 proteins may have occurred; (iv) finally, limited AAV2 diffusion could have contributed to the failure of the treatment. This last AAV2 characteristic is exploited for treating specific neurological diseases with localized pathology. In particular, putaminal convection-enhanced delivery (CED) of an AAV2 vector, containing the human aromatic L-amino acid decarboxylase (hAADC) gene for the treatment of Parkinson disease, has recently completed a phase I clinical trial [237]. Moreover, in an open-label phase I trial, gene delivery of the trophic factor neurturin via an AAV2 was well tolerated and seemed to improve motor function in patients with advanced Parkinson's disease [238].

In order to avoid some biases in subsequent experiments and to improve ScFvD18 diffusion, we inoculated the same strain of mice (CD1) with the AAV9-ScFvD18 vectors and we infected them intraperitoneally (i.p.) with RML. The first important data that we collected is that the animals well tolerated AAV9-ScFvD18 inoculation and slight astrocyte reaction was mainly confined to the site of AAV injection. Neither the intracerebral injection of the vector nor the viral particles themselves had any obvious effect on the

behavior of the mice. Also MRI and histological analysis, periodically performed, confirmed the lack of toxic or pathological effects related to the ScFvD18 expression into the CNS.

Animals sacrificed 166 days post infection gave important results. In particular, AAV9-ScFvD18 treated mice showed less-advanced disease compared to their untreated counterpart. Before being sacrificed, untreated animals had evident hyperactivity in the open field, fear and hind limb clasping while treated mice behaved normally. These data were also confirmed by neuropathological findings, which showed severe thalamic, hippocampal and septal pathology into the brain of untreated animals, while the same areas in ScFvD18 treated group were less affected. Immunohistochemical and biochemical analysis showed very low level of PrP^{res} in the brain of treated mice while untreated animals were characterized by higher levels of PrP deposition. Peripheral infection may have regulated the amount of prion that has been able to reach the CNS during disease progression. In the early stage of the disease, when a low amount of PrP^{Sc} reached the brain, ScFvD18 may have exerted a sufficient activity against PrP^{res} deposition and neurodegeneration.

Progressive neuronal loss and the increasing accumulation of the protein into the brain could have progressively masked the protective effects of ScFvD18, leading to a loss of therapeutic efficacy. In fact, even if ScFvD18 treated mice developed clinical signs of disease significantly later than untreated animals, no statistically significant difference in survival between groups has been observed and all mice succumbed to disease. An immune response mounted against the ScFvD18 or the AAV9 itself could have limited the efficacy of the

treatment. As we hypothesized in the previous therapeutic approach, the presence of a more aggressive PK-sensitive PrP may be responsible for this faster disease progression in treated mice. Some specific conformers of PrP^{Sc} over the others may have prevailed and, the experimental conditions in which they were challenged could have influenced the propagation of a subtype instead of another. Particularly, in this case, the involvement of the lymphoreticular system may have further influenced this selection. As already reported in the literature, after peripheral infection, uptake of the prion agent is followed by an initial phase of replication in the lymphoreticular system. Lymphatic organs such as the spleen, tonsils, lymph nodes or gut associated lymphoid tissue contain high concentrations of PrP^{Sc} long before PrP^{Sc} replication starts in the brain. Cells found to be particularly important for peripheral PrP^{Sc} replication are the follicular dendritic cells (DC) and the migratory bone-marrow derived DC.

DC from infected animals are capable of spreading the disease. The presence of PrP^{Sc} in peripheral lymphoid organs of all vCJD cases strongly underscores the importance of the lymphoreticular system [239, 240] after peripheral infection. For these reasons, the efficiency of our last approach could be improved by a combinatorial therapy able to target both the CNS and the lymphoreticular system. An emerging therapeutic approach effective against prion peripheral infection is immunomodulation [241]. Perhaps the treatment of mice with both AAV9-ScFvD18 and immunomodulant molecules could improve their efficacy.

In the last tested AAV-based therapeutic approach, both mouse and prion strains were changed in order to test whether they have an influence on AAV9-ScFvD18 efficacy.

For this purpose, we injected AAV9-ScFvD18 into the brain of C57Bl/6J mice infected with a mouse adapted strain of BSE. Also this mouse strain well tolerated the AAV inoculation and moderate astrocyte reaction was restricted to the injection site. Neither the treatment by intracerebral AAV injection nor the viral particles themselves caused behavioral or neuropathological harmful effects in treated mice. Most importantly, the AAV9 vector genome was present into the brain of mice even after 34 weeks from the day of inoculation. This is an important data because it shows again that the neuronal transduction was successful. One month after AAV administration, at the time of highest ScFvD18 expression, mice have been intracerebrally (i.c.) infected with BSE.

Unfortunately, the treatment was not effective in modifying or delaying neither the incubation time nor the survival of treated animals compared to their untreated counterparts. Also neuropathological changes were comparable between groups and mainly characterized by vacuolation preferentially involving the medulla oblongata, thalamus, hippocampus, septum and cerebral cortex. In particular, cochlear nucleus was severely affected. This nucleus is involved in the auditory system and projects to the vestibulocochlear nerve, a sensory nerve that conducts both hearing (audition) and balance (vestibular). Pathological changes observed in the cochlear nucleus may had an indirect effect on the vestibular nucleus, leading to the clinical signs of disease such as ataxia

observed in mice at the terminal stage of the disease. Ataxia due to alteration in the cochlear nucleus was also detected in cattle affected with BSE. The hippocampus was also affected. This area is part of the limbic system, implicated in emotion and its expression, and is mainly involved in learning and long-term memory storage. For this reason, hippocampus degeneration was responsible for mice behavioral disturbances. In particular, animals were hypoactive and lethargic in the home cage and also in the open field.

Immunohistochemical and biochemical data showed a statistically significant lower level of PrP^{res} concentration into the brain of treated mice compared to that of untreated animals. Again, it seems that the expression of ScFvD18 antibody exerted a moderate activity against PrP^{res} deposition but, unfortunately, the infectivity was not reduced. Therefore, in addition to PrP^{res}, further mechanisms of neurodegeneration have to be considered. A study of Lasmézas et al. [231] demonstrated that C57Bl/6J mice injected with homogenate from BSE-infected cattle brain exhibited neurological symptoms and neuronal death but, more than 55 percent had no detectable PrP^{res}. Thus, further unidentified agent, that might be an alternative PrP^{Sc} isoform more or less susceptible to PK treatment, could transmit BSE.

In addition, a crucial involvement of the host genome in modulating BSE prion strain propagation in mice was demonstrated by Lloyd and co-workers [242]. For this reason, the expression of ScFvD18 antibody into the brain of treated mice infected with BSE could have modulated the propagation of PrP^{res}.

Other possible reasons for the failure of the first attempt may be the following: (i) the lack of ScFvD18 effectiveness could be partially

explained by the high amount and the low dilution of infective material used for animals' intracererbal infection following standardized procedures. The injection of devastating amount of infective PrP^{Sc} into the brain of mice could have masked a potential benefit of ScFvD18 antibody; (ii) the incomplete protection could be related to a downregulation of ScFvD18 expression due to the progressive reduction of scFv expressing neurons, thereby leading to the loss of therapeutic efficacy; (iii) an immune response of mice against a foreign preformed viral vector or expressed ScFvD18 proteins may have occurred.

Innovative therapeutic approaches have been studied applying nanotechnology to the field of neurology (nanoneurology). Many existing neurologic treatments are at the nanoscale, such as pharmaceuticals and anticoagulants for stroke [179]. In particular gold nanoparticles (AuNPs) are emerging as a lead candidate in the field of nanotechnology as they can be easily prepared and tailored to a desirable size from 0.8 to 200 nm, they can be readily modified to various functionalities and good biocompatibility and can be conjugated to proteins without altering the biological activity of the conjugated species. They result in excellent therapeutic compounds due to the intrinsic properties as being non-toxic and inert to most chemical reactions [225]. Citrate-stabilized nanogold particles maintain good long-term stability in solution. Gold nanoparticles can be functionalized using Layer-by-Layer (LbL) deposition [220, 226]. Polyelectrolyte assembling on gold nanoparticles is induced by electrostatic interactions between the positively and negatively

charged polyelectrolytes. The range of the number of layers for these experiments was chosen to be in the precursor region of the LbL technique. From the LbL technique it is known that the first five layers of deposited polyelectrolytes differ from the following set of layers in terms of composition and thickness. These first five layers are the so-called precursor region. The polyelectrolyte absorption in the precursor layers is influenced by the attractive forces to the underlying layer, and also by the influence of the core. For example, if the core is negatively charged, the first positively charged polyelectrolyte layer will be self-assembled by pure attractive forces of the core, and will overcompensate the core charge. In the next layer, the attractive forces of the first polyelectrolyte layer are present, together with the repulsive forces of the core. The polyelectrolyte layers penetrate each other in the precursor region, and are thinner than the following set of layers, which are more distant and detached from the core [243]. We used the intercalation of polycations and polyanions, containing either sulfonate or primary amine groups, to selectively bind and inhibit prion formation, in order to create a surface exposing both moieties randomly and in varying ratios.

There is some reported evidence that polyamines can have an effect on PrP^{Sc} [244]. Indeed, Supattapone et al. found that branched polyamines are able to disintegrate aggregates of PrP^{Sc} to undetectable levels. For polysulfates, the influence of their chemical structure on the selective binding to either PrP^{C} or PrP^{Sc} lead to prion inhibitory activity [152]. In our work, both functional groups were combined on the surface of the nanogold particles in varying ratios, in order to obtain a platform of possible interactive sites for the misfolded PrP.

In addition, there are two studies to be considered about the bio-distribution of citrate stabilized nanogold. The results of these studies though were somehow contradictory: De Jong and co-workers found that only 10 nm particles were crossing the BBB, while Sonavane et al. found also 50 nm particles in the brain [245, 246]. Our particles showed in dynamic light scattering a hydrodynamic diameter 90 to 130 nm. But, under electron microscopy the fully hydrated polyelectrolyte matrix was deprived in the ultra high vacuum and was only 1-2 nm thick. This indicates that the shell of hydrated polyelectrolyte molecules is quite flexible and this can facilitate the entrance in the CNS throughout the BBB.

From previous experiments with porcine brain capillary endothelial cells, it is known that coated nanogold particles are cytotoxic. A strong dependence from the number of layers and surface charge was observed [220]. Polycations are more cytotoxic than polyanions and a lower number of layers is more cytotoxic than a higher number of layers. This toxicity was diminished by an additional binding of albumin to the final polyelectrolyte layer, and the animal experiments confirmed that after intracranial inoculation no toxicity leading to morphological changes in the brain was present.

Our *in vivo* experiments showed the efficacy of both 2A and 5S coated gold nanoparticles to interfere with prion propagation. Because of the limited information available about the toxic effects of these particles when injected in animals, we started our experiments by using dosages of compound lower than those generally reported in the literature for other therapeutic approaches [152].

Nanomolar concentrations of both 2A and 5S AuNPs were used. After infection, animal monitoring was periodically performed and confirmed the lack of adverse effects related to both 2A and 5S nanoparticles injection.

Similar behavioral and neuropathological alterations were found between groups and, in particular, lesions into the hippocampus, ventro-medial portion of the hypothalamus, caudate, putamen and septal nuclei and gave rise to specific behavioral alterations. Unfortunately all mice succumbed to the disease and, whereas nanogold 5S significantly increased only the incubation time of treated mice, nanogold 2A significantly increased both incubation and survival time. Indeed, even if animals were treated with a single dose of nanoparticles, 2A AuNPs were more efficient than 5S AuNPs against prion propagation.

Immunohistochemical and biochemical analysis showed similar alterations between groups, except for an higher amount of PrP^{res} into the CNS of 2A AuNPs treated mice compared to 5S AuNPs or untreated animals. These data further support our hypothesis regarding a possible dissociation between PrP^{Sc} and infectivity.

We could speculate that beneficial effects related to the treatment with 2A AuNPs may arise from the binding of nanoparticles to PrP^{Sc} or to specific cofactors necessary for PrP^{Sc} propagation.

In fact, since now, specific binding between nanoparticles and PrP^{Sc} have not been demonstrated, so the action of the nanoparticles on molecules different from PrP has to be taken into account.

2. SUMMARY

Prion diseases, or transmissible spongiform encephalopathies (TSEs), are neurodegenerative disorders of humans and animals that are sporadic or inherited in origin and can be transmitted. Creutzfeldt-Jakob disease (CJD) is the most prevalent form of TSE in humans, with a worldwide incidence of 1 case per million population per year. The typical clinical presentation of CJD is of a rapidly progressive dementia with ataxia and myoclonus, usually leading to death within 1 year from the onset of symptoms. The pathogenic mechanism shared by all TSEs is a post-translational modification of the prion protein from a normal cellular isoform (PrP^{C}) to insoluble and protease-resistant disease-specific species (termed PrP^{Sc}). PrP^{Sc} accumulates in the brain and is responsible for propagation of the pathologic process and transmissibility of the disease, by converting PrP^{C} into PrP^{Sc}.

Over the past several years, several compounds have been tested for treatment of prion diseases but most of them resulted ineffective. The main objective of this project was to evaluate the efficacy of innovative therapeutic compounds gained from emerging areas of gene therapy and nanomedicine. Among them, ScFvD18, an antibody fragment composed by the variable regions of the heavy and light chains, that was found to be efficient in clearing PrP^{Sc} in prion infected cells. Once engineered in Adeno-Associated Viral vectors serotype 9 (AAV9-ScFvD18) this compound has been delivered into the brain of prion-infected mice for studying the effectiveness in delay the appearance of symptoms and prolong survival. Polyelectrolyte gold nanoparticles represent another important class of molecules that

has been gained from the field of nanomedicine. Picomolar amount of polyelectrolyte-coated gold nanoparticles (AuNPs) with layer-wise deposition of oppositely charged synthetic polyelectrolytes were able to hamper the accumulation of PrP^{Sc} in cell culture. Their efficacy *in vivo* was tested for the first time in this work. In particular we evaluated the efficacy of ScFvD18 antibody and polycationic (2A) or polyanyionic (5S) functionalized AuNPs as prophylactic treatment in C57Bl/6J and CD1 mice subjected to different kind of prion infection.

Prions occur in the form of distinct strains, originally characterized by the incubation time and the neuropathology they elicit in a particular host. Many different strains can be propagated indefinitely in hosts expressing PrP protein; the protein-only hypothesis assumes that each strain is associated with a different conformer of PrP^{Sc}, which implies that there are as many stable conformations of PrP as there are stable prion strains that can be propagated in a particular mouse strain. Recent works of Li and co-workers [247], indicated that the concept of "conformation templating" at the protein level was first supported by cell-free conversion experiments and extended by the development of protein misfolding cyclic amplification (PMCA), which mimics PrP^{Sc} autocatalytic replication in vitro. A prion strain, transferred from one species to another and subsequently returned to the original host, may in some instances have changed or "mutated". Novel strains may arise not only by mutation of naturally occurring strains, but also de novo, in transgenic mice or in cell-free systems, mediated by PMCA.

The conversion reaction itself is critical to neurotoxicity in prion diseases: increasing evidences suggest that neither loss of PrP^{C} function nor deposition of PrP^{Sc} is sufficient to cause pathology. In

effect, the precise identity of the neurotoxic prion species and the exact mechanism of neurotoxicity are still unknown.

This hypothesis agrees well with the experimental data that we obtained.

Indeed, none of the therapies adopted was able to cure prion diseases. Conversely, the specific treatment with AAV2-ScFvD18 caused a faster disease progression in treated animals compared to untreated mice. Generally, we have never found a correlation between the amount of PrP^{res} and the infectivity. In particular, ScFvD18 treated animals always showed less PrP^{res} deposition in comparison to that found into the brain of untreated mice. These data clearly indicated the efficacy of ScFvD18 in modify PrP^{C}/PrP^{Sc} interaction thus reducing the amount of PK resistant PrP into the CNS. Despite less amount of PrP^{res}, neither important behavioral nor neuropathological modifications were detected. In addition, AAV2 or AAV9 administration and ScFvD18 expression into the brain have never induced toxic or adverse effects in mice. For this reason, the high diffusion and transduction efficiency of AAV9 vectors make them important tool for gene therapeutic approaches for prion and other neurodegenerative diseases involving the whole brain, such as Alzheimer's disease.

Interesting results were collected from the experiment with AuNps. Even in this case, all the treatments were not effective in curing prion diseases. To note, the field of nanoparticles is currently expanding and most information regarding pharmacodynamic and pharmacokinetics of AuNPs are still unknown. Important studies aimed to determine these parameters are actually ongoing. In our study, AuNPs were

administrated at nanomolar concentration in order to avoid eventual toxic or adverse effects in mice. The incubation periods of mice treated with nanomolar concentrations of 2A or 5S particles resulted significantly longer compared to that of untreated animals. In particular, polycationic 2A gold nanoparticles were the most effective in modify disease progression. Their exact mechanism of action is unknown. The functional groups exposed on their surface can selectively bind PrP^{Sc}, inhibit or prevent PrP^{Sc}/PrP^{C} interaction and disrupt PrP^{Sc} structure. In addition, they may bind other cofactors useful for PrP^{Sc} propagation. This interaction has to be investigated.
This finding represents the first report of nanoparticles as novel anti-prion drugs in mice.

These therapies provide important information about prion diseases. In fact, we may conclude that probably PrP^{res} itself is not responsible for neurodegeneration and the severity of the disease could not be correlated with the amount of PrP^{res} found into the brain. This allow us to think about the role of alternative PrP isoforms or specific cofactors (plasminogen, RNA, etc.) associated with PrP^{res} in brain damage. Contrary to classical drugs, our molecules can be optimized for a customized therapy. Moreover, designing of drugs with greater degree of cell specificity improves efficacy and minimizes adverse effects. In addition, therapies targeted only to PrP may not be sufficient in curing prion diseases and combinatorial approaches have to be considered. Learning about the molecular mechanisms responsible for the onset of prion diseases may help to decipher the age-dependent onset of several other degenerative disorders, the

incidences of which increases with age. These age-dependent diseases are becoming an increasingly serious public health problem in developed countries, where modern medicine as well as improved hygiene and lifestyles contribute to extending the average life span.

3. FUTURE PERSPECTIVES

To conclude, let us mention some lines for future research suggested by the approaches taken in this thesis.

General observations

By exploiting the potential of recent analytic methods, all samples will be reanalyzed to detect the presence of PK-sensitive, disease-related forms of PrP.

In particular, conformation-dependent immunoassay (CDI), treatment with thermolysin (a protease that preserves both PK-sensitive and PK-resistant disease-related isoforms of PrP but digests PrP^C in both rodent and human brain) [248] and immunoblotting after biochemical purification, will be performed.

Future prion infections will be performed either intracerebrally or intraperitoneally by inoculating lower dosage of infective material. In addition, our compounds will be inoculated both before and after prion infection in order to analyzes their efficacy as prophylactic or therapeutic treatments.

Gene therapy approaches

In order to confirm the presence of pathological PrP isoforms different from PrP^{Sc} in the brain of treated mice, we will perform a second passage transmission of brain homogenates from AAV9-ScFvD18 treated CD1 and C57Bl/6J mice infected with RML and BSE, respectively. We will characterize these new strains and we will compare them with the original ones to verify whether differences are detectable.

In the previous experiments AAV9-ScFvD18 has been injected one month before prion infection. In the future, detailed amount of AAV9-ScFvD18 will be inoculated concomitantly or after prion infection. In addition, it will be also interesting to study the effects of a combinatorial therapy with intracerebral and intravenous AAV9-ScFvD18 injection. In fact, tail vein injection of AAV9 in adult mice leads to robust transduction of astrocytes throughout the entire CNS, with limited neuronal transduction [249, 250]. This approach along with the intracerebral AAV9 injection (which leads to prevalent neuronal transduction) may further enhance the effect of the treatment. Indeed, *in vitro* studies showed that both neurons and astrocytes can sustain prion propagation, but the role of infected astrocytes in neurodegeneration remains controversial. Astrocytes play a critical role in normal brain development, neuronal plasticity, axonal conduction, synaptic transmission throughout adult life, and neuronal survival particularly following injury. These functions are mediated by astrocyte-neuron interactions, as well as by the extracellular matrix (ECM) and secreted factors produced by astrocytes [251]. Therefore,

it is possible that astrocyte alterations may also affect neuronal networking and survival.

Nanomedicine approaches

Different studies will be undertaken to determine the most effective composition and concentration of nanoparticles able to inhibit or completely block disease progression without causing toxic effects. In particular, AuNPs with different layer-wise deposition of oppositely charged synthetic polyelectrolytes will be tested. Based on our previous results with 2A and 5S AuNPs, several mice will be intracerebrally infected with RML brain homogenate, pre-incubated with higher dosages of 2A AuNPs.

Since the 2A nanoparticles, modified with the addition of albumin in the outermost layer, were able to cross BBB [252], new therapeutic approaches based on their systemic injection will be planned. Intraperitoneally or intracerebrally infected mice will be subjected to periodical intravenous AuNPs administration both before or after prion inoculation.

Aim of these experiments will be to establish the optimal and non-toxic dosage of AuNPs efficient to halt or delay disease progression.

REFERENCES

REFERENCES

[1] De Girolami U. et al. "Pathology of degenerative diseases of the nervous system." Manual of basic neuropathology. Chapter 8, pg 169; ISBN: 0-7506-7405-9.

[2] Prusiner S.B. (2001). "Shattuck lecture - Neurodegenerative diseases and prions." N Engl J Med 344(20): 1516-1526.

[3] Carrell, R. W. and D. A. Lomas (1997). "Conformational disease." Lancet 350(9071): 134-138.

[4] Blake, C. C., L. C. Serpell, et al. (1996). "A molecular model of the amyloid fibril." Ciba Found Symp 199: 6-15; discussion 15-21, 40-16.

[5] Ross, C. A. and M. A. Poirier (2004). "Protein aggregation and neurodegenerative disease." Nat Med 10 Suppl: S10-17.

[6] Dickson, D. W. (2009). "Neuropathology of non-Alzheimer degenerative disorders." Int J Clin Exp Pathol 3(1): 1-23.

[7] Ciechanover, A. and P. Brundin (2003). "The ubiquitin proteasome system in neurodegenerative diseases: sometimes the chicken, sometimes the egg." Neuron 40(2): 427-446.

[8] Zeng, B. Y., A. D. Medhurst, et al. (2005). "Proteasomal activity in brain differs between species and brain regions and changes with age." Mech Ageing Dev 126(6-7): 760-766.

[9] Lue, L. F., Y. M. Kuo, et al. (1999). "Soluble amyloid beta peptide concentration as a predictor of synaptic change in Alzheimer's disease." Am J Pathol 155(3): 853-862.

[10] McLean, C. A., R. A. Cherny, et al. (1999). "Soluble pool of Abeta amyloid as a determinant of severity of neurodegeneration in Alzheimer's disease." Ann Neurol 46(6): 860-866.

[11] Gu, Y., N. Sanjo, et al. (2004). "The presenilin proteins are components of multiple membrane-bound complexes that have different biological activities." J Biol Chem 279(30): 31329-31336.

[12] Yankner, B. A., L. R. Dawes, et al. (1989). "Neurotoxicity of a fragment of the amyloid precursor associated with Alzheimer's disease." Science 245(4916): 417-420.

[13] Price, D. L., R. E. Tanzi, et al. (1998). "Alzheimer's disease: genetic studies and transgenic models." Annu Rev Genet 32: 461-493.

[14] Hardy, J. (2006). "Has the amyloid cascade hypothesis for Alzheimer's disease been proved?" Curr Alzheimer Res 3(1): 71-73.

[15] Spillantini, M. G. and M. Goedert (1998). "Tau protein pathology in neurodegenerative diseases." Trends Neurosci 21(10): 428-433.

[16] Ironside, J. W., M. W. Head, et al. (2000). "Laboratory diagnosis of variant Creutzfeldt-Jakob disease." Histopathology 37(1): 1-9.

[17] McKinley, M. P., R. K. Meyer, et al. (1991). "Scrapie prion rod formation in vitro requires both detergent extraction and limited proteolysis." J Virol 65(3): 1340-1351.

[18] Prusiner, S. B. (1982). "Novel proteinaceous infectious particles cause scrapie." Science 216(4542): 136-144.

[19] Büeler, H., A. Aguzzi, et al. (1993). "Mice devoid of PrP are resistant to scrapie." Cell 73(7): 1339-1347.

[20] Hsiao, K., H. F. Baker, et al. (1989). "Linkage of a prion protein missense variant to Gerstmann-Straussler syndrome." Nature 338(6213): 342-345.

[21] Grundke-Iqbal, I., K. Iqbal, et al. (1986). "Microtubule-associated protein tau. A component of Alzheimer paired helical filaments." J Biol Chem 261(13): 6084-6089.

[22] Lindwall, G. and R. D. Cole (1984). "Phosphorylation affects the ability of tau protein to promote microtubule assembly." J Biol Chem 259(8): 5301-5305.

[23] Nieznanski, K., K. M. Osieka, et al. (2010). "Tau protein inhibits tubulin oligomerization induced by prion protein." Prion 4(3): 170. [Abstract].

[24] Hutton, M., C. L. Lendon, et al. (1998). "Association of missense and 5'-splice-site mutations in tau with the inherited dementia FTDP-17." Nature 393(6686): 702-705.

[25] Lewis, J., E. McGowan, et al. (2000). "Neurofibrillary tangles, amyotrophy and progressive motor disturbance in mice expressing mutant (P301L) tau protein." Nat Genet 25(4): 402-405.

[26] Binder, L. I., A. Frankfurter, et al. (1985). "The distribution of tau in the mammalian central nervous system." J Cell Biol 101(4): 1371-1378.

[27] Brion, J. P., D. P. Hanger, et al. (1991). "Tau in Alzheimer neurofibrillary tangles. N- and C-terminal regions are differentially associated with paired helical filaments and the location of a putative abnormal phosphorylation site." Biochem J 273(Pt 1): 127-133.

[28] Galvin, J. E., V. M. Lee, et al. (2001). "Synucleinopathies: clinical and pathological implications." Arch Neurol 58(2): 186-190.

[29] Clayton, D. F. and J. M. George (1998). "The synucleins: a family of proteins involved in synaptic function, plasticity, neurodegeneration and disease." Trends Neurosci 21(6): 249-254.

[30] Iwai, A., E. Masliah, et al. (1996). "The synaptic protein NACP is abnormally expressed during the progression of Alzheimer's disease." Brain Res 720(1-2): 230-234.

[31] Polymeropoulos, M. H., C. Lavedan, et al. (1997). "Mutation in the alpha-synuclein gene identified in families with Parkinson's disease." Science 276(5321): 2045-2047.

[32] Spillantini, M. G., M. L. Schmidt, et al. (1997). "Alpha-synuclein in Lewy bodies." Nature 388(6645): 839-840.

[33] Paulson, H. L., N. M. Bonini, et al. (2000). "Polyglutamine disease and neuronal cell death." Proc Natl Acad Sci U S A 97(24): 12957-12958.

[34] Kwong, L. K., K. Uryu, et al. (2008). "TDP-43 proteinopathies: neurodegenerative protein misfolding diseases without amyloidosis." Neurosignals 16(1): 41-51.

[35] Amador-Ortiz, C., W. L. Lin, et al. (2007). "TDP-43 immunoreactivity in hippocampal sclerosis and Alzheimer's disease." Ann Neurol 61(5): 435-445.

[36] Hasegawa, M., T. Arai, et al. (2007). "TDP-43 is deposited in the Guam parkinsonism-dementia complex brains." Brain 130(Pt 5): 1386-1394.

[37] Nakashima-Yasuda, H., K. Uryu, et al. (2007). "Co-morbidity of TDP-43 proteinopathy in Lewy body related diseases." Acta Neuropathol 114(3): 221-229.

[38] Guest, W. C., A. Das, et al. (2010). "Probing structural transition in Superoxide Dismutase 1, a protein with prion-like template-directed misfolding activity. " Prion 4(3): 223. [Abstract].

[39] Dohm, C. P., P. Kermer, et al. (2008). "Aggregopathy in neurodegenerative diseases: mechanisms and therapeutic implication." Neurodegener Dis 5(6): 321-338.

[40] Brundin, P., R. Melki, et al. (2010). "Prion-like transmission of protein aggregates in neurodegenerative diseases." Nat Rev Mol Cell Biol 11(4): 301-307.

[41] Prusiner, S. B. (1991). "Molecular biology of prion diseases." Science 252(5012): 1515-1522.

[42] Ghetti, B., P. Piccardo, et al. (1996). "Prion protein amyloidosis." Brain Pathol 6(2): 127-145.

[43] Williams, E. S. and S. Young (1980). "Chronic wasting disease of captive mule deer: a spongiform encephalopathy." J Wildl Dis 16(1): 89-98.

[44] Prusiner, S. B. and K. K. Hsiao (1994). "Human prion diseases." Ann Neurol 35(4): 385-395.

[45] Casalone, C., G. Zanusso, et al. (2004). "Identification of a second bovine amyloidotic spongiform encephalopathy: molecular similarities with sporadic Creutzfeldt-Jakob disease." Proc Natl Acad Sci U S A 101(9): 3065-3070.

[46] The National Creutzfeldt-Jakob Disease Surveillance Unit (NCJDSU). http://www.cjd.ed.ac.uk

[47] Ladogana, A., M. Puopolo, et al. (2005). "Mortality from Creutzfeldt-Jakob disease and related disorders in Europe, Australia, and Canada." Neurology 64(9): 1586-1591.

[48] Prusiner, S. B. (1994). "Biology and genetics of prion diseases." Annu Rev Microbiol 48: 655-686.

[49] Westergard, L., H. M. Christensen, et al. (2007). "The cellular prion protein (PrP(C)): its physiological function and role in disease." Biochim Biophys Acta 1772(6): 629-644.

[50] Mouillet-Richard, S., M. Ermonval, et al. (2000). "Signal Transduction Through Prion Protein." Science 289(5486): 1925-1928.

[51] Aguzzi, A. and M. Polymenidou (2004). "Mammalian prion biology: one century of evolving concepts." Cell 116(2): 313-327.

[52] Zahn, R., A. Liu, et al. (2000). "NMR solution structure of the human prion protein." Proc Natl Acad Sci U S A 97(1): 145-150.

[53] Taraboulos, A., K. Jendroska, et al. (1992). "Regional mapping of prion proteins in brain." Proc Natl Acad Sci U S A 89(16): 7620-7624.

[54] Stack M: 2004, Western immunoblotting techniques for the study of transmissible spongiform encephalopathies. *In*: Methods and tools in biosciences and medicine—techniques in prion research, ed. Lehmann S, Grassi J, pp. 97–116. Birkha¨user Verlag, Berlin.

[55] Parchi, P., A. Giese, et al. (1999). "Classification of sporadic Creutzfeldt-Jakob disease based on molecular and phenotypic analysis of 300 subjects." Ann Neurol 46(2): 224-233.

[56] Telling, G. C., M. Scott, et al. (1995). "Prion propagation in mice expressing human and chimeric PrP transgenes implicates the interaction of cellular PrP with another protein." Cell 83(1): 79-90.

[57] WHO manual for surveillance of human transmissible spongiform encephalopathies including variant Creutzfeldt-Jakob

diseases. World Health Organization Communicable Disease Surveillance and Response.

[58] Lloyd, S. E., O. N. Onwuazor, et al. (2001). "Identification of multiple quantitative trait loci linked to prion disease incubation period in mice." Proc Natl Acad Sci U S A 98(11): 6279-6283.

[59] Gajdusek, D. C. (1977). "Unconventional viruses and the origin and disappearance of kuru." Science 197(4307): 943-960.

[60] Will, R. G., J. W. Ironside, et al. (1996). "A new variant of Creutzfeldt-Jakob disease in the UK." Lancet 347(9006): 921-925.

[61] Zeidler, M., R. J. Sellar, et al. (2000). "The pulvinar sign on magnetic resonance imaging in variant Creutzfeldt-Jakob disease." Lancet 355(9213): 1412-1418.

[62] Zou, W. Q., G. Puoti, et al. (2010). "Variably protease-sensitive prionopathy: A new sporadic disease of the prion protein." Ann Neurol 68(2): 162-172.

[63] Gambetti, P., Z. Dong, et al. (2008). "A novel human disease with abnormal prion protein sensitive to protease." Ann Neurol 63(6): 697-708.

[64] Zerr, I., W. J. Schulz-Schaeffer, et al. (2000). "Current clinical diagnosis in Creutzfeldt-Jakob disease: identification of uncommon variants." Ann Neurol 48(3): 323-329.

[65] Sanchez-Juan, P., A. Green, et al. (2006). "CSF tests in the differential diagnosis of Creutzfeldt-Jakob disease." Neurology 67(4): 637-643.

[66] Otto, M., J. Wiltfang, et al. (2002). "Tau protein and 14-3-3 protein in the differential diagnosis of Creutzfeldt-Jakob disease." Neurology 58(2): 192-197.

[67] Riemenschneider, M., S. Wagenpfeil, et al. (2003). "Phospho-tau/total tau ratio in cerebrospinal fluid discriminates Creutzfeldt-Jakob disease from other dementias." Mol Psychiatry 8(3): 343-347.

[68] Zerr, I., K. Kallenberg, et al. (2009). "Updated clinical diagnostic criteria for sporadic Creutzfeldt-Jakob disease." Brain 132(Pt 10): 2659-2668.

[69] Zerr, I. (2009). "Therapeutic trials in human transmissible spongiform encephalopathies: recent advances and problems to address." Infect Disord Drug Targets 9(1): 92-99.

[70] Hill, A. F., R. J. Butterworth, et al. (1999). "Investigation of variant Creutzfeldt-Jakob disease and other human prion diseases with tonsil biopsy samples." Lancet 353(9148): 183-189.

[71] Rossetti, A. O., J. Bogousslavsky, et al. (2004). "Mimicry of variant Creutzfeldt-Jakob disease by sporadic Creutzfeldt-Jakob disease: importance of the pulvinar sign." Arch Neurol 61(3): 445-446.

[72] Telling, G. (2001). "Protein-based PCR for prion diseases?" Nat Med 7(7): 778-779.

[73] Pan, K. M., M. Baldwin, et al. (1993). "Conversion of alpha-helices into beta-sheets features in the formation of the scrapie prion proteins." Proc Natl Acad Sci U S A 90(23): 10962-10966.

[74] Krammer, C., I. Vorberg, et al. (2009). "Therapy in prion diseases: from molecular and cellular biology to therapeutic targets." Infect Disord Drug Targets 9(1): 3-14.

[75] Brandner, S., S. Isenmann, et al. (1996). "Normal host prion protein necessary for scrapie-induced neurotoxicity." Nature 379(6563): 339-343.

[76] Mallucci, G., A. Dickinson, et al. (2003). "Depleting neuronal PrP in prion infection prevents disease and reverses spongiosis." Science 302(5646): 871-874.

[77] Gauczynski, S., C. Hundt, et al. (2001). "Interaction of prion proteins with cell surface receptors, molecular chaperones, and other molecules." Adv Protein Chem 57: 229-272.

[78] Supattapone, S. (2010). "Biochemistry. What makes a prion infectious?" Science 327(5969): 1091-1092.

[79] Provost, P. (2010). "MicroRNAs as a molecular basis for mental retardation, Alzheimer's and prion diseases." Brain Res 1338: 58-66.

[80] Soto, C. and J. Castilla (2004). "The controversial protein-only hypothesis of prion propagation." Nat Med 10 Suppl: S63-67.

[81] Chandler, R. L. (1961). "Encephalopathy in mice produced by inoculation with scrapie brain material." Lancet 1(7191): 1378-1379.

[82] Chandler, R. L. and B. A. Turfrey (1972). "Inoculation of voles, Chinese hamsters, gerbils and guinea-pigs with scrapie brain material." Res Vet Sci 13(3): 219-224.

[83] Griffith, J. S. (1967). "Self-replication and scrapie." Nature 215(5105): 1043-1044.

[84] Outram, G. W. (1976). The pathogenesis of scrapie in mice. In *Slow Virus Diseases of Animals and Man,* pp. 325-357. Edited by R. H. Kimberlin. New York: Elsevier.

[85] Thackray, A. M., L. Hopkins, et al. (2007). "Mouse-adapted ovine scrapie prion strains are characterized by different conformers of PrPSc." J Virol 81(22): 12119-12127.

[86] Fraser, H., M. E. Bruce, et al. (1992). "Transmission of bovine spongiform encephalopathy and scrapie to mice." J Gen Virol 73 (Pt 8): 1891-1897.

[87] Groschup, M. H. and A. Buschmann (2008). "Rodent models for prion diseases." Vet Res 39(4): 32.

[88] Moore, R. C., N. J. Redhead, et al. (1995). "Double replacement gene targeting for the production of a series of mouse strains with different prion protein gene alterations." Biotechnology (N Y) 13(9): 999-1004.

[89] Bishop, M. T., P. Hart, et al. (2006). "Predicting susceptibility and incubation time of human-to-human transmission of vCJD." Lancet Neurol 5(5): 393-398.

[90] Asante, E. A., J. M. Linehan, et al. (2002). "BSE prions propagate as either variant CJD-like or sporadic CJD-like prion strains in transgenic mice expressing human prion protein." EMBO J 21(23): 6358-6366.

[91] Windl, O., M. Buchholz, et al. (2005). "Breaking an absolute species barrier: transgenic mice expressing the mink PrP gene are

susceptible to transmissible mink encephalopathy." J Virol 79(23): 14971-14975.

[92] Buschmann, A., E. Pfaff, et al. (2000). "Detection of cattle-derived BSE prions using transgenic mice overexpressing bovine PrP(C)." Arch Virol Suppl(16): 75-86.

[93] Crozet, C., F. Flamant, et al. (2001). "Efficient transmission of two different sheep scrapie isolates in transgenic mice expressing the ovine PrP gene." J Virol 75(11): 5328-5334.

[94] Tamguney, G., K. Giles, et al. (2006). "Transmission of elk and deer prions to transgenic mice." J Virol 80(18): 9104-9114.

[95] Fischer, M., T. Rulicke, et al. (1996). "Prion protein (PrP) with amino-proximal deletions restoring susceptibility of PrP knockout mice to scrapie." EMBO J 15(6): 1255-1264.

[96] Telling, G. C., P. Parchi, et al. (1996). "Evidence for the conformation of the pathologic isoform of the prion protein enciphering and propagating prion diversity." Science 274(5295): 2079-2082.

[97] Gavier-Widen, D., M. J. Stack, et al. (2005). "Diagnosis of transmissible spongiform encephalopathies in animals: a review." J Vet Diagn Invest 17(6): 509-527.

[98] Arima, K., N. Nishida, et al. (2005). "Biological and biochemical characteristics of prion strains conserved in persistently infected cell cultures." J Virol 79(11): 7104-7112.

[99] Fraser, H. and A. G. Dickinson (1968). "The sequential development of the brain lesion of scrapie in three strains of mice." J Comp Pathol 78(3): 301-311.

[100] Prusiner, S. B. 2004. Prion biology and diseases, 2nd ed. Cold Spring Harbor Laboratory Press, Cold Spring Harbor, NY.

[101] Bruce, M. E., I. McConnell, et al. (1991). "The disease characteristics of different strains of scrapie in Sinc congenic mouse lines: implications for the nature of the agent and host control of pathogenesis." J Gen Virol 72 (Pt 3): 595-603.

[102] Safar, J., H. Wille, et al. (1998). "Eight prion strains have PrP(Sc) molecules with different conformations." Nat Med 4(10): 1157-1165.

[103] World Alzheimer Report, Alzheimer Diseases International (ADI). http://www.alz.co.uk/research/worldreport/

[104] Brandt T, Caplan LR, Dichgans J, Diener HC, Kennard C (eds): Neurological Disorders. Course and Treatment. San Diego, Academic Press, 2003.

[105] Wei, C., N. Liu, et al. (2007). "From bench to bedside: successful translational nanomedicine: highlights of the Third Annual Meeting of the American Academy of Nanomedicine." Nanomedicine 3(4): 322-331.

[106] Russell, J. H., P. D. Stahl, et al. (2004). "Biomedical education in the 21st century." Mo Med 101(5): 484-486.

[107] Haik, S., J. P. Brandel, et al. (2004). "Compassionate use of quinacrine in Creutzfeldt-Jakob disease fails to show significant effects." Neurology 63(12): 2413-2415.

[108] May, B. C., A. T. Fafarman, et al. (2003). "Potent inhibition of scrapie prion replication in cultured cells by bis-acridines." Proc Natl Acad Sci U S A 100(6): 3416-3421.

[109] Tagliavini, F., R. A. McArthur, et al. (1997). "Effectiveness of anthracycline against experimental prion disease in Syrian hamsters." Science 276(5315): 1119-1122.

[110] Peretz, D., R. A. Williamson, et al. (2001). "Antibodies inhibit prion propagation and clear cell cultures of prion infectivity." Nature 412(6848): 739-743.

[111] Heppner, F. L., C. Musahl, et al. (2001). "Prevention of scrapie pathogenesis by transgenic expression of anti-prion protein antibodies." Science 294(5540): 178-182.

[112] Sigurdsson, E. M., M. S. Sy, et al. (2003). "Anti-prion antibodies for prophylaxis following prion exposure in mice." Neurosci Lett 336(3): 185-187.

[113] Perrier, V., J. Solassol, et al. (2004). "Anti-PrP antibodies block PrPSc replication in prion-infected cell cultures by accelerating PrPC degradation." J Neurochem 89(2): 454-463.

[114] Chabry, J., B. Caughey, et al. (1998). "Specific inhibition of in vitro formation of protease-resistant prion protein by synthetic peptides." J Biol Chem 273(21): 13203-13207.

[115] Zuber, C., S. Knackmuss, et al. (2008). "Single chain Fv antibodies directed against the 37 kDa/67 kDa laminin receptor as therapeutic tools in prion diseases." Mol Immunol 45(1): 144-151.

[116] White, A. R., P. Enever, et al. (2003). "Monoclonal antibodies inhibit prion replication and delay the development of prion disease." Nature 422(6927): 80-83.

[117] Proske, D., S. Gilch, et al. (2002). "Prion-protein-specific aptamer reduces PrPSc formation." Chembiochem 3(8): 717-725.

[118] Sayer, N. M., M. Cubin, et al. (2004). "Structural determinants of conformationally selective, prion-binding aptamers." J Biol Chem 279(13): 13102-13109.

[119] Soto, C., R. J. Kascsak, et al. (2000). "Reversion of prion protein conformational changes by synthetic beta-sheet breaker peptides." Lancet 355(9199): 192-197.

[120] Supattapone, S., H. O. Nguyen, et al. (1999). "Elimination of prions by branched polyamines and implications for therapeutics." Proc Natl Acad Sci U S A 96(25): 14529-14534.

[121] Winklhofer, K. F. and J. Tatzelt (2000). "Cationic lipopolyamines induce degradation of PrPSc in scrapie-infected mouse neuroblastoma cells." Biol Chem 381(5-6): 463-469.

[122] Whittle, I. R., R. S. Knight, et al. (2006). "Unsuccessful intraventricular pentosan polysulphate treatment of variant Creutzfeldt-Jakob disease." Acta Neurochir (Wien) 148(6): 677-679; discussion 679.

[123] Mange, A., N. Nishida, et al. (2000). "Amphotericin B inhibits the generation of the scrapie isoform of the prion protein in infected cultures." J Virol 74(7): 3135-3140.

[124] Caughey, B., K. Brown, et al. (1994). "Binding of the Protease-Sensitive Form of Prion Protein Prp to Sulfated Glycosaminoglycan and Congo Red." Journal of Virology 68(4): 2135-2141.

[125] Adjou, K. T., S. Simoneau, et al. (2003). "A novel generation of heparan sulfate mimetics for the treatment of prion diseases." J Gen Virol 84(Pt 9): 2595-2603.

[126] Kimberlin, R. H. and C. A. Walker (1983). "The antiviral compound HPA-23 can prevent scrapie when administered at the time of infection." Arch Virol 78(1-2): 9-18.

[127] Farquhar, C. F. and A. G. Dickinson (1986). "Prolongation of scrapie incubation period by an injection of dextran sulphate 500 within the month before or after infection." J Gen Virol 67 (Pt 3): 463-473.

[128] Masullo, C., G. Macchi, et al. (1992). "Failure to ameliorate Creutzfeldt-Jakob disease with amphotericin B therapy." J Infect Dis 165(4): 784-785.

[129] Pocchiari, M., S. Schmittinger, et al. (1987). "Amphotericin B delays the incubation period of scrapie in intracerebrally inoculated hamsters." J Gen Virol 68 (Pt 1): 219-223.

[130] Amyx, H., A. M. Salazar, et al. (1984). "Chemotherapeutic trials in experimental slow virus diseases. " Neurology 34 (Suppl. 1).

[131] Adjou, K. T., N. Privat, et al. (2000). "MS-8209, an amphotericin B analogue, delays the appearance of spongiosis,

astrogliosis and PrPres accumulation in the brain of scrapie-infected hamsters." J Comp Pathol 122(1): 3-8.

[132] Marella, M., S. Lehmann, et al. (2002). "Filipin prevents pathological prion protein accumulation by reducing endocytosis and inducing cellular PrP release." J Biol Chem 277(28): 25457-25464.

[133] Caughey, W. S., L. D. Raymond, et al. (1998). "Inhibition of protease-resistant prion protein formation by porphyrins and phthalocyanines." Proc Natl Acad Sci U S A 95(21): 12117-12122.

[134] Priola, S. A., A. Raines, et al. (2000). "Porphyrin and phthalocyanine antiscrapie compounds." Science 287(5457): 1503-1506.

[135] Forloni, G., S. Iussich, et al. (2002). "Tetracyclines affect prion infectivity." Proc Natl Acad Sci U S A 99(16): 10849-10854.

[136] Doh-Ura, K., T. Iwaki, et al. (2000). "Lysosomotropic agents and cysteine protease inhibitors inhibit scrapie-associated prion protein accumulation." J Virol 74(10): 4894-4897.

[137] Murakami-Kubo, I., K. Doh-Ura, et al. (2004). "Quinoline derivatives are therapeutic candidates for transmissible spongiform encephalopathies." J Virol 78(3): 1281-1288.

[138] Meier, P., N. Genoud, et al. (2003). "Soluble dimeric prion protein binds PrP(Sc) in vivo and antagonizes prion disease." Cell 113(1): 49-60.

[139] Roikhel, V. M., G. I. Fokina, et al. (1984). "Influence of aminasine on experimental scrapie in mice." Acta Virol 28(4): 321-324.

[140] Kocisko, D. A., A. Vaillant, et al. (2006). "Potent antiscrapie activities of degenerate phosphorothioate oligonucleotides." Antimicrob Agents Chemother 50(3): 1034-1044.

[141] Ertmer, A., S. Gilch, et al. (2004). "The tyrosine kinase inhibitor STI571 induces cellular clearance of PrPSc in prion-infected cells." J Biol Chem 279(40): 41918-41927.

[142] Engelstein, R., N. Grigoriadis, et al. (2005). "Inhibition of P53-related apoptosis had no effect on PrP(Sc) accumulation and prion disease incubation time." Neurobiol Dis 18(2): 282-285.

[143] Gresser, I., C. Maury, et al. (1983). "Failure to modify scrapie in mice by administration of interferon or anti-interferon globulin." J Gen Virol 64 (Pt 6): 1387-1389.

[144] Sethi, S., G. Lipford, et al. (2002). "Postexposure prophylaxis against prion disease with a stimulator of innate immunity." Lancet 360(9328): 229-230.

[145] Leucht, C., S. Simoneau, et al. (2003). "The 37 kDa/67 kDa laminin receptor is required for PrP(Sc) propagation in scrapie-infected neuronal cells." EMBO Rep 4(3): 290-295.

[146] Daude, N., M. Marella, et al. (2003). "Specific inhibition of pathological prion protein accumulation by small interfering RNAs." J Cell Sci 116(Pt 13): 2775-2779.

[147] Mabbott, N. A., J. Young, et al. (2003). "Follicular dendritic cell dedifferentiation by treatment with an inhibitor of the lymphotoxin pathway dramatically reduces scrapie susceptibility." J Virol 77(12): 6845-6854.

[148] Otto, M., L. Cepek, et al. (2004). "Efficacy of flupirtine on cognitive function in patients with CJD: A double-blind study." Neurology 62(5): 714-718.

[149] Caughey, B., L. D. Raymond, et al. (2003). "Inhibition of protease-resistant prion protein accumulation in vitro by curcumin." J Virol 77(9): 5499-5502.

[150] Shaked, G. M., R. Engelstein, et al. (2003). "Dimethyl sulfoxide delays PrP sc accumulation and disease symptoms in prion-infected hamsters." Brain Res 983(1-2): 137-143.

[151] Taraboulos, A., M. Scott, et al. (1995). "Cholesterol depletion and modification of COOH-terminal targeting sequence of the prion protein inhibit formation of the scrapie isoform." J Cell Biol 129(1): 121-132.

[152] Trevitt, C. R. and J. Collinge (2006). "A systematic review of prion therapeutics in experimental models." Brain 129(Pt 9): 2241-2265.

[153] Diringer, H. and B. Ehlers (1991). "Chemoprophylaxis of scrapie in mice." J Gen Virol 72 (Pt 2): 457-460.

[154] Richt, J. A., P. Kasinathan, et al. (2007). "Production of cattle lacking prion protein." Nat Biotechnol 25(1): 132-138.

[155] Ludewigs, H., C. Zuber, et al. (2007). "Therapeutic approaches for prion disorders." Expert Rev Anti Infect Ther 5(4): 613-630.

[156] Stewart, L. A., L. H. Rydzewska, et al. (2008). "Systematic review of therapeutic interventions in human prion disease." Neurology 70(15): 1272-1281.

[157] Terzano, M. G., E. Montanari, et al. (1983). "The effect of amantadine on arousal and EEG patterns in Creutzfeldt-Jakob disease." Arch Neurol 40(9): 555-559.

[158] The National Creutzfeldt-Jakob Disease Surveillance Unit (NCJDSU). http://www.cjd.ed.ac.uk/TREAT.htm

[159] David, A. S., R. Grant, et al. (1984). "Unsuccessful treatment of Creutzfeldt-Jakob disease with acyclovir." Lancet 1(8375): 512-513.

[160] Ratcliffe, J., A. Rittman, et al. (1975). "Creutzfeldt-Jakob disease with focal onset unsuccessfully treated with amantadine." Bull Los Angeles Neurol Soc 40(1): 18-20.

[161] Kovanen, J., M. Haltia, et al. (1980). "Failure of interferon to modify Creutzfeldt-Jakob disease." Br Med J 280(6218): 902.

[162] Beringue, V., J. P. Deslys, et al. (1997). "Creutzfeldt-Jakob disease: therapeutic strategies." Expert Opin Investig Drugs 6(4): 345-348.

[163] Rudyk, H., M. H. Knaggs, et al. (2003). "Synthesis and evaluation of analogues of Congo red as potential compounds against transmissible spongiform encephalopathies." Eur J Med Chem 38(6): 567-579.

[164] Bone, I., L. Belton, et al. (2008). "Intraventricular pentosan polysulphate in human prion diseases: an observational study in the UK." Eur J Neurol 15(5): 458-464.

[165] Klingenstein, R., S. Lober, et al. (2006). "Tricyclic antidepressants, quinacrine and a novel, synthetic chimera thereof clear prions by destabilizing detergent-resistant membrane compartments." J Neurochem 98(3): 748-759.

[166] Dohgu, S., A. Yamauchi, et al. (2004). "Uptake and efflux of quinacrine, a candidate for the treatment of prion diseases, at the blood-brain barrier." Cell Mol Neurobiol 24(2): 205-217.

[167] Themis, M., D. May, et al. (2003). "Mutational effects of retrovirus insertion on the genome of V79 cells by an attenuated retrovirus vector: implications for gene therapy." Gene Ther 10(19): 1703-1711.

[168] Manservigi, R., R. Argnani, et al. (2010). "HSV recombinant vector for gene therapy. " Open Virol J 4: 123-156.

[169] Bjorklund, A., D. Kirik, et al. (2000). "Towards a neuroprotective gene therapy for Parkinson's disease: use of adenovirus, AAV and lentivirus vectors for gene transfer of GDNF to the nigrostriatal system in the rat Parkinson model." Brain Res 886(1-2): 82-98.

[170] Wilson, J. M., B. Gansbacher, et al. (2008). "Good news on the clinical gene transfer front." Hum Gene Ther 19(5): 429-430.

[171] Schnepp, B. C., K. R. Clark, et al. (2003). "Genetic fate of recombinant adeno-associated virus vector genomes in muscle." J Virol 77(6): 3495-3504.

[172] Mandel, R. J., F. P. Manfredsson, et al. (2006). "Recombinant adeno-associated viral vectors as therapeutic agents to treat neurological disorders." Mol Ther 13(3): 463-483.

[173] Clinical Trials. http://clinicaltrials.gov/

[174] Chan, W. C. and S. Nie (1998). "Quantum dot bioconjugates for ultrasensitive nonisotopic detection." Science 281(5385): 2016-2018.

[175] Vaseashta, A. and D. Dimova-Malinovska (2005). "Nanostructured and nanoscale devices, sensors and detectors." Sci Technol Adv Mat 6(3-4): 312-318.

[176] Langer, R. (2001). "Drug delivery. Drugs on target." Science 293(5527): 58-59.

[177] Jin, S. and K. Ye (2007). "Nanoparticle-mediated drug delivery and gene therapy." Biotechnol Prog 23(1): 32-41.

[178] Kabanov, A. V. and H. E. Gendelman (2007). "Nanomedicine in the diagnosis and therapy of neurodegenerative disorders." Prog Polym Sci 32(8-9): 1054-1082.

[179] Rutledge Ellis-Behnke (2007). “Nano neurology and the four P’s of central nervous system regeneration: preserve, permit, promote, plasticity.” Med Clin North Am 91(5): 937-962.

[180] Quintana, A., E. Raczka, et al. (2002). "Design and function of a dendrimer-based therapeutic nanodevice targeted to tumor cells through the folate receptor." Pharm Res 19(9): 1310-1316.

[181] Hong, M. S., S. J. Lim, et al. (2002). "pH-sensitive, serum-stable and long-circulating liposomes as a new drug delivery system." J Pharm Pharmacol 54(1): 51-58.

[182] Alexiou, C., R. Jurgons, et al. (2003). "Magnetic drug targeting-biodistribution of the magnetic carrier and the chemotherapeutic agent mitoxantrone after locoregional cancer treatment." J Drug Target 11(3): 139-149.

[183] Radt, B., T. A. Smith, et al. (2004). "Optically addressable nanostructured capsules." Adv Mater 16 (23-24): 2184-2189.

[184] Nelson, J. L., B. L. Roeder, et al. (2002). "Ultrasonically activated chemotherapeutic drug delivery in a rat model." Cancer Res 62(24): 7280-7283.

[185] Kong, G., R. D. Braun, et al. (2001). "Characterization of the effect of hyperthermia on nanoparticle extravasation from tumor vasculature." Cancer Res 61(7): 3027-3032.

[186] Maguire, A. M., F. Simonelli, et al. (2008). "Safety and efficacy of gene transfer for Leber's congenital amaurosis." N Engl J Med 358(21): 2240-2248.

[187] Chakraborty, C., B. Sarkar, et al. (2009). "Future prospects of nanoparticles on brain targeted drug delivery." J Neurooncol 93(2): 285-286.

[188] De Jong, W. H. and P. J. Borm (2008). "Drug delivery and nanoparticles: applications and hazards." Int J Nanomedicine 3(2): 133-149.

[189] Calvo, P., B. Gouritin, et al. (2001). "Long-circulating PEGylated polycyanoacrylate nanoparticles as new drug carrier for brain delivery." Pharm Res 18(8): 1157-1166.

[190] Silva, G. A. (2008). "Nanotechnology approaches to crossing the blood-brain barrier and drug delivery to the CNS." BMC Neurosci 9 Suppl 3: S4.

[191] Kreuter, J. (2001). "Nanoparticulate systems for brain delivery of drugs." Adv Drug Deliv Rev 47(1): 65-81.

[192] Edetsberger, M., Gaubitzer, E, et al. (2005). "Detection of nanometer-sized particles in living cells using modern fluorescence

fluctuation methods." Biochem Biophys Res Commun 332(1): 109-116.

[193] Owens, D. E., 3rd and N. A. Peppas (2006). "Opsonization, biodistribution, and pharmacokinetics of polymeric nanoparticles." Int J Pharm 307(1): 93-102.

[194] Mayor, H. D. and J. L. Melnick (1966). "Small deoxyribonucleic acid-containing viruses (picodnavirus group)." Nature 210(5033): 331-332.

[195] Athanasopoulos, T., S. Fabb, et al. (2000). "Gene therapy vectors based on adeno-associated virus: characteristics and applications to acquired and inherited diseases (review)." Int J Mol Med 6(4): 363-375.

[196] Gao, G., L. H. Vandenberghe, et al. (2005). "New recombinant serotypes of AAV vectors." Curr Gene Ther 5(3): 285-297.

[197] Gao, G., L. H. Vandenberghe, et al. (2004). "Clades of Adeno-associated viruses are widely disseminated in human tissues." J Virol 78(12): 6381-6388.

[198] Davidson, B. L., C. S. Stein, et al. (2000). "Recombinant adeno-associated virus type 2, 4, and 5 vectors: transduction of variant cell types and regions in the mammalian central nervous system." Proc Natl Acad Sci U S A 97(7): 3428-3432.

[199] Nakai, H., S. Fuess, et al. (2005). "Unrestricted hepatocyte transduction with adeno-associated virus serotype 8 vectors in mice." J Virol 79(1): 214-224.

[200] Akache, B., D. Grimm, et al. (2006). "The 37/67-kilodalton laminin receptor is a receptor for adeno-associated virus serotypes 8, 2, 3, and 9." J Virol 80(19): 9831-9836.

[201] Wu, Z., A. Asokan, et al. (2006). "Adeno-associated virus serotypes: vector toolkit for human gene therapy." Mol Ther 14(3): 316-327.

[202] Chirmule, N., K. Propert, et al. (1999). "Immune responses to adenovirus and adeno-associated virus in humans." Gene Ther 6(9): 1574-1583.

[203] Bishop, K. M., E. K. Hofer, et al. (2008). "Therapeutic potential of CERE-110 (AAV2-NGF): targeted, stable, and sustained NGF delivery and trophic activity on rodent basal forebrain cholinergic neurons." Exp Neurol 211(2): 574-584.

[204] Kaplitt, M. G., A. Feigin, et al. (2007). "Safety and tolerability of gene therapy with an adeno-associated virus (AAV) borne GAD gene for Parkinson's disease: an open label, phase I trial." Lancet 369(9579): 2097-2105.

[205] Mastakov, M. Y., K. Baer, et al. (2002). "Immunological aspects of recombinant adeno-associated virus delivery to the mammalian brain." J Virol 76(16): 8446-8454.

[206] Zaiss, A. K., Q. Liu, et al. (2002). "Differential activation of innate immune responses by adenovirus and adeno-associated virus vectors." J Virol 76(9): 4580-4590.

[207] Manno, C. S., G. F. Pierce, et al. (2006). "Successful transduction of liver in hemophilia by AAV-Factor IX and limitations imposed by the host immune response." Nat Med 12(3): 342-347.

[208] Vandenberghe, L. H., L. Wang, et al. (2006). "Heparin binding directs activation of T cells against adeno-associated virus serotype 2 capsid." Nat Med 12(8): 967-971.

[209] Wang, L., J. Figueredo, et al. (2007). "Cross-presentation of adeno-associated virus serotype 2 capsids activates cytotoxic T cells but does not render hepatocytes effective cytolytic targets." Hum Gene Ther 18(3): 185-194.

[210] Broekman, M. L., L. A. Comer, et al. (2006). "Adeno-associated virus vectors serotyped with AAV8 capsid are more efficient than AAV-1 or -2 serotypes for widespread gene delivery to the neonatal mouse brain." Neuroscience 138(2): 501-510.

[211] Taymans, J. M., L. H. Vandenberghe, et al. (2007). "Comparative analysis of adeno-associated viral vector serotypes 1, 2, 5, 7, and 8 in mouse brain." Hum Gene Ther 18(3): 195-206.

[212] Gabizon, R., M. P. McKinley, et al. (1988). "Immunoaffinity purification and neutralization of scrapie prion infectivity." Proc Natl Acad Sci U S A 85(18): 6617-6621.

[213] Solforosi, L., J. R. Criado, et al. (2004). "Cross-linking cellular prion protein triggers neuronal apoptosis in vivo." Science 303(5663): 1514-1516.

[214] Wuertzer, C. A., M. A. Sullivan, et al. (2008). "CNS delivery of vectored prion-specific single-chain antibodies delays disease onset." Mol Ther 16(3): 481-486.

[215] Zuber, C., G. Mitteregger, et al. (2008). "Delivery of single-chain antibodies (scFvs) directed against the 37/67 kDa laminin receptor into mice via recombinant adeno-associated viral vectors for prion disease gene therapy." J Gen Virol 89(Pt 8): 2055-2061.

[216] Campana, V., L. Zentilin, et al. (2009). "Development of antibody fragments for immunotherapy of prion diseases." Biochem J 418(3): 507-515.

[217] Sahoo, S. K. and V. Labhasetwar (2003). "Nanotech approaches to drug delivery and imaging." Drug Discov Today 8(24): 1112-1120.

[218] Liu, G., P. Men, et al. (2006). "Nanoparticle iron chelators: a new therapeutic approach in Alzheimer disease and other neurologic disorders associated with trace metal imbalance." Neurosci Lett 406(3): 189-193.

[219] Supattapone, S., J. R. Piro, et al. (2009). "Complex polyamines: unique prion disaggregating compounds." CNS Neurol Disord Drug Targets 8(5): 323-328.

[220] Chanana, M., A. Gliozzi, et al. (2005). "Interaction of polyelectrolytes and their composites with living cells. " NanoLetters 5(12): 2605-2612.

[221] Aguzzi, A. (2009). "Cell biology: Beyond the prion principle." Nature 459(7249): 924-925.

[222] Salvadores, N., D. Morales-Scheihing, et al. (2010). "In vivo transmission of Type-2 diabetes by a prion-like mechanism. Prion." 4(3): 124. [Abstract].

[223] Guenther, K., R. M. Deacon, et al. (2001). "Early behavioural changes in scrapie-affected mice and the influence of dapsone." Eur J Neurosci 14(2): 401-409.

[224] Giaccone, G., B. Canciani, et al. (2000). "Creutzfeldt-Jakob disease: Carnoy's fixative improves the immunohistochemistry of the proteinase K-resistant prion protein." Brain Pathol 10(1): 31-37.

[225] Turkevich, J., P. C. Stevenson, (1951). "A study of the nucleation and growth processes in the synthesis of colloidal gold." Disc Farad Soc 11: 55-75.

[226] Schneider, G. and G. Decher. (2004). "From functional core/shell nanoparticles prepared via layer-by-layer deposition to empty nanospheres." NanoLetters 4: 1833-1839.

[227] Liu, X., M. Atwater, et al. (2007). "Extinction coefficients of gold nanoparticles with different sizes and different capping ligands." Colloids Surf B Biointerfaces 58: 3-7.

[228] Colby, D. W., Q. Zhang, et al. (2007). "Prion detection by an amyloid seeding assay." Proc Natl Acad Sci U S A 104(52): 20914-20919.

[229] Korth, C., B. C. May, et al. (2001). "Acridine and phenothiazine derivatives as pharmacotherapeutics for prion disease." Proc Natl Acad Sci U S A 98(17): 9836-9841.

[230] Cearley, C. N. and J. H. Wolfe (2006). "Transduction characteristics of adeno-associated virus vectors expressing cap

serotypes 7, 8, 9, and Rh10 in the mouse brain." Mol Ther 13(3): 528-537.

[231] Lasmezas, C. I., J. P. Deslys, et al. (1997). "Transmission of the BSE agent to mice in the absence of detectable abnormal prion protein." Science 275(5298): 402-405.

[232] Barron, R. M., S. L. Campbell, et al. (2007). "High titers of transmissible spongiform encephalopathy infectivity associated with extremely low levels of PrPSc in vivo." J Biol Chem 282(49): 35878-35886.

[233] Chiesa, R. and D. A. Harris (2001). "Prion diseases: what is the neurotoxic molecule?" Neurobiol Dis 8(5): 743-763.

[234] Thackray, A. M., L. Hopkins, et al. (2007). "Mouse-adapted ovine scrapie prion strains are characterized by different conformers of PrPSc." J Virol 81(22): 12119-12127.

[235] Klohn, P. C., L. Stoltze, et al. (2003). "A quantitative, highly sensitive cell-based infectivity assay for mouse scrapie prions." Proc Natl Acad Sci U S A 100(20): 11666-11671.

[236] Chiesa, R., P. Piccardo, et al. (2003). "Molecular distinction between pathogenic and infectious properties of the prion protein." J Virol 77(13): 7611-7622.

[237] Valles, F., M. S. Fiandaca, et al. (2010). "Qualitative imaging of adeno-associated virus serotype 2-human aromatic L-amino acid decarboxylase gene therapy in a phase I study for the treatment of Parkinson disease." Neurosurgery 67(5): 1377-1385.

[238] Marks, W. J., Jr., R. T. Bartus, et al. (2010). "Gene delivery of AAV2-neurturin for Parkinson's disease: a double-blind, randomised, controlled trial." Lancet Neurol 9(12): 1164-1172.

[239] Sethi, S., K. M. Kerksiek, et al. (2007). "Role of the CD8+ dendritic cell subset in transmission of prions." J Virol 81(9): 4877-4880.

[240] Daude, N. (2004). "Prion diseases and the spleen." Viral Immunol 17(3): 334-349.

[241] Wisniewski, T. and E. M. Sigurdsson (2007). "Therapeutic approaches for prion and Alzheimer's diseases." FEBS J 274(15): 3784-3798.

[242] Lloyd, S. E., J. M. Linehan, et al. (2004). "Characterization of two distinct prion strains derived from bovine spongiform encephalopathy transmissions to inbred mice." J Gen Virol 85(Pt 8): 2471-2478.

[243] Decher, G. (2003). Polyelectrolyte multilayers, an Overview. In Multilayer thin films. Edited by G. Decher, J. Schlenoff. Wiley-VCH, Weinheim, pp. 1-17.

[244] Supattapone, S., H. Wille, et al. (2001). "Branched polyamines cure prion-infected neuroblastoma cells." J Virol 75(7): 3453-3461.

[245] De Jong, W. H., W. I. Hagens, et al. (2008). "Particle size-dependent organ distribution of gold nanoparticles after intravenous administration." Biomaterials 29(12): 1912-1919.

[246] Sonavane, G., K. Tomoda, et al. (2008). "Biodistribution of colloidal gold nanoparticles after intravenous administration: effect of particle size." Colloids Surf B Biointerfaces 66(2): 274-280.

[247] Li, J., S. Browning, et al. (2010). "Darwinian evolution of prions in cell culture." Science 327(5967): 869-872.

[248] Cronier, S., N. Gros, et al. (2008). "Detection and characterization of proteinase K-sensitive disease-related prion protein with thermolysin." Biochem J 416(2): 297-305.

[249] Foust, K. D., E. Nurre, et al. (2009). "Intravascular AAV9 preferentially targets neonatal neurons and adult astrocytes." Nat Biotechnol 27(1): 59-65.

[250] Duque, S., B. Joussemet, et al. (2009). "Intravenous administration of self-complementary AAV9 enables transgene delivery to adult motor neurons." Mol Ther 17(7): 1187-1196.

[251] Fields, R. D. and B. Stevens-Graham (2002). "New insights into neuron-glia communication. " Science 298: 556-562.

[252] Sousa, F., S. Mandal, et al. (2010). "Functionalized gold nanoparticles: a detailed in vivo multimodal microscopic brain distribution study." Nanoscale. 2010 Oct 15. [Epub ahead of print]. PMID: 20949211.

[253] Barret, A., F. Tagliavini, et al. (2003). "Evaluation of quinacrine treatment for prion diseases." J Virol 77(15): 8462-8469.

PUBLICATIONS and ACKNOWLEDGEMENTS

1. PUBLICATIONS

1. Ai Tran HN, Sousa F, Moda F, Mandal S, Chanana M, Vimercati C, Morbin M, Krol S, Tagliavini F, Legname G. A novel class of potential prion drugs: preliminary in vitro and in vivo data for multilayer coated gold nanoparticles. Nanoscale. 2010 Oct 14.
   [Epub ahead of print] PMID: 20944860.

2. Giaccone G, Morbin M, Moda F, Botta M, Mazzoleni G, Uggetti A, Catania M, Moro ML, Redaelli V, Spagnoli A, Rossi RS, Salmona M, Di Fede G, Tagliavini F. Neuropathology of the recessive A673V APP mutation: Alzheimer disease with distinctive features. Acta Neuropathol. 2010 Dec;120(6):803-12

2. ACKNOWLEDGEMENTS

Ringrazio il dott. Fabrizio Tagliavini per avermi dato l'opportunità di raggiungere questo importante traguardo, mettendo costantemente a mia disposizione la sua fondamentale e vasta competenza e professionalità. Lo ringrazio per la fiducia riposta in me, nell'affidarmi un progetto tanto importante che mi ha permesso di crescere sia lavorativamente che personalmente, e grazie al quale ho avuto modo di conoscere e collaborare con diversi professionisti del settore.

Un doveroso e sincero ringraziamento è rivolto al mio mentor, il dott. Giuseppe Legname, della Scuola Internazionale Superiore di Studi Avanzati di Trieste, per avermi guidato, consigliato e supportato, insieme al dott. Fabrizio Tagliavini, nella stesura dei protocolli terapeutici sperimentali, con il quale si è creata anche una autentica amicizia.

Ringrazio la dott.ssa Lorena Zentilin e parte del suo staff, in particolare le sig.re Marina Dapas e Michela Zotti, dell'International Centre for Genetic Engineering and Biotechnology di Trieste, per averci fornito il materiale genetico utilizzato nelle sperimentazioni, aiutandoci con competenza ed esperienza nella realizzazione degli studi di terapia genica.

Ringrazio la dott.ssa Silke Krol e la dott.ssa Maria Fernanda Costa de Sousa, del Centro Europeo di Nanomedicina dell'Istituto Neurologico Besta di Milano, per averci fornito le nano particelle e per aver messo a nostra disposizione la loro esperienza nel campo della nanomedicina per la conduzione degli esperimenti sugli animali.

Un ringraziamento speciale è dedicato a tutti i professionisti del laboratorio in cui ho condotto gli esperimenti, per le disponibilità e capacità con le quali hanno contribuito alla buona riuscita del progetto. In particolare voglio citare, la dott.ssa Chiara Vimercati per il preziosissimo lavoro di monitoraggio e cura degli animali in sperimentazione; la dott.ssa Ruggerone Margherita e la dott.ssa Ilaria Campagnani per la costanza e la dedizione nella raccolta e nella processazione dei campioni; il dott. Giorgio Giaccone per l'eccellente supporto con le analisi neuropatologiche; la dott.ssa Michela Morbin ed il dott. Andrea Uggetti per le analisi di microscopia elettronica ed

infine, la dott.ssa Marcella Catania e la dott.ssa Elena Piccoli per le analisi genetiche.

Vorrei esprimere gratitudine e riconoscenza ad alcune persone che hanno contribuito alla mia formazione e il cui supporto mi ha consentito di affrontare con attenzione, passione e professionalità gli studi con gli animali, gli studi immunoistochimici e biochimici. In particolare, la dott.ssa Michela Mangieri per avermi trasmesso la passione del lavorare con gli animali e quella per gli studi immunoistochimici; la dott.ssa Lucia Limido e la dott.ssa Silvia Suardi per avermi insegnato la parte biochimica necessaria allo svolgimento del lavoro, ed infine la sig.ra Cinzia Francesca Cacciatore e la sig.ra Sonia Spinello per avermi istruito sulla parte tecnica, tutte fondamentali per la realizzazione e la redazione di questo lavoro.

Ultimo, ma non meno importante, un sincero grazie al supporto dei miei genitori, Giuliana e Filippo e a quello di Anna e Davide che hanno sempre condiviso con me sia gli insuccessi che le soddisfazioni lavorative. Li ringrazio per aver creduto in me e per avermi accompagnato al raggiungimento di questo traguardo.